Universidade Federal de Juiz de Fora
Programa de Pós-Graduação em
Engenharia Elétrica

Luís Guilherme da Silva Costa

Non-Adaptive and Adaptive Coupling Circuits for Power Line Communication System

Juiz de Fora
2017

Luís Guilherme da Silva Costa

Non-Adaptive and Adaptive Coupling Circuits for Power Line Communication System

Tese de doutorado apresentada ao Programa de Pós-Graduação em Engenharia Elétrica da Universidade Federal de Juiz de Fora, na área de concentração em sistemas eletrônicos, como requisito parcial para obtenção do título de Doutor em Engenharia Elétrica.

Orientador: Prof. Moisés Vidal Ribeiro, Phd.
Co-orientador: Prof. Antônio Carlos Moreirão de Queiroz, D.Sc.

Juiz de Fora
2017

Ficha catalográfica elaborada através do programa de geração
automática da Biblioteca Universitária da UFJF,
com os dados fornecidos pelo(a) autor(a)

Costa, Luís Guilherme da Silva.
Non-Adaptive and Adaptive Coupling Circuits for Power Line Communication System : / Luís Guilherme da Silva Costa. -- 2017.
154 p. : il.

Orientador: Moisés Vidal Ribeiro
Coorientador: Antônio Carlos Moreirão de Queiroz
Tese (doutorado) - Universidade Federal de Juiz de Fora, Faculdade de Engenharia. Programa de Pós-Graduação em Engenharia Elétrica, 2017.

1. Power line communication. 2. Access impedance. 3. Coupling circuit. 4. Statistical modeling. 5. Electric power grid. I. Ribeiro, Moisés Vidal, orient. II. Queiroz, Antônio Carlos Moreirão de, coorient. III. Título.

Luís Guilherme da Silva Costa

Non-Adaptive and Adaptive Coupling Circuits for Power Line Communication System

Tese apresentada ao Programa de Pós-Graduação em Engenharia Elétrica da Universidade Federal de Juiz de Fora, na área de concentração em Sistemas Eletrônicos, como requisito parcial para obtenção do título de Doutor em Engenharia Elétrica.

Aprovada em 06 de setembro de 2017.

BANCA EXAMINADORA:

Prof. Moisés Vidal Ribeiro
Universidade Federal de Juiz de Fora, UFJF
Orientador

Prof. Antônio Carlos Moreirão de Queiroz, Dr.
Universidade Federal do Rio de Janeiro, UFRJ
Orientador

Prof. Carlos Augusto Duque, Dr.
Universidade Federal de Juiz de Fora, UFJF

Prof. Cássio Gonçalves do Rego, Dr.
Universidade Federal de Minas Gerais, UFMG

Prof. Elnatam Chagas Ferreira, Dr.
Universidade Estadual de Campinas, UNICAMP

Prof. Luciano Manhães de Andrade Filho, Dr.
Universidade Federal de Juiz de Fora, UFJF

ACKNOWLEDGEMENTS

To my parents, Maria Lúcia and Ayrton, for always encourage me to study and for teaching me important values.

To may belove wife Tereza and my sons Vinícius and Vitor for their support and companionship during my entire doctorate.

To my sister Cláudia and my brothers Carlos Augusto, Alexandre e Leonardo for all support, motivation, and trust placed in me.

To my advisor Moisés, who believed in my potential and was a nice friend.

To my co-advisor Moreirão for important contributions in my work and teachings.

To my friends Guilherme Colen and Picorone for their friendship during my walk in doctorate degree in which contributed directly with my thesis.

" Engineering is not merely knowing and being knowledgeable, like a walking encyclopedia; engineering is not merely analysis; engineering is not merely the possession of the capacity to get elegant solutions to non-existent engineering problems; engineering is practicing the art of the organizing forces of technological change···Engineers operate at the interface between science and society. "

Gordon Stanley Brown

Esta tese de doutorado apresenta, inicialmente, uma revisão sobre acopladores para power line communication (PLC), utilizados para acoplar o sinal dos transceptores PLC à rede de energia elétrica. As questões predominantes para o projeto de acopladores e, consequentemente, os diferentes tipos de acopladores são discutidos. Uma classificação dos acopladores PLC baseada nos tipos de acoplamentos (capacitivo, indutivo, resistivo e por antenas), níveis de tensão, largura de banda de frequência, modos de propagação e números de conexões com a rede de energia elétrica é apresentada. Em seguida, o projeto de circuitos PLC de acoplamento capacitivo não adaptativos, single input single output (SISO) de baixa tensão para aplicações banda larga e banda estreita são discutidos. O acoplador PLC banda estreita é projetado para a banda de frequência de 9 kHz-500 kHz, enquanto os acopladores banda larga são projetados para a banda de frequência de 1.7-50 MHz, 1.7-100 MHz e 1.7-500 MHz. Além disso, discute-se as especificações e o projeto dos protótipos desses circuitos de acoplamento PLC medindo seus parâmetros de espalhamento. A seguir, é discutida a medida da impedância de acesso da rede de energia elétrica de baixa tensão na banda de frequência 2-500 MHz, visando apresentar prévio conhecimento da impedância de acesso da rede de energia elétrica no Brasil com base em uma campanha de medição realizada em várias instalações em três cidades brasileiras diferentes. Além disso, é proposto um procedimento para obter um modelo estatístico da impedância de acesso na referida faixa de frequência. Com base em uma série de medidas de impedâncias de acesso da rede de energia elétrica e critérios para a escolha de modelos estatísticos, esta tese sugere duas distribuições para modelar as componentes resistência e reatância da impedância de acesso da rede de energia elétrica. Uma vez que, os parâmetros de tais modelos mudam com a frequência e que a impedância de acesso é um processo aleatório no domínio da frequência, um modelo simples para gerar amostras em função desse processo aleatório, que leva em consideração as distribuições sugeridas, é detalhado. Por fim, é proposto um circuito de acoplamento adaptativo PLC, capacitivo, SISO de baixa tensão. Estes circuitos de acoplamento adaptativos usam três diferentes filtros analógicos passa-baixa com diferentes impedâncias de entrada. A impedância de entrada de cada filtro analógico é projetado de acordo com os valores obtidos através da campanha de medição, e a impedância de saída é projetada para 50 Ω. A escolha do filtro analógico que proporciona melhor casamento de impedância com a rede de energia elétrica é obtido por um microcontrolador, que através de um conversor analógico digital, monitora a tensão fornecida por um circuito que mede a potência dos sinais injetados nos acopladores PLC pelos transceptores PLC. A monitoração da potência é realizada continuamente pelo conversor analógico digital do microcontrolador que

escolhe qual o filtro analógico proporciona o melhor casamento de impedância com a rede de energia elétrica e comuta os filtros analógicos através de uma chave de analógica conectando os transceptores PLC a rede de energia elétrica através dos acopladores PLC. Além disso, as medições dos valores do parâmetro de espalhamento S_{11} confirmam que a componente resistiva da impedância de acesso da rede de energia elétrica apresentou melhor casamento de impedância entre 50 Ω e 100 Ω. Por fim, os valores medidos do parâmetro de espalhamento S_{12} mostram que a atenuação cresce com o aumento da frequência devido ao comportamento indutivo da rede de energia elétrica.

Palavras-chave: power line communications, impedância de acesso, circuito de acoplamento, rede de energia elétrica, modelagem estatística.

ABSTRACT

This work outlines a comprehensive review of PLC coupling circuits, which are required for narrowband and broadband PLC transceivers. Prevailing issues that protract the design of couplers and consequently subtended the inventions of different types of couplers are clearly described. Also, it provides a useful classification of PLC couplers based on the type of physical couplings, voltage levels, frequency bandwidth, propagation modes and a number of connections. Next, the focus is on the design of non-adaptive capacitive, SISO and low-voltage (LV) PLC coupling circuits for both broadband and narrowband applications. The narrowband cover the frequency band 9 kHz-500 kHz, while broadband frequency bands are 1.7-50 MHz, 1.7-100 MHz and 1.7-500 MHz. Moreover, it discusses the specification and design of the prototypes of the PLC coupling circuits measuring their scattering parameters. The access impedance of Brazilian in-home, broadband and low-voltage electric power grid in the frequency band 2-500 MHz is taken into account. Based on the use of a measurement setup a large measurement campaign that was carried out in several facilities in three different Brazilian cities is discussed. Also, a procedure to obtain a statistical model of the access impedance in the aforementioned broadband frequency is outlined. Based on a number of measured access impedances and well-known criteria for choosing statistical models, two distributions to model the resistance and reactance components of the access impedance are suggested. Due to the fact that the parameters of such models change with the frequency and the access impedance is a random process in the frequency domain, a simple and effective model to generate samples function of such random process, which takes into account the suggested distributions, is addressed. Finally, adaptive capacitive, SISO and LV PLC coupling circuits are proposed for broadband power line communication. These adaptive coupling circuits use three different analog low-pass filter for impedance matching. This filter is an array of analog low-pass irregular filters that separate the input and output signal into three analog low-pass filters, each one matching the impedance between the electric power grid and PLC transceiver. The input impedance of each filter has a different impedance value, chosen according to the impedance of the measurement campaign, and the output impedance is fixed in 50 Ω for all analog low-pass filter. The choice of the analog filter that provides better impedance matching to the electrical power grid is obtained by a microcontroller,

which through an analog-to-digital converter (ADC), measure the voltage provided by a circuit that measures the power of the signals injected into the PLC coupling circuit by the PLC transceivers. The power is continuously measured by an ADC of the microcontroller which chooses which analog filter provides the best impedance matching with the electric power grid and switches the analog filters through an analog switcher connecting the PLC transceivers to the electric power grid through the PLC coupling circuit. In addition, the measured values of the scattering parameter S_{11} show that the best impedance matching occurs when the resistive impedance component of the access impedance is between 50 Ω and 100 Ω. For the scattering parameter S_{12} it has been found that the attenuation increases as the frequency increases because of the inductive behavior of the electric power grid.

Keywords: power line communication, access impedance, coupling circuit, electric power grid, statistical modeling.

LIST OF FIGURES

LIST OF TABLES

ACRONYMS

AC alternating current

ADC analog-to-digital converter

ADS Advanced Design System

AIC Akaike Information Criterion

ANATEL Agência Nacional de Telecomunicações

BALUN balanced to unbalanced

BIC Bayesian Information Criterion

CCVTs Coupling Capacitor Voltage Transformers

CDF cumulative distribution function

CM common mode

DAC digital-to-analog converter

DC direct current

DFT discrete Fourier Transform

DM differential mode

EDC Efficient Determination Criterion

EMC electromagnetic compliance

EMI electromagnetic interference

GDT gas discharge tube

GPIO general purpose input/output

HV high-voltage

LV low-voltage

LVDC low voltage direct current

MIMO multiple input multiple output

MISO multiple input single output

MOV metal oxide varistor

MV medium-voltage

PCB printed circuit board

PLC power line communication

PTH plated-through holes

RF radio frequency

SAR successive-approximation-register

SIMO single input multiple output

SISO single input single output

SMD surface mount device

SPD surge protection device

SRF self resonant frequency

TVS transient voltage suppressor

TVSP transient voltage surge protection

UHF ultra-high-frequency

VNA vector network analyzer

CONTENTS

1 INTRODUCTION

Currently, there is a great interest in the widespread use of PLC technologies because they allow the use of electric power grid as data transmission medium. In fact, electric power grid can have its usefulness expanded by delivering electric energy and providing data communication at HV, MV and LV in outdoor (e.g. electric power system) and indoor facilities (e.g. home, buildings, and vehicles).

The use of electric power grid to support the maintenance and operation of electric power companies begins in the 20th Century. For instance, Electric utilities use low-data rate transmission technology to remotely switch relays on and off, to perform maintenance of circuits and electrical protection, automatically collecting and monitoring the electricity consumption [1], among other applications. However, the use of electric power grid for high-data rates emerged after 1980 [2] [3].

The use of electric power grid as a medium for data communication is a challenging, since these media are characterized by time-frequency varying nature of the loads connected to electric power grid, leading to relevant impedance mismatching, increasing attenuation with the increase of distance and/or frequency, related to the characteristics of power cables, the presence of high power impulsive noise, and electromagnetic interference due to the use of unshielded cables [4].

Since electric power grid was not designed for data communication, there are several issues that must be addressed to design effective and efficient PLC transceivers [5]. Regarding PLC transceivers, the main obstacle is to accomplish the coupling among electric power grid and PLC transceivers. Traditionally, the coupling of PLC transceivers with electric power grid are accomplished by using passive electrical components, which are combined to provide adequate isolation between the hardware of a PLC transceiver and the electric power grid. It can be stated that coupling is a challenging problem for the PLC technology because, as stated earlier, the electric power grid is not designed to transmit telecommunications signals with low power and high-frequency content [6] and are characterized by the presence of dynamic loads.

Consequently, the electronic circuits of PLC transceivers are not designed to operate at high voltages levels associated with the mains signal of the electric power system [7] and existing impedance mismatching.

The impedance mismatching between the PLC coupling circuit and electric power grid can severely attenuate the PLC signals injected into or extracted from the electric power grid by PLC transceiver. The maximum power transfer is achieved when the impedance of the PLC coupling circuit is equal to the complex conjugate of the electric power grid impedance. However, the temporal and spectral dynamics behaviors of impedances of the electric power grid make it very hard task to be accomplished because it must be designed to adjust the dynamics variation of the access impedance and provide strength signal. For this purpose, the design of an adaptive impedance circuit between the transmitter and the receiver would allow that the loss of power between the transmitter and the receiver to be minimized. However, to design an adaptive impedance matching circuit, preliminary we must measure the values of the access impedance of electric power grid.

Measuring and characterizing impedance behaviors at connection points and proposing solutions to improve impedance matching and increasing the throughput of a PLC system is a matter of great interest and applicability [8]. In this context, it becomes important to know the values of the access impedance of electric power grid to design adaptive impedance matching circuits to dynamically adjust the impedance of the PLC coupling circuit with the electric power grid. On the other hands, the majority of the current researches regarding PLC coupling are directed to the use of non-adaptive circuits, since they present the lowest cost and are very simple to implement by dealing with LV electric circuits.

A comprehensive review of PLC coupling show that the focus was on impedance matching of the PLC transceiver with electric power grid designing different types of techniques such as using a different ratio of turns from the primary to secondary windings of the RF transformer. In this type of impedance matching the ratio N:1 is used to match the impedance between the PLC transceiver and electric power grid [9]. Another work proposed the use of band-pass filter designed in the T or π configuration [10], transformerless power line coupling circuit to match the impedance with the electric power grid. However, these techniques do not predict the time-varying behavior of the access impedance behavior of the electric power grid, since they consider a single impedance value and assume that the impedance of the PLC transceiver is 50 Ω.

In such scenario, the investigation of non-adaptive and adaptive PLC coupling circuit plays a vital role for understanding coupling between PLC transceiver and the electric power grid, and improving the maximum power transfer and, as a consequence, the signal to noise ratio (SNR) at the receiver side.

1.1 OBJECTIVES

Regarding the aforementioned motivations, the main objectives of this dissertation are as follows:

1. To present a comprehensive review of PLC coupling circuits, which are required for narrowband and broadband PLC transceivers. In Chapter 2, the discussion of important issues related to the design of PLC coupling circuits, such as PCB design, insertion loss and return loss, galvanic isolation, impedance matching, analog filtering, protection and performance due to the type of components, costs and complexities, are addressed. We also provided a classification of couplings which considers the type of physical coupling (capacitive, inductive, resistive and antenna), the voltage levels (HV, MV and LV), the type of voltage (alternating current (AC) or direct current (DC)), the frequency band (narrowband and broadband), the type of signal propagation (common mode (CM) or differential mode (DM)) and the number of connections.

2. To describe the designs and prototype non-adaptive capacitive, SISO and LV PLC coupling circuits that cover narrowband frequency (9 kHz to 500 kHz) and broadband frequency (1.7 MHz to 50 MHz, 1.7 MHz to 100 MHz and 1.7 MHz to 500 MHz). The Chapter 4 discusses the prototypes of the designed PLC coupling circuits, which ones can be easily reproduced and used to interface with any PLC transceiver and it shows the results obtained by measuring their scattering parameters.

3. To discuss measurement, characterization, and analysis of access impedance of electric power grid in some urban, suburban and farm residences in the frequency band of 1.7-500 MHz. Also, present a statistical model of the access measured impedance. The measurement investigates the resistance and reactance part of the access impedance on in-home, broadband and LV electric power grid. The setup used to perform the measurements consists of a vector network analyzer (VNA) instrument and a PLC coupling circuit, which is used as an

interface between the VNA instrument and the outlet. The Chapter 3 outlines a simple and straightforward procedure to obtain a statistical model of the access impedance in the frequency domain. Finally, statistical analysis of the data set of measured access impedances, which was obtained with the measurement campaign, is performed.

4. To propose an adaptive PLC coupling circuit which its input impedance is designed according to the impedance measurement campaign. This Chapter 5 proposes a PLC coupling circuit for impedance matching using an adaptive concept switching analog filters with different input impedances. The proposed PLC coupling circuit is designed using RF Switch which is controlled by a control circuit composed of a microcontroller and a logarithmic amplifier, responsible for the conversion of the signal level from the PLC transceiver. This control circuit provides a reference voltage level to the ADC input port of the microcontroller, to choose the analog filter that best matches the impedance with the electric power grid. A highlight of the PLC coupling circuit is that it can work properly under fairly harsh environments e.g., high current and time and frequency varying impedance on in-home and LV electric power grid.

1.2 THESIS OUTLINE

This thesis is organized as follows:

Chapter 2 presents a review of PLC coupling circuit design, describing in details a useful classification of PLC couplers, such as high-pass and low-pass filters, impedance matching, PCB design, insertion loss (scattering parameters S_{12} and S_{21}) and return loss (scattering parameters S_{11} and S_{22}), galvanic isolation, the behavior of components, like inductor and capacitor, in high-frequency and efficient electrical protection against surges. In addition, it is proposed a classification of couplers according to the following characteristics: based on the types of physical connection (capacitive, inductive, resistive and antenna coupling), voltage level (HV, MV and LV), type of voltage (AC or DC), frequency band, propagation mode and number of connections. The importance of literature review is to evaluate relevant articles research limitations and future research recommendation, collect more information about their research topic, find the relevant research methods, instruments, survey questionnaire, provide supporting proof, precedent for an argument and claim capture what literature was reviewed.

Chapter 4 addresses the designs and specifications of the non-adaptive, capacitive, SISO and LV PLC coupling circuit designed for a narrowband frequency of 9-500 kHz and for broadband frequencies of 1.7-50 MHz, 1.7-100 MHz and 1.7-500 MHz, as well as, reporting results of the insertion and return loss curves. Important issues in designing a PLC coupling circuit such as the PCB, types of components and protection devices are detailed. The analog filters of all prototypes were designed using the Advanced Design System (ADS) Software [11].

Chapter 3 focuses on measurement, characterization, modeling, and analysis of access impedance in several in-home, broadband, and LV Brazilian electric power grid. Moreover, it discusses the measurement setup and campaign of the access impedances of electric power grid covering the frequency band between 2-500 MHz. A statistical analysis of the access impedance is shown and the results are important to design PLC coupling circuits knowing the typical access impedances values of the electric power grid.

The so-called adaptive broadband, SISO, capacitive and LV PLC coupling circuit is presented in Chapter 5 and stated important results and discussions about this kind of impedance matching between adaptive and non-adaptive PLC coupling circuit and the electric power grid for Brazilian in-home scenarios.

Chapter 6 addresses the main conclusions of this thesis.

1.3 SUMMARY

This Chapter presents, in a simplified way, the objectives and organization of the present thesis.

2 COUPLING FOR POWER LINE COMMUNICATIONS: A SURVEY

The use of power cables for data communication purposes, known as PLC, dated back to the early 1910s when Major George Squier of US Army demonstrated the transmission of analog voice signals (multiple telephony channels) over a pair of power cables to support the operation of distribution power systems by electric utilities. At that time, this type of analog data transmission was called wired wireless [12]. The period from 1910 to 1930 was characterized by the introduction of some technologies which involve the transmission of telephone signals through power cables.

The PLC has since moved from the little-known technology in the 30s to a competitive technology of the 21st century. As a consequence, coupling issues have become more relevant. Essentially, couplers are devices which inject data signals into electric power cables. These power cables could be AC or DC power lines and the signals of PLC transceivers are subsequently coupled to them via a coupling circuit. In the case of power lines used to transmit AC power, the coupling circuit has also to filter out the AC mains signal. On the other hand, the coupling circuit simply has to block the DC mains voltage of the DC electric power grid.

During the late 1970s and early 1980s, new investigations to characterize electric power grid as a medium for data communication showed a higher potential in the range of frequencies between 5 kHz and 500 kHz [13]. Some years later, it was demonstrated that, given some constraints (transmission power and distance), the frequency range from 9 kHz to 30 MHz could be used [14]. Currently, there are research and development efforts focusing on the use of electric power grid in the frequency band between 0 and 500 MHz.

Moreover, PLC systems can be distinguished based on two classes of frequencies: narrowband and broadband. Usually, narrowband PLC refers to data communication over the frequency band between 0 and 500 kHz [15]. On the other hand, broadband PLC covers the frequency band between 1.7 MHz and 500 MHz and high-speed data rate [16–18].

It is important to mention that the main focus on PLC technologies is to provide data communication over AC and DC electric power grid. The use of PLC technologies over the DC bus in distributed energy generation, airplanes, automobiles and trains reduce wiring complexity, weight, space requirement and ultimately installation cost of telecommunication infrastructures. Thus, the PLC technologies eliminate the need for extra wires dedicated to data communication, which, for instance, reduces the weight of the vehicle and prevent problems when passing wires through dashboard and instrumentation panels. They also decrease cost and complexity of cable connectors and raise the benefit-cost ratio to any new device requiring extra wiring [19]. Therefore, the investigation of low-cost couplings is of utmost importance for such kind of environments.

Electric power systems have the advantage of being a ubiquitous infrastructure [20]. Also, no changes in the installed power cables infrastructure are necessary to implement the PLC system. As a result, the payback can be quicker with reduced capital expenditures. PLC networks can be used as a backbone of data communication networks and considered as a technology for replacing, completing, serving or interconnecting with other data networks. The cost of PLC systems is moderate for long-term purposes, especially when compared to the conventional data network systems. For example, the replacements of these power cables are not comparable in cost with the replacement of the conventional data communication system devices such as cables, switches and outlets [21].

Reviewing the literature about PLC technologies, measurement [22, 23], characterization [24] and modeling, as well as the development of techniques to improve the performance of PLC systems at the physical and link layers [25–28], there are a number of technical contributions providing understanding into how PLC systems work and pointing out challenging issues related to the advancement of the PLC technology. Although there are a plethora of literature on the general PLC systems, a similar volume is currently not available for coupling techniques in PLC systems. Hence, the relevance of this survey.

In the literature, antenna coupling was the first type of coupling used with the electric power grid due to its simplicity, cost and easy installation. However, impedance mismatching with the power cables, which reduces the transfer of energy between the power cable and the antenna, motivated investigations which resulted in the introduction of capacitive couplers [12, 29]. It is interesting to note that one century later, researchers are reinvestigating the use of antennas to introduce the so-called PLC

wireless system [30, 31]. In the sequel, inductive coupling was introduced. Due to the characteristics of inductive couplings such as electromagnetic isolation between the power cable and the PLC transceiver, they have been successfully applied in Medium-Voltage-based (MV) PLC systems since it is possible to install them to the live power line. On the other hand, their usage in electric power systems Low-Voltage (LV) was not widely adopted due to the high insertion loss. For LV levels, capacitive coupling is common due to its low cost and simplicity. Most recently, resistive PLC couplers have gained some interest due to their low cost and simple circuitry features [32].

Above all, coupling is a very important issue in PLC systems. Since the dynamism of electric power systems at HV, MV and LV levels and, as a consequence, the lack of perfect impedance matching at the point of connection with the PLC transceiver both in the time and frequency domains may result in remarkable insertion loss and signal distortion [33].

In this context, this Chapter aims to present a comprehensive review on coupling for PLC systems. With this in mind, we first discuss important issues related to the design of PLC couplers, such as PCB design, insertion loss and return loss, galvanic isolation, impedance matching, analog filtering, protection and performance due to the type of components, costs and complexities. Second, we present a classification of couplings which considers the type of physical coupling (capacitive, inductive, resistive and antenna), the voltage levels (HV, MV and LV), the type of voltage (AC or DC), the frequency band (narrowband and broadband), the type of signal propagation (CM or DM) and the number of connections. Additionally, we highlight future tendencies and critical issues which must be pursued to introduce PLC couplers which will comply with the constraints imposed by the electric power systems and fulfill the needs and demands associated with the novel generation of PLC systems.

The remaining parts of this chapter are organized as follows: Section 2.1 briefly and concisely addresses the main issues for designing PLC couplers; Section 2.2 discusses a classification of PLC couplers based on a comprehensive review of this subject; Section 2.3 highlights open problems and future trends for advancing the design of PLC coupling devices.

2.1 DESIGN OF A PLC COUPLER: IMPORTANT ISSUES

The coupling of PLC transceivers with electric power grid is considered to be a difficult task to be accomplished mainly because the access impedance (impedance

at the point of connection) changes with frequency and time due to the dynamism of loads connected to electric power grid. Also, the low impedance of power cables, which is desired for reducing technical losses associated with the energy delivery, yields a problem because the usual coupling devices are designed to have access impedance equal to 50 Ω or 75 Ω.

The design of a PLC coupler considering impedance matching, flat frequency response to minimize distortions, efficient electrical protection against transients and low cost have been the major challenges in recent years. To carry out such design, several issues must be addressed in order to come up with a PLC coupler which may be useful for the target application. In this context, it is necessary to understand all main issues which must be taken into account to correctly design a PCB, such as measuring S scattering parameters for quantifying insertion and return losses, providing galvanic isolation, dealing with impedance matching, designing the analog filters with passive components and choosing the appropriate electric protection scheme. These relevant issues are briefly described in the following subsections.

2.1.1 PRINTED CIRCUIT BOARD DESIGN

The electrical characteristics of the PCB used to physically assemble the components of the coupling device significantly impact on the coupling performance [34]. In [35], the author showed that the transmission line properties of signal traces in the PCB considerably changes when multiple circuits or components are connected to a given signal trace. Characteristics such as impedance mismatching and skin effect usually result in an increase of the conductor impedance as the frequency rises.

Moreover, as frequency increases, parasitic elements may impact the design of the PCB of PLC couplers and their modeling for circuit simulation and design become relevant [36]. In a high-frequency circuit, it is simple to visualize how a long thin track of a PCB will behave as an inductor, a large pad over a ground plan will behave as a capacitor and performance degradation may occur due to the crosstalk among tracks [37]. In [38], the authors discussed the impedance mismatching in the connections among tracks, capacitors, pathways, stubs, and welds.

In [20], high-frequency transmission line effects were studied and a fundamental concept called electrically long trace was defined. If a distance from transmitter to receiver exceeds $\lambda/20$, where λ is the wavelength in meters or terminates the transmission line in its characteristic impedance when the one-way propagation delay

of the PCB track is equal to or greater than one-half the applied signal rise/fall time, then the PCB should be treated as a transmission line and a routing topology should be created to match the trace impedance of a PCB. To match impedance line in a PCB, several techniques are available for designing a transmission line structure. There are two techniques which are most frequently used to control trace impedance, stripline, and microstrip. In stripline, the transmission lines exist on internal routing layers and require a minimum of 3 board layers (2 ground planes and a routing layer). The insulating material of the substrate forms a dielectric. The width of the strip, the thickness of the substrate and the relative permittivity of the substrate determine the characteristic impedance of the strip, which is a transmission line. The use of microstrips is a popular method used to provide controlled trace impedance when microwave frequency is taken into account. Microstrip lines are exposed to both air and dielectric material referenced to the planar structure. Fig. 1 shows a microstrip transmission line structure, where T is the thickness of the track, W is the width of the track and h is the distance between signal track and the reference plane.

The stripline technique has the advantage of greater isolation of transmission lines and bandwidth, resulting in lower radiation loss. Although better isolation and good electromagnetic shielding can be achieved, the stripline technique has the disadvantage of complexity and cost in its fabrication, as tuning or troubleshooting is complex and stripline trace width is smaller compared to a microstrip line of same impedance and height. Microstrip has the advantage of less dielectric losses (when using identical materials), being cheaper and presenting easier debugging due to the location of traces on the top and bottom layers [39].

Characteristic impedance Z_0 of microstrip is also a function of the ratio of the height to the width W/h (and the ratio of width to height h/W) of the transmission line. The characteristic impedance Z_0 of a microstrip is calculated by [40]

$$Z_0 = \left(\frac{87}{\sqrt{\varepsilon_r + 1.41}}\right) \ln\left(\frac{5.98h}{0.8W + T}\right) \Omega \qquad \text{for} \quad 15 < \text{W} < 25 \text{ mils} \tag{2.1}$$

or

$$Z_0 = \left(\frac{79}{\sqrt{\varepsilon_r + 1.41}}\right) \ln\left(\frac{5.98h}{0.8W + T}\right) \Omega \qquad \text{for} \quad 5 < \text{W} < 15 \text{ mils}, \tag{2.2}$$

where ε_r denotes the dielectric constant of the PCB material.

To implement a ground plane, one side of a double-sided PCB is made of continuous copper plate and used as ground. The theory behind it is that the larger the amount of metal, the lower the attained resistance. An analytical method for characterizing

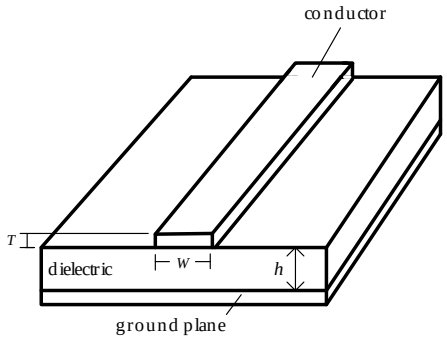

Figure 1: A PCB microstrip transmission line.

the impedance behavior of the ground planes in the frequency domain is presented in [41]. The importance of maintaining a large area of low-impedance ground plane is critical to all analog circuits today. The ground plane not only acts as a low impedance return path for decoupling high-frequency currents but also minimizes electromagnetic interference (EMI) emissions [42].

To make full use of PLC couplers for data communication purposes or in order to analyze the impedance matching, it is important to know how signals propagate on a PCB to obtain low insertion loss in a microstrip transmission line.

2.1.2 INSERTION LOSS AND RETURN LOSS

Assuming that the two ports use the same reference impedance the insertion loss (I_L) is the magnitude of the S_{21} scattering parameter, given (in dB) by:

$$I_L(dB) = -20\log_{10}|S_{21}|, \tag{2.3}$$

where S_{21} represents the voltage gain from Port 1 to Port 2 [43], which is often used to show the frequency response of passive circuit which is supposed to be linear and time-invariant [44]. The Insertion Loss is defined as the drop in power as a signal enters in the two-port networks. This value not only includes the reflected incoming signal but also the attenuation of the component and it is the ratio between output power and input power [45].

The return loss (R_L) is the magnitude of the S_{11} scattering parameter, which represents the reflection coefficient because it describes what fraction of an incident wave is reflected back to the input port. In other words, the S_{11} scattering parameter is a measure of how close the source and input impedances are matched. The R_L given

(in dB) by

$$R_L(dB) = -20\log_{10}|S_{11}|\,. \tag{2.4}$$

In order to measure S_{12} and S_{11} scattering parameters, the impedances of a VNA are matched to 50 Ω, the passive PLC coupler is considered as a two-port network and, as a consequence, we characterize it through its scattering matrix, as shown in Fig. 2 [46]. In Fig. 2, the $Z_{network}$ represents the impedance of the electric power network at the connection point, Γ_{in} and Γ_{out} represent the reflection coefficients of PLC coupler and $Z_{network}$, respectively. Finally, Z_2 represents the impedance of port 2 - 2' of the PLC coupler. With knowledge of the scattering parameters, we can completely characterize PLC coupler and precisely quantify the distortion introduced by the PLC coupler in the transmitted signal.

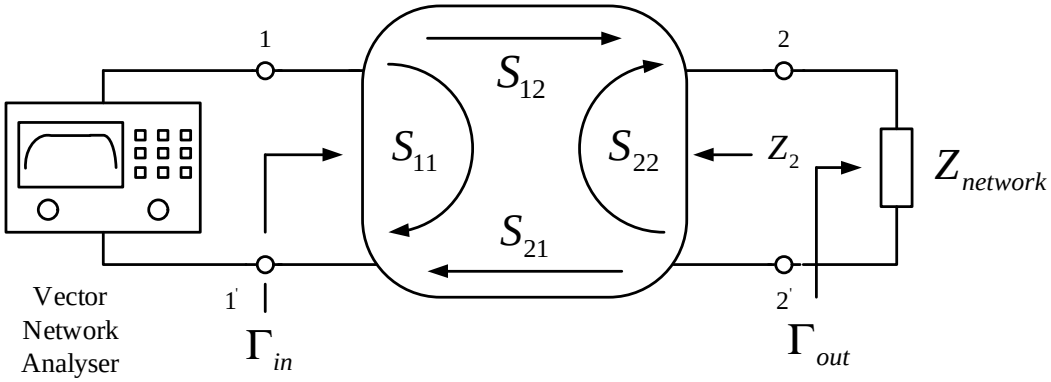

Figure 2: Measurement of scattering parameters.

2.1.3 GALVANIC ISOLATION

Galvanic isolation is usually necessary when two or more electric circuits are connected, but their grounds may be at different potentials. Also, it is an effective approach for breaking ground loops by preventing undesirable current flowing between two distinct circuits sharing a ground conductor. Moreover, it protects transceiver circuits and people from shocks and short circuits. Regarding the PLC coupler, a RF transformer is normally responsible for the galvanic isolation [26] between the transceiver and the power line. Also, as discussed in [27, 41, 47], it can be applied to impedance matching purposes through the transformation ratio 1:N between the primary and secondary windings of the transformer, where N denotes the turns ratio of secondary to the primary windings.

In [45], it was shown that an RF transformer has some non-ideal characteristic properties which must be observed, such as the maximum magnetic flux density in the

core to avoid non-linear effects, frequency band specification, impedance levels/winding ratio, maximum voltage levels, maximum power and currents, skin effect, number of strands, number of turns, leakage inductance, enlarging of leakage inductance, magnetizing inductance and distortion of signal in secondary winding.

In [48], a model of an RF transformer was proposed and analyzed by Kazimierczuk. Fig. 3 depicts such model. It consists of ideal transformer, magnetizing inductance L_M, core-loss shunt resistance R_C, leakage inductances L_{lP} and L_{lS}, winding resistances R_P and R_S and stray capacitances C_P and C_S. The stray capacitances model the effect of turn-to-turn capacitance, layer-to-layer capacitance, winding-to-winding capacitance, winding-to-core capacitance, winding-to-shield capacitance, core-to-shield capacitance and the capacitance between the outer winding and surrounding circuitry [47, 49–51].

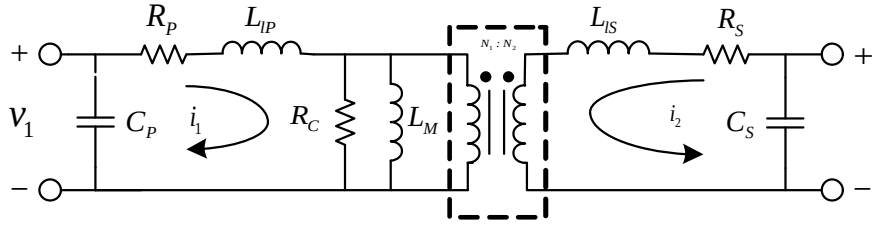

Figure 3: Model of RF Transformer.

In order to determine the bandwidth of an RF transformer, low frequency and high frequency are analyzed. For a low frequency of an RF transformer, the magnetizing impedance is calculated by $j\omega L_m \backslash\backslash R_C$. The values of L_M and R_C are determined by the core material and the cut-off frequency can be calculated by the core material with high relative permeability. High-frequency cut-off is attributed to intra-winding capacitance (C_P, C_S) and series leakage inductance (L_{lP},L_{lS}), core and conductor losses (R_P,R_S). To achieve a high value of frequency, the stray capacitance (C_P, C_S) and leakage inductance (L_{lP},L_{lS}) should be reduced.

2.1.4 IMPEDANCE MATCHING

The impedance matching between the PLC coupler and the power cable at the connection point is a challenging task to be accomplished due to the time-frequency varying nature of the loads connected to electric power grid [8, 52, 53]. Due to the wide range of values that the impedance at the connector point (access impedance) can assume when the frequency and time vary [54–56], it definitely must be brought to the center of discussion when designing a PLC coupler. In fact, the lack of impedance matching may considerably reduce the transmission power [6,57–62] even though impedance matching

is ensured within the PCB of the PLC coupler.

Impedance matching techniques for narrowband PLC couplers were proposed in [62, 63]. The impedance matching technique based on the change of the tap of an RF transformer was outlined in [64]. In [65] the authors described a technique for measuring the impedance at the connection point of an electric power grid to feed a microcontroller, which is capable of switching a bank of capacitors [66] aiming to eliminate the reactive component of the access impedance. The complexity of this technique increases along with the number of capacitors in the bank. Moreover, the variation step of the impedance depends on the number of branches of the bank of capacitors. Then, [62, 67, 68] proposed a new circuit, which is capable of adapting the impedance, changing the series inductance and the turns ratio of the RF transformer. Transformerless coupling circuits and impedance adaptation for narrowband PLC, with a view of simplifying the design and minimizing costs of a PLC transceiver, were discussed in [10, 69].

Impedance matching techniques for broadband PLC were discussed in [70, 71]. These works addressed an optimization method to calculate the values of the parameters of 5^{th} order band-pass filters for matching the access impedance. Moreover, [62] focused on another design method which is capable of offering an optimization procedure to synthesize broadband impedance matching circuits for the equalization of the power transfer gain in a wide frequency band. The method is based on a parametric representation of the driving impedance of the broadband impedance matching circuit, which is optimized by means of a meta particle swarm optimization method [72].

Impedance matching to improve the maximum power transfer of transmission/reception of the signal into/from power line cable becomes an important and challenging issue. Different designs of impedance matching circuit have been studied in the literature. Frequency and time dependencies of access impedance, which renders adaptive matching circuits to be developed, are the major challenge of PLC coupler.

2.1.5 ANALOG FILTERING

In a typical PLC coupler design, analog filtering is performed by a cascade of a high-pass filter and a low-pass filter, in this order, and their combination results in a passband filter. The design of an equivalent passband filter is not recommended because the purposes of designing the high-pass and low-pass filters are totally different. In fact, the former aims to block the high power mains signal [73], while the latter limits the

upper edge of frequency bandwidth to comply with the analog-to-digital conversion [74]. Fig. 4 shows a typical capacitive SISO PLC coupler, where T_1 is an RF transformer, C_{BLOCK} is a high-pass filter and L_1, L_2, C_1 up to C_5 constitute a low-pass filter.

The design of the high-pass filter is very simple because it is realized with a capacitor with a reasonable working voltage and a self-resonant frequency higher than the maximum mains frequency. On the order hand, the low-pass filter is more sophisticated and can be realized with a Butterworth, Chebyshev or an elliptic filter. Usually, the choice is in favor of an elliptic filter due to the sharpness of its frequency response [75–78]. However, a careful analysis of the low-pass filter must be carried out when multi-carrier scheme based on discrete Fourier Transform (DFT) is used because it can increase the effective delay spread of the channel between the digital-to-analog converter (DAC) of the transmitter and the ADC of the receiver. Moreover, a practical approach for reducing the order of a low-pass filter is to concatenate a low-order high-pass filter (less selective) with a 2nd or 3rd order notch filter with notch frequency located in the stopband. Additionally, the analog filter can be used to mitigate interference from radio signals (AM, FM and TV) [79, 80]. The order of the analog filter can be determined by the designer according to the desired selectivity, keeping in mind that the insertion loss increases along with it. Therefore, a rule of thumbs is to keep the analog filter order below or equal to six.

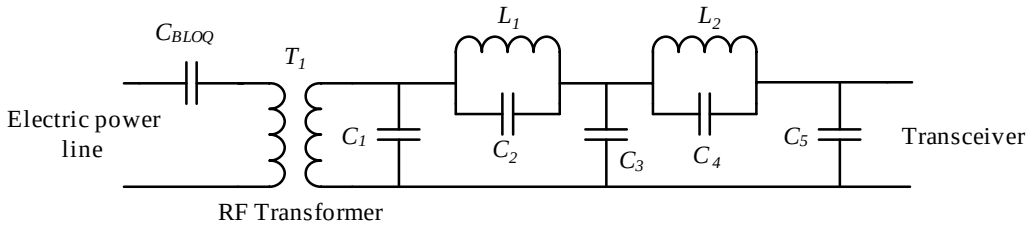

Figure 4: Circuit of a capacitive PLC coupler.

2.1.6 ELECTRIC PROTECTION

All telecommunication technologies are bound to comply with electromagnetic compliance (EMC) standards, whose requirements depend on the environment [81, 82]. The PLC coupling circuit, which is physically connected to power cables, is occasionally subjected to significant high voltage and current transients and, as a consequence, damages to the circuits of the PLC transceiver may happen [83, 84]. For instance, in HV and MV, a strong current pulse of short rise time is created when a distribution transformer fails due to a short circuit or when power cables fall to the ground (high

impedance faults) or touch each other. Similarly, a lightning strike near the power cable yields a traveling wave that may destroy the PLC transceiver.

With this in mind, SPD attempt to limit the voltage supplied to an electric device by either blocking or shorting to ground any unwanted voltages above a safe threshold. An SPD must simultaneously provide low insertion loss in all operating frequency band and adequate surge protection in all ports of the PLC coupler. The SPD must not interfere with the frequency spectrum of the transmitted signal. Typical SPD used in PLC couplers are MOV, Zener diodes, high-speed switching diodes and GDT.

In [85], a surge protection circuit for HV-based PLC systems was proposed aiming to achieve protection against an induced surge in one conductor of the transmission line, to offer protection against a common mode surge induced in both conductors of the transmission line and to yield protection against the potential rise of the earth conductor during an occurrence of high surge current through the earth conductor.

The authors of [86] analyzed the influence of capacitance of an MOV on the insertion loss of a PLC coupler. Although the capacitance characteristics of an MOV and diodes, such as Zener and high-speed switching diodes [6], may cause distortion in the frequency response (S_{12} or S_{21} scattering parameter) of PLC couplers, their usage is widely adopted because the cost-benefit is the best available. In order to avoid the disturbing effect of MOVs, GDTs can replace them in PLC couplers designed to operate at frequencies above 35 MHz. Regarding the frequency band between 1.7 and 100 MHz, Fig. 5 shows the effect of an MOV and Zener diode working together in concatenated way on the frequency response magnitude of a PLC coupler in comparison with a GDT. It is important to mention that the majority of studies and simulations of SPD effect covers the frequencies up to 30 MHz [87]. However, nothing has been discussed in the literature about its protection efficiency capabilities and its impact on the signal distortion at the frequencies higher than 30 MHz. Furthermore, the use of transient voltage surge protection (TVSP) [88] can also be investigated to replace Zener diodes or high-speed switching diodes for frequencies above 35 MHz in PLC coupler.

Fig. 6 shows a typical protection for inductive and capacitive PLC coupler circuits. The capacitive coupler requires the use of MOV, fuse and Zener diodes to protect the transceiver circuit. The inductive coupler does the same by exploiting the limitations of the maximum magnetic flux density of the ferrite core to avoid spikes of current in the secondary windings and by concatenating high-speed switching diodes at the secondary windings of the ferrite core to limit the voltage. The use of MOV [89] and

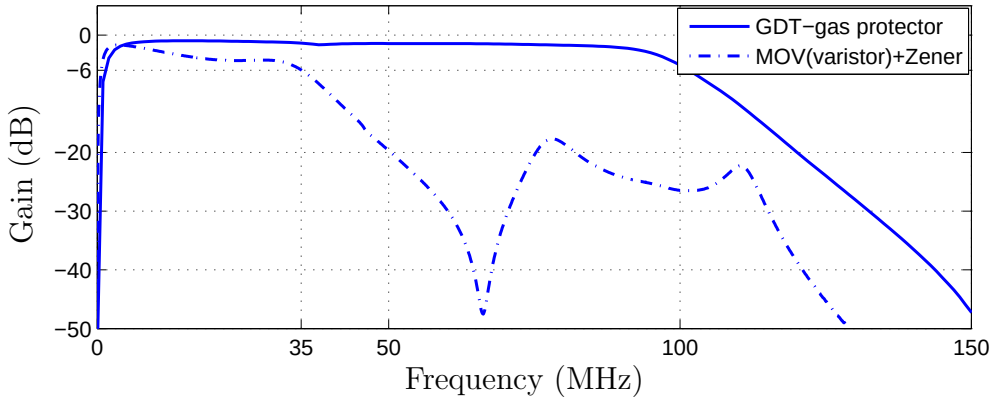

Figure 5: Distortion of frequency response magnitude of a capacitive and low voltage PLC coupler in the frequency band 1.7 - 100 MHz due to the use of different types of protective circuit.

diodes for protection purposes needs to be analyzed based on the operating frequency of the PLC system and the voltage level of the mains signal in the electric power line.

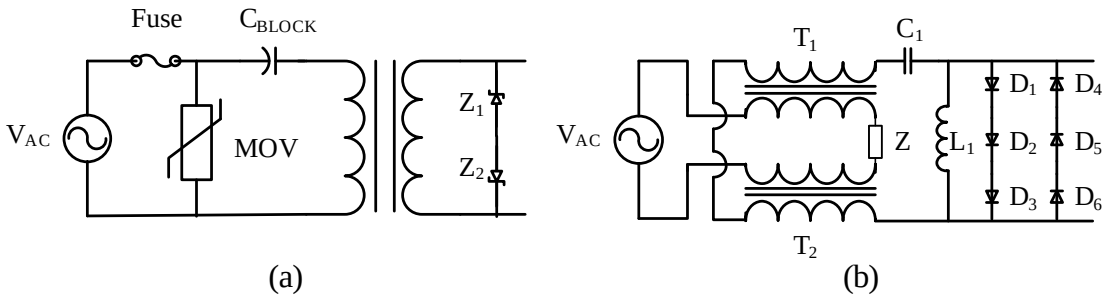

Figure 6: Typical protection circuit for PLC coupler. (a) Capacitive coupler and (b) Inductive Coupler.

2.1.7 COMPONENTS

Due to cost and size, the components used in a PLC coupler circuit are passive (resistors, capacitors, transformers, and inductors). Therefore, particular attention must be paid to the self resonant frequency (SRF) frequency of inductors and capacitors as well as to the frequency response of the transformer. Additionally, the behavior of other components due to the chosen operating frequency of the PLC system needs to be carefully taken into account, especially at high frequencies [90], as the skin effect, i.e. the increase in the apparent resistance of a wire along with the frequency, becomes more relevant. If a voltage is maintained at a constant DC level, current flow will be uniform throughout the area of the wire. However, as the frequency increases, the magnetic field near the center of the wire increases the local reactance. The charge carriers then move towards the edge of the wire, decreasing the effective area and increasing the

apparent resistance of the inductor winding [91, 92], capacitor [93], and resistor.

In fact, at high frequencies, the physical length, width and height of components, the properties of the conductors and dielectrics, as well as the types of electrodes for attachment to external circuits have influence on the performance of a PLC coupler circuit. Fig. 7 shows high-frequency lumped circuit models for a resistor, a capacitor and an inductor. Note that the additional capacitance due to the attached electrodes is usually included in the nominal value of the capacitance. Despite the parasitic resistances and reactances, attaching devices on a PCB can introduce significant additional capacitance to the body of the component [49]. This capacitance and the added inductance of the pads and traces, which are used to attach a component and are typically considered part of the circuit, affect the frequency response and impedance matching of a PLC coupler. In the design of PLC the coupler for broadband data communication, it is important to take it into account.

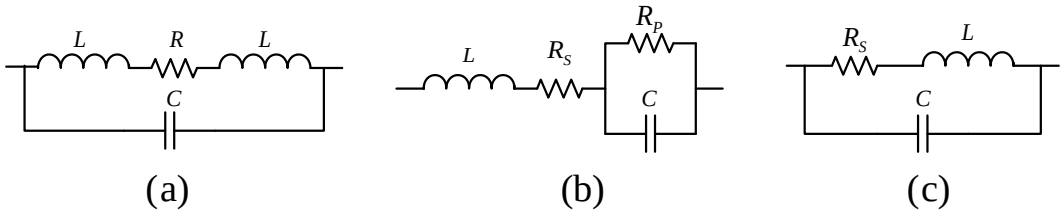

Figure 7: Equivalent circuit for RF model. (a) Resistor, (b) Capacitor and (c) Inductor.

2.1.8 COST AND COMPLEXITY

The main advantages of the PLC technology are the use of electric power system infrastructures for costs and expenditures reduction and the easy deployment of new telecommunication networks over such infrastructure [94]. Regarding HV and MV PLC couplers, some care must be taken into account due to the complexity of the coupler construction, which may increase costs due to the isolation need at these voltages levels. Moreover, PLC coupler designers must pay particular attention to the external environment which is subject to rain, snow and lightning on the power cable [95]. Due to these constraints and environment issues, the cost of the capacitive coupler is very high and high at HV and MV, respectively. Due to saturation of magnetic flux inside the core and the cost to handle it, inductive coupling is only used at MV and LV. Moreover, at LV, PLC couplers are constructed at a relatively low cost. Usually, a PLC capacitive coupler requires low complexity and cost since the components are available commercially. In [69], a PLC coupler without transformer was proposed for

eliminating this costly component, while maintaining impedance matching with the electric power grid. Overall, complexity and cost of a PLC coupler increase along with voltage levels and bandwidth. Also, they increase when perfect impedance matching is mandatory.

2.2 CLASSIFICATION OF PLC COUPLERS

In general, PLC couplers can be grouped according to different criteria. In this sense, this work outlines a classification based on the type of physical couplings, voltage levels, frequency bandwidths, propagation modes and numbers of connections.

2.2.1 BASED ON THE TYPE OF PHYSICAL CONNECTION

Based on the type of physical connection, the coupling can be capacitive, inductive, resistive and by an antenna. Note that the antenna could be seen as a kind of inductive coupling, but we prefer to keep it separate because its mechanical construction is totally different.

2.2.1.1 CAPACITIVE

Capacitive coupling is the serial insertion of one or more capacitors in direct contact with the power cable. It offers low impedance path to the high-frequency components of the power line signal and, at the same time, it blocks the mains signal by presenting a high impedance to it. Among the four types of PLC couplers, it has the lowest insertion loss, thus ensuring the highest power transfer [96]. As shown in Fig. 8, there are two types of capacitive coupler: (a) one with a transformer to provide galvanic isolation (T_1) and to limit transients based on the core saturation; (b) and one without transformer, which is a low-cost option with the disadvantage of not providing galvanic isolation. While the use of capacitive coupling with transformer is strongly recommended in AC electric circuits, mainly when the voltage amplitude of the mains signal increases, the use of capacitive coupler may also be useful for DC buses [97, 98] in which the voltage level is low, such as in-vehicle [99], ships and spacecraft environments. In [100], the author proposed a capacitive coupler to operate in low-voltage DC electric power grid when the frequency bandwidth is between 1 MHz and 30 MHz and the voltage level of mains signal is up to 750 V_{DC}.

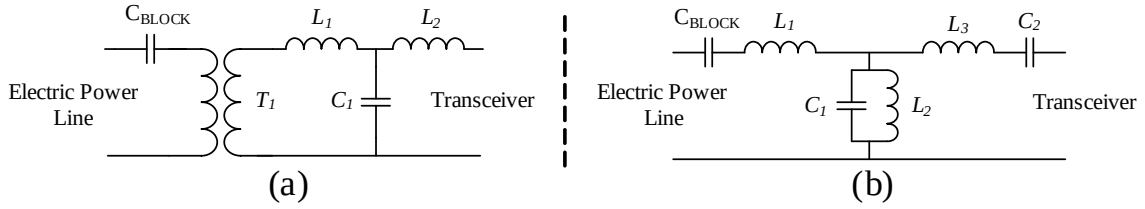

Figure 8: Equivalent circuit for a capacitive PLC coupler. (a) Coupling with galvanic isolation and (b) Transformerless coupling.

2.2.1.2 INDUCTIVE

The inductive PLC coupler can be accomplished with (series inductive coupling) or without (shunt inductive coupling) galvanic isolation to the power cable [101]. In the inductive PLC coupler, electric current flows through the winding coil and yields an electromagnetic field which inductively loads the signal into the conductor, as showed in Fig. 9, where T_1 and T_2 are inductive couplers. Structurally, it consists of a magnetic core with gaps and the output coil is connected to the transceiver, both of which are wound around the core. Its installation does not require lockout of the electric power grid because there is no electric connection between power cables and the PLC coupler.

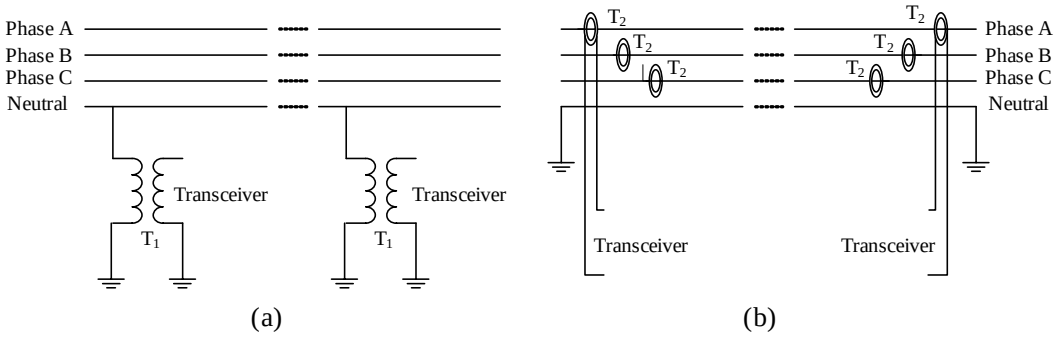

Figure 9: (a) Serial inductive coupler and (b) Shunt inductive coupler.

In inductive PLC couplers, the mains current can flow unlimited through the magnetic core clamped over the wires as shown in [102]. Toroidal transformers typically have copper wire wrapped around a toroidal core so that the magnetic flux remains trapped in the coil and does not leak out. The properties of toroidal core current transformers, such as maximum transmissible primary current, amplitude, phase error as well as linearity, are basically determined by the material used in the core [103]. High magnetic coupling coefficient values are desirable in inductive couplers for offering low insertion loss and return loss, as well as for covering wide frequency bandwidth.

In [104], insertion losses of inductive couplers based on Rogowski coil and a conventional (ferrite based) inductive coupler were compared. The authors measured the variation of insertion loss response of an inductive coupler in high current test in the frequency range of 1.7 MHz and 40 MHz. The performance of couplers based on Rogowski coil is stable because the relative permeability of an implemented coupler is very low and it is not saturated according to an increase of current.

The inductive coupling offers many degrees of freedom for system design by varying geometric parameters to tune parasitic elements, such as the crossover capacitance between the spirals, the magnetic coupling coefficient, inductance ratio and impedance terminations. The geometry and electromagnetic properties of coiled wire over the ferrite core result in a high impedance for high-frequency signals. In [105] was shown that the inductance of a choke depends not only on the geometry of the windings and the core but also on the permeability of the core material. The distributed capacitance between the winding turns acts as a shunt capacitor on the inductor resulting in the occurrence of resonance at a given frequency. Furthermore, the inductive PLC coupler shows good performance in low impedance power cable and yields low energy radiation [106]. The coupling efficiency varies according to distinct factors such as the shape and magnetic characteristics of the magnetic core, the length of the gaps and the characteristic impedance of power cable [106].

It is important to emphasize that the nonlinearity of the magnetic material together with the magneto-motive force rising from zero to a maximum, twice each cycle of the mains signal, causes distortions, such as amplitude modulation of the transmitted and received signals.

2.2.1.3 RESISTIVE

The resistive coupler is constituted by a voltage divider, a bandpass filter and an amplifier. The voltage divider drops the voltage signal from the power cable and, in the following, the bandpass filter attenuates the out of band signals. Finally, the amplifier boosts the voltage signal amplitude for a further analog-to-digital conversion. Theoretically, injection and extraction of signals into/from the power cable are possible; however, only the extraction of the signal seems to be practicable. For instance, [32] proposed a circuit for a resistive coupler, see Fig. 10. As we can see, it is constituted by a voltage divider, a buffer, a band-pass filter and an amplifier. Due to its nature, the resistive PLC coupler may be suitable for coupling narrowband PLC system in

low-voltage electric power grid.

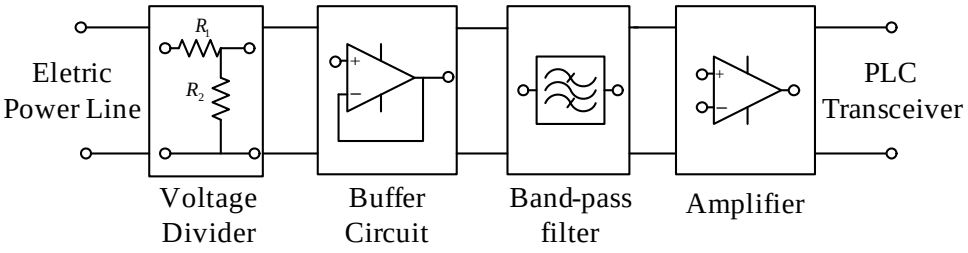

Figure 10: The block diagram of the resistive PLC coupler.

2.2.1.4 ANTENNA

The first form of coupling PLC transceivers to power cables was based on an antenna due to its simplicity, low cost and easy installation and operation [29]. Fig. 11 shows a typical antenna coupling. These antennas were mounted below the power lines on the tower structure and the high-frequency carrier signal was induced in parallel with the power cable. The size of antennas exceeded 300 feet in length and was designed to the carrier frequency employed for voice communication [99]. However, coupling antennas are quite inefficient because there is a lot of power lost in the coupling with the electric power grid.

In 1921, AT&T began to develop the first PLC transceiver with an antenna coupling (analog modulation, simplex transmission and transmission power of 50 W) for voice signals communication, control, operation and maintenance of the distribution electric power system. However, problems such as impedance mismatching between the antenna and the power cable and the length of the antenna for working with the low frequencies motivated the development of capacitive and inductive couplers.

Currently, the use of antenna coupling is under investigation for broadband PLC to offer mobility to PLC users, introducing both PLC and wireless transceivers called hybrid PLC-wireless [31, 107, 108]. Furthermore, the power cable can be seen as an antenna for the propagation of RF signals, such as WiFi, [109–111] which can reduce the investment with cabling and repeaters. In [112], the authors characterized the LV power cable to use as an antenna to propagate RF signals in ultra-high-frequency (UHF). The range of tested frequencies in power cable extends to 550 MHz beyond the current IEEE 802.11g standard which has a center frequency of 2.45 GHz and an 80 MHz frequency bandwidth. It experimentally demonstrated that LV electric power grid can be used as an antenna in the UHF in the frequency range from 1 GHz to 3 GHz.

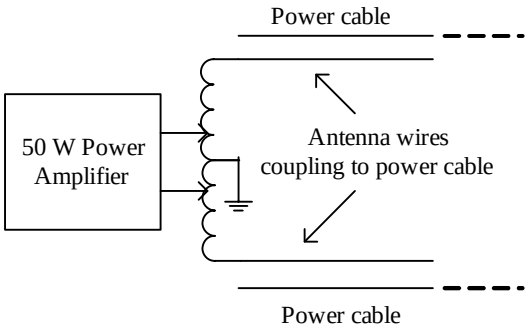

Figure 11: Equivalent circuit of antenna wires.

2.2.2 BASED ON VOLTAGE LEVEL

Regardless of the electric power grid to be AC or DC, the coupling can be classified according to their voltage level as follows [113]:

2.2.2.1 HIGH-VOLTAGE

The coupling capacitor is the most widely used component which enables the signal coupling to and from the HV power cable [114]. Standards have been established for ratings and tests power capacitor (i.e., isolation) which must be met by coupling capacitors in HV. The requirements and essential characteristics of capacitive coupling for HV have been standardized in ANSI C93.1 [115].

In [116], the author describes capacitive and SISO couplers for HV transmission lines designed for narrowband and broadband PLC transceivers between the phase conductor and the earth. Basically, there are two types of phase to ground narrowband resonant schemes for coupling. Fig. 12 shows the single-frequency and the two-frequency resonant circuits that implement such scheme.

The modeling approach and analysis of a component influence on the performance of a PLC transceiver show the behavior of complex coupling with many co-existing carrier frequencies are discussed in [117]. Also, it addressed the development and application of a PLC modem components, including single and double-frequency line traps, line tuning units, Coupling Capacitor Voltage Transformers (CCVTs), transmitters, receivers, balanced and skewed hybrids and signal level probes in a 115 kV transmission line.

The inductive coupling for HV transmission lines is more sensitive to HV fluctuations, impulsive noise, corona effects and voltage arcing between phases than capacitive

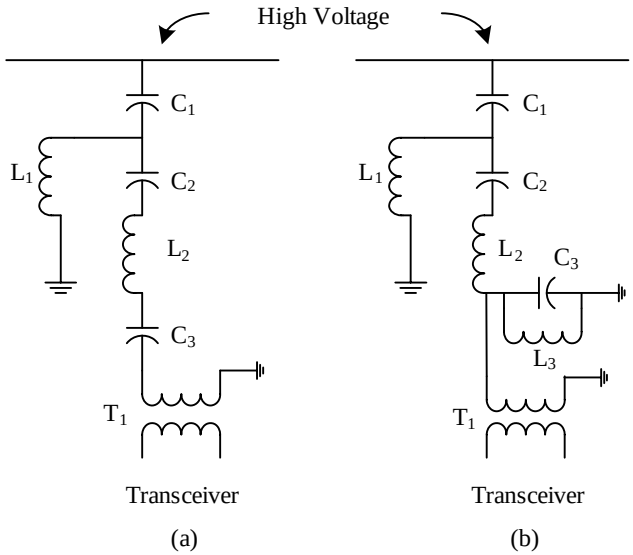

Figure 12: Typical coupling schemes for HV transmission lines. (a) Phase-to-ground coupled single frequency narrowband and (b) Phase-to-ground coupled two frequency narrowband.

coupling because it results in the saturation of the core [117]. Also, it provides more insertion loss than capacitive coupling. On the other hand, the greatest advantages of the inductive couplers, when compared to capacitive couplers, are: during installation, there is no interruption in the electricity supply, low cost of production and installation and the galvanic isolation among the HV transmission lines and the transceiver circuit [118]. The inductive coupling in HV transmission lines acts as an electrical protection. For instance, if there is an increase in electrical current in the HV transmission lines due to short-circuit or short discharges, the voltage is limited by the saturation of the magnetic flux inside the core of the inductive coupler, due to the saturation of the RF transformer core.

2.2.2.2 MEDIUM-VOLTAGE

In recent years, the idea of using the existing MV electric distribution grid as a medium for data communications became a reality. In fact, such infrastructure can be used to constitute data communication backbone to meet protection, metering, distribution, automation and control, by connecting several substations [119].

The MV coupler must withstand high differential voltages among phases and earth. As a consequence, it requires special components, which make these devices more expensive and more complex to implement than LV couplers but much less expensive than HV couplers. The requirements for the installation of capacitors in MV must also

follow the ANSI C93.1 [115].

Similar to HV PLC couplers, MV PLC couplers must be in compliance with the requirement of the utility and applicable regulation (e.g. insulation level of feeding cable, grounding, mechanical strength, lifetime and climatic category). In the case of switching the MV switchboard or in the case of short circuit, the MV PLC coupler must be able to support transient currents higher than 20 kA with no mechanical damage or change of frequency response not exceeding 1.5 dB [120].

In [121, 122], a capacitive SISO PLC coupler for broadband PLC was proposed. Fig. 13 shows a MV PLC coupler device which can work with voltage levels as high as 11 kV. In this proposal, the PLC coupler is connected to phases insulated from the power grid by line trap circuits. The line trap circuit is a parallel resonant circuit, mounted in-line on AC transmission power lines to prevent the transmission of high-frequency carrier signals of power line communication to unwanted destinations. It does not affect the low-frequency signal of the AC power line but offers a high impedance to the high-frequency signal of the PLC transceivers. Two RF transformers are used to achieve the desired isolation. The series combination of L_S and C_S form a band-pass filter to block the AC power line and present a low impedance for the signal of PLC transceivers. The resonant frequencies of the three circuits (L_S, C_S, L and C) are designed as the midband frequency of the PLC coupler. The MOV together with D_{Z1} and D_{Z2} (Zener diodes) are responsible for the electric protection.

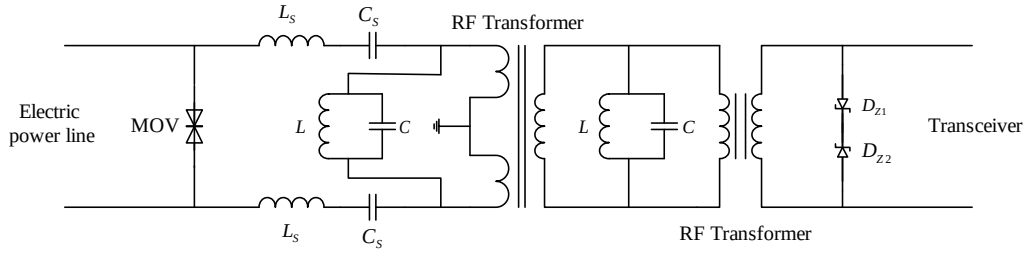

Figure 13: Typical capacitive coupling circuit for MV.

When the inductive PLC coupler comes to matter, there are two options available for installation: the inductive PLC coupler is clamped around a MV power cable, or the inductive PLC coupler is serially connected between the neutral line of the MV circuit and the ground wire if it is available [118]. The former has the advantage of offering galvanic isolation from the power cable and its installation is done without powering off. On the other hand, its disadvantage is that high current on the MV power cable causes the magnetic saturation of the RF transformer and, as a consequence, the insertion of relevant loss. The latter has the advantage of facing low saturation magnetic

flux density because of the low-level current flowing between neutral and ground lines resulting in low insertion loss. Moreover, it offers an interesting cost-effective solution because the PLC coupler has a small size in comparison to the capacitive MV PLC coupler [123]. In addition, due to its characteristics, the distance for signal transmission can be long [124–126].

2.2.2.3 LOW-VOLTAGE

Typical LV power cables consist of three conductors, a phase, a neutral and ground. Two of these three conductors can be used to create a communication channel. The scenario for the LV electric power grid is different compared with HV and MV ones, as discussed in [125] because the LV power cable is derived from secondary windings of the MV/LV power transformer and the energy is delivered to a large number small consumers. The dynamic of the loads in LV electric power grid yields emissions and interference associated with appliances, motors and other loads, which make them the most hostile environment for data communication purposes [22, 127] and difficulty impedance matching among PLC transceivers and power lines. Due to the low cost of LV PLC couplers, some features can be improved, such as impedance matching with electric power grid by using, for instance, the RF transformer ratio transformation or the design of adaptive matching impedance and selective filters that is capable of attenuating unwanted frequencies which may cause interference with the PLC system.

In [73] it was shown that the analog filter is the key issue of LV PLC capacitive couplers. The authors showed how to build the filter circuit model for LV, and the Butterworth band-pass filter which frequency band is from 1 MHz up to 30 MHz was designed. The main issues for designing a capacitive SISO PLC coupler was discussed in Section II.

The inductive coupling has been studied in motor cable communication [70] for a voltage of 400 V_{DC}. The inductive PLC coupler for motor cable communication is tuned for the low voltage direct current (LVDC) [128]. The inductive couplers are not commonly used in consumer applications, in which the connection with the power cable is made through an electrical wall outlet. The typical circuit of LVDC and the basic structure of the proposed PLC-base communication architecture can be accessed in [129]. Also, we point that a LVDC is very common in vehicles.

2.2.3 BASED ON TYPE OF VOLTAGE

The use of PLC in AC electric power grid is widespread, but the voltage of electric circuits can be classified into two categories: AC and DC. However, despite the popularity of PLC system over AC electrical circuits, there are a lot of researches focused on facilitating communication over DC electric circuits. In [97], the DC PLC coupler is developed on the basis of AC PLC coupler. Essentially, the fundamental structure of a DC PLC coupler is very similar to the AC PLC coupler. In [130] were investigated the possibility of using the PLC technology to transmit data along differential DC power buses employed in spacecraft.

The inductive and capacitive PLC coupler can be designed to work in different levels of voltage in AC or DC electrical circuits. A DC PLC coupler uses a series capacitor connected with the power cable such as an AC PLC coupler does. The capacitor blocks the AC or DC mains signal and passes high frequencies for a wide range of frequencies. In inductive coupling without galvanic contact with the DC bus voltage, the inductive PLC coupler, installed in parallel with DC bus, injects the PLC signal following the principle of magnetic induction, which is exploited in inductive coupling, see Section III-A-2.

The applicability of narrowband and broadband PLC for the LVDC electrical circuits communication is shown in [131]. In [15] narrowband capacitive couplers that are differentially connected between the neutral and DC conductors in bipolar ± 750 V_{DC} is proposed. An inductive coupler is used in [132] for analysis of noise in broadband PLC in DC power cables.

2.2.4 BASED ON FREQUENCY BAND

The PLC system has a range of frequency bands allocated to narrowband and broadband PLC data communications. Therefore, PLC couplers can be classified as narrowband (frequency range between 0 kHz and 500 kHz) [9], [6] and broadband (frequency range from 1.7 MHz to 500 MHz) [106], [121]. The frequency bandwidth is determined by low and high cut-off frequencies at 3 dB attenuation and can be modified in function of filter design. The parameters of the RF transformer, analog filter and electric protection must be designed in accord with the chosen frequency band desired [48], [50].

2.2.5 BASED ON PROPAGATION MODE

Power cable wiring installations in a residence make use of three wires, namely phase, neutral and protective ground, which can be modeled as parallel conductors sheathed in a dielectric material [133]. PLC couplers can inject a signal in the power cable along the wire in two ways: DM and CM [134].

The DM is the normal current conduction mode by a two-wire circuit. The current flows in a wire in phase opposition of the other wire, the electromagnetic fields generated by the currents actually cancel out each other. On the other hand, in the CM, the current goes through all the wires in the same direction causing the addition of electromagnetic fields, yielding significant levels of EMI [135].

Fig. 14 shows a high-frequency equivalent circuit of a PLC channel illustrating the creation of CM signals due to current I_{cm} and voltage V_{cm} with respect to the ground, originated unintentionally in an unbalanced electric power cable. It creates a parasitic capacitance with respect to ground and causes a CM current to return to the source through the parasitic capacitance (C_{para}). In this model, we have a three-wire power line cable in which the Ground wire is the reference conductor. The I_{dm} current flows in the Phase wire from/to PLC Couplers and returns via the Neutral wire. The I_{cm} currents flow from/to PLC Couplers in the Live and Neutral wires and return to PLC Couplers via the Ground wire. The I_{cm} flows back to the location where it was converted via unwanted parasitic components C_{para}, ground and any other asymmetry.

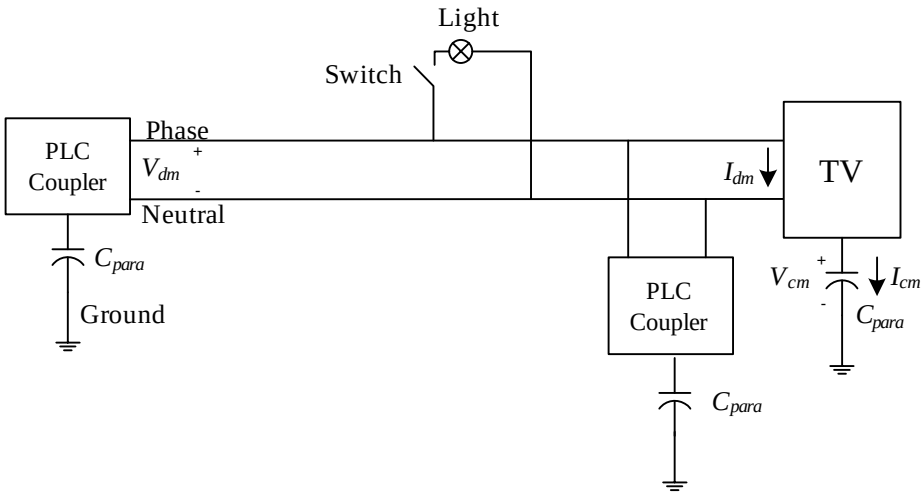

Figure 14: High-frequency equivalent circuit of a DM.

2.2.6 BASED ON NUMBER OF CONNECTIONS

The wires in HV, MV and LV electric power grid can be used to provide more than one path for data communication. Hence, the coupling circuits can be classified according to the number of connections. The power cable in HV and MV consists of three phase wires where the same signal can be sent by three different paths. The power cable in LV is composed of three phase conductors and one neutral conductor and, therefore, there are four paths available for data communication [136, 137]. In this context, the connection between two PLC transceivers can be classified in terms of SISO, single input multiple output (SIMO), multiple input single output (MISO) and multiple input multiple output (MIMO).

The SISO coupling is the simplest form of coupling with power cable. In LV, the connection of PLC couplers can be performed by the phase and neutral wires or phase to phase wires. Such connection in HV and MV occurs among phases. The advantage of the SISO PLC coupler is its simplicity and low cost. The majority of PLC systems are SISO.

To have SIMO and MISO PLC couplers, connecting at HV and MV, all three phases wires must be available. The SIMO PLC coupler is connected in two phases to transmit the signal from the transceiver circuit and it receives the signal in three phases. In that case, the signal is induced in the third phase.

In MIMO coupling at HV and MV, all three phase wires can be used, simultaneously. The MIMO PLC coupler is connected in three phases to transmit the signal and it receives the signal in two phases. For LV electric power grid the electrical protective wire and protective earth (PE) allows the creation of another path between two PLC couplers [138]. Table 1 and Fig. 15 show the configuration mode of SISO, SIMO and MIMO. In [138], the authors show the results of channel measurements motivated to implement a MIMO PLC equivalent circuit explaining the creation and reception of CM signals. Two RF transformers are connected in triangle and star configuration providing several paths for data communication.

2.3 FUTURE WORKS

Although there is a scarce effort toward PLC coupling research, the coupling unit is perhaps one of the most important components in a PLC transceiver. Therefore, the design of a PLC coupler capable of handling the complexity, dynamic and diversity

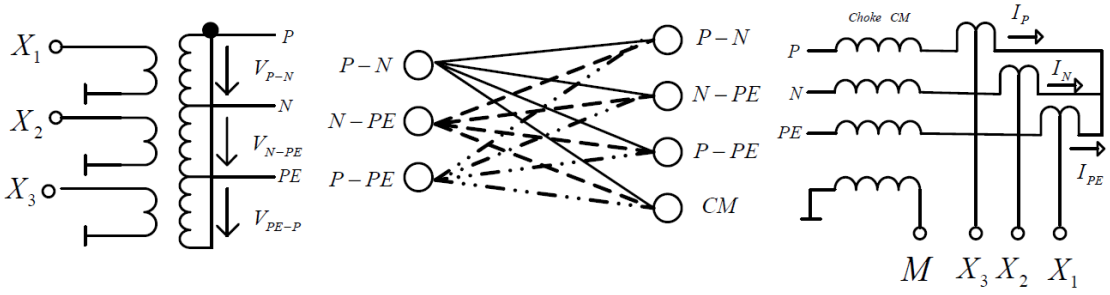

Figure 15: MIMO PLC Coupler.

Table 1: Types of connections.

Mode	*Transformer (Tx)*	*Transformer (Rx)*
1X1 (SISO)	*P-N*	*P*
1X2 (SIMO)	*P-N*	*P, CM*
1X3 (SIMO)	*P-N*	*P, N, PE*
1X4 (SIMO)	*P-N*	*P, N, PE, CM*
2X2 (MIMO)	*P-N, P-PE*	*P, PE*
2X3 (MIMO)	*P-N, P-PE*	*P, N,PE*
2X4 (MIMO	*P-N, P-PE*	*P, N, PE, CM*

of electric power system is a challenging issue for the PLC research community. With this regards, in the following, we enumerate some important question deserving more attention in order to come up with improved coupling solution:

- The measurement of access impedances is of particular importance since it is necessary for designing efficient and effective couplers, for improving the performance of the PLC coupling [139]. It is important to know time and frequency behaviors of resistive and reactive components of such impedance. Lack of this very important information has led to the design of poor quality and low efficient coupling devices in the past. In order to address this issue, Chapter 3 focuses on measurement, characterization, and statistical analysis of access impedance in LV and indoor facilities.

- Research and development of new components and material for electrical protection of transceiver circuits for broadband PLC. Very limited research efforts have been expended in the area of special materials for couplers, especially when compared to the work on materials for the design of advanced transformers. For instance, the use of nanocrystalline magnetic materials to substitute the ferrite and nanomaterials for capacitive devices. This kind of material will considerably reduce the cost of current coupling devices used in medium and high voltage electric power systems.

- The design of low-cost surge protective components when the frequency is over 35 MHz. Our review showed that GDT and TVSP are the most recommended if the mains voltage is high; however, their cost may limit the use of them in commercial coupling devices.

- The development of simple and effective coupling circuits that is capable of performing impedance matching to maximize power transfer. The introduction of such kind of coupler will result in a remarkable improvement of PLC technology. This issue is addressed in Chapter 5.

2.3.1 SUMMARY

A review on the use of couplers to enable data communications over AC and DC electric power grid has been presented. PLC couplers enable data communications over power lines by injecting/extracting data signals into or from these power lines either by differential mode or by common mode. The review showed that the introduction of couplers to connect PLC transceivers to electric power circuits could be used to minimize both signal distortion and insertion loss to improve PLC systems performance. In this regard, we isolated the key issues related to the design of a PLC coupler, such as the PCB design, insertion and return loss, galvanic isolation, impedance matching, filtering and protection. Additionally, we provided a classification of PLC couplers based on the type of physical coupling, voltage levels, frequency bandwidth, propagation mode and number of connections. These fundamental concepts are provided to suffice basic understanding about some relevant issues related to the design of PLC couplers. Finally, we pointed out some important research questions whose investigations can result in the design of new generations of efficient and effective PLC couplers.

In the next chapter, the design and prototype of non-adaptive SISO PLC coupling circuit will be addressed.

3 ACCESS IMPEDANCE IN BRAZILIAN IN-HOME BROADBAND AND LOW-VOLTAGE ELECTRIC POWER GRIDS

The usefulness and suitability of PLC technology for smart grid, in-vehicle and in-home data communication have been demonstrated worldwide. Currently, PLC technology is being considered to support Internet of Things (IoT) applications [25,157–161]. In spite of the advantages offered by this technology, there are some important issues related to data communication through electric power grid that must be deeply addressed in order to efficiently use the available resources of such kind of *no new wire* data communication medium. Among these issues, deserves attention the temporal and spectral behaviors of access impedances at the connection points with the electric power grid.

The underlying sources of such issue are the load dynamics, circuit topologies and the use of unshielded power lines [157, 162, 163]. In fact, according to [164–167], the access impedances of the electric power grid are disturbed by the presence of harmonics, household appliances connected to the electric power grid, frequency modulation (FM) carriers, amateur radio service, and other short wave radio disturbances. To ensure that data communication through electric power grid will succeed, the knowledge of access impedances (resistance and reactance components) is of utmost importance. In fact, the *a priori* availability of such kind of knowledge is essential to design impedance matching circuits (adaptive or not) that are capable of maximizing the power transfer between PLC transceiver and electric power grid [66, 162, 168, 169].

In general, conventional telecommunication transceivers are designed with input and output impedance of 50, 75, 150 and 600 Ω, depending on the characteristic impedance of the transmission media. However, this is not valid for the electric power grid, in which the access impedance may vary from few ohms up to few kiloohms [58, 170].

The frequency and time-varying behaviors of the access impedance at the point of connection (e.g., outlets) of the electric power grid [59] reveal the complexity involved with the design of PLC coupling circuits. In fact, impedance mismatching between PLC

coupling circuit and electric power grid results in coupling losses, which can severely shorten the PLC signal propagation or coverage [171,172]. Note that coupling loss is, in our context, defined as the signal power loss which occurs between PLC transceiver and the electric power grid at the connection point due to impedance mismatching [173].

Characterization and modeling of the access impedance of in-home, broadband and LV electric power grid were presented in [174], in which was shown that the measured access impedance in the frequency band from 1 MHz up to 10 MHz varies between 20 Ω and 190 Ω. In [14], the low-voltage single-phase power line was modeled as a transmission line in the frequency band from 1 MHz up to 30 MHz to compute two intrinsic transmission line parameters, namely the characteristic impedance and the propagation constant. This model considered the type of cable and its length. Moreover, [175] investigated the indoor LV electric power grid attenuation profile and the access impedance. In addition, [176] addressed the characteristic impedances of the electric power grid to understand the broadband signals propagation in the frequency band between 1 MHz and 30 MHz, when the outdoor and LV electric power grid between a pole holding a medium-voltage to low-voltage (MV/LV) transformer and an end user is taken into account.

In [177], four methods of measuring access impedances of electric power grid were summarized. They are based on current probe, resonance, voltmeter and ratio approaches. The authors compared the performance of four methods and showed that the two-current-probe method is effective for measuring access impedances of the electric power grid in the frequency band from 500 kHz up to 20 MHz. Also, [162] outlined a methodology, based on current probes, for measuring the access impedance for the frequency band from 1 MHz up to 30 MHz. Actually, it showed the construction and characterization of a PLC coupling circuit to analyze the access impedance of the electric power grid without loads or with resistive loads. Additionally, [178] presented a statistical characterization of the access impedance for China in-home electric circuits in the frequency band between 1 MHz and 30 MHz. Based on a measurement campaign, carried out in seven Brazilian residences, preliminary results of impedance characterization in some Brazilian in-home power line grid were reported in [179].

Regarding access impedance measurement, characterization and modeling in in-home, LV and broadband electric power grid, we state that more investigations and information need to be extracted from these grid in order to obtain a good picture and/or deep knowledge of their access impedance dynamics and, as a consequence, to allow the development of PLC coupling circuits that correctly and efficiently take into

account the impedance matching functionality. In this regard, this Chapter focuses on measurement, characterization, modeling and statistical analysis of access impedance in several in-home, broadband and LV Brazilian electric power grid.

The remainder of this Chapter is organized as follows: the measurement setup is addressed in Sec. 3.1. Sec. 3.2 describes the procedure to obtain a statistical model for the access impedance. Results and analyses are summarized in Sec. 3.3.

3.1 THE MEASUREMENT SETUP

This section describes the measurement setup used to investigate the resistance and reactance components of the access impedance in in-home, broadband and LV electric power grid. This setup consists of a VNA instrument and a PLC coupling circuit, which is used as an interface between the VNA instrument and an outlet inside of the house or apartment [31, 111]. Moreover, the PLC coupling circuit is responsible for providing galvanic isolation between the electric power grid and the VNA instrument by avoiding physical contact between VNA instrument and these grid [6].

Fig. 16 shows the schematic of a capacitive broadband coupling circuit for SISO and LV PLC system used to measure the access impedance of in-home and LV electric power grid. In Fig. 16, the capacitor C_1 is used to block the mains voltage of the electric power grid (at 60 Hz) and works as a first order high-pass analog filter with a flat magnitude of frequency response for $f \geq f_l$, where f_l denotes the cut-off frequency. The RF transformer T_1 has a 1:1 relation between primary and secondary windings to provide the galvanic isolation between the VNA instrument and the electric power grid. It works like a balanced to unbalanced (BALUN) line and isolates the grounds of the VNA instrument and the electric power grid [96]. In addition, it is also used to provide electrical safety to the VNA instrument operator, avoiding accidental shocks.

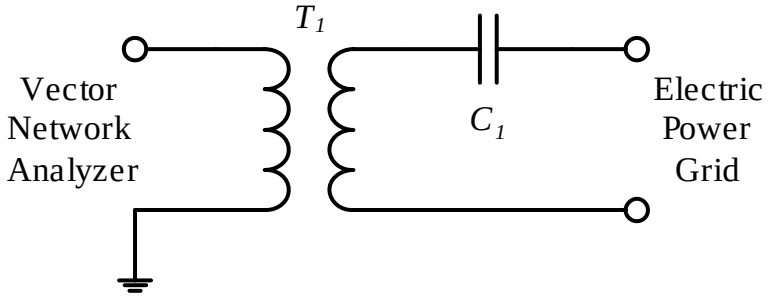

Figure 16: Schematic of the capacitive broadband coupling circuit for SISO and LV PLC system.

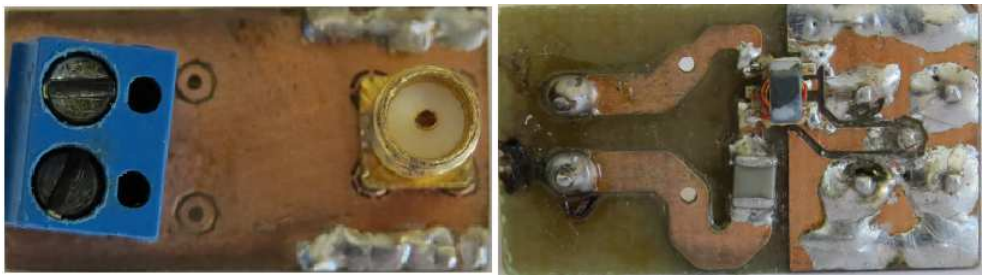

Figure 17: The prototype of the designed PLC coupling circuit.

Two measurements were made through the VNA. In the first one, the scattering parameters of the PLC coupling circuit was measured. The port 1 of the VNA is connected on the RF transformer, and port 2 is connected on the capacitor, see Fig. 16. Based on the use of aforementioned prototype, the PLC coupling circuit shows the frequency magnitude attenuation lower than 5 dB in the band-pass, which is from $f_l = 2$ MHz up to $f_h = 500$ MHz. Moreover, Fig. 18 shows the frequency magnitude of the scattering parameters of the designed capacitive broadband coupling circuit for SISO and LV PLC system.

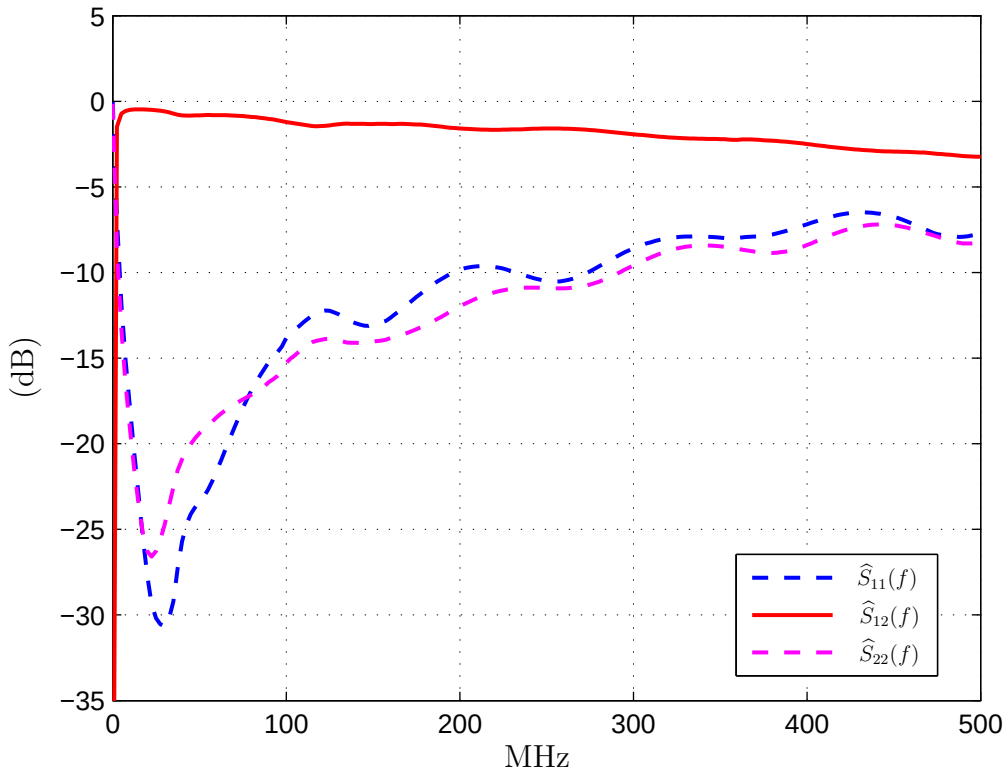

Figure 18: Frequency magnitude of scattering parameters of the designed PLC coupling circuit with the impedance matching of 50 Ω.

The second measurement used only the port 1 of the VNA to measure the S_{11}

parameter. Fig. 19 shows the block diagram of the measurement setup that was used to measure the scattering parameters in the frequency domain.

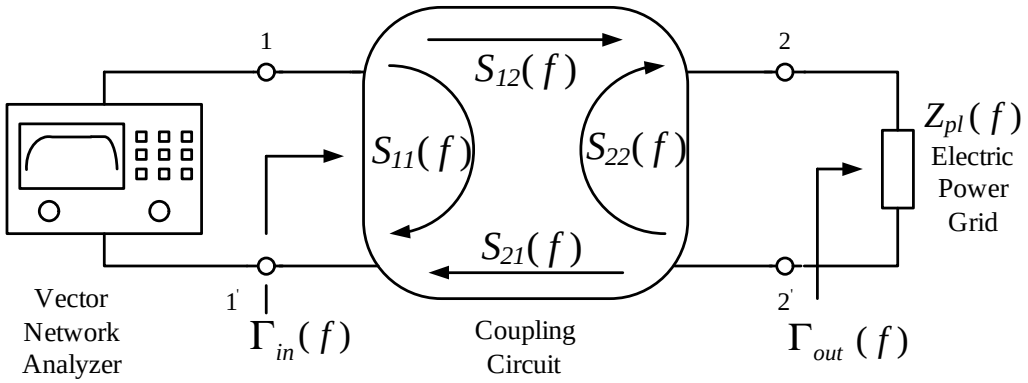

Figure 19: The block diagram of the measurement setup used to measure $Z_{pl}(f)$.

The measurement setup makes uses of a VNA Agilent Field Fox N9912A instrument and the PLC coupling circuit with C_1 and T_1 specified as follows:

- The ceramic capacitor C_1 is a SMD of 1.5 nF with insulation voltage of 1 kV_{rms} working as a high-pass filter with low cut-off frequency of 2 MHz.
- The RF transformer T_1 has characteristic of band-pass filter from 0.4 MHz to 500 MHz and insertion loss of 2 dB with the impedance matching of 50 Ω [151].

The cascade of high-pass filter, capacitor C_1, and RF transformer T_1, in this order, results in a band-pass filter.

Fig. 20 illustrates the equivalent circuit of the measurement setup, which considers the presence of the PLC coupling circuit and the access impedance of the electric power grid. In this circuit, $Z_c(f)$ is the impedance of capacitor C_1, which is expressed by

$$Z_c(f) = \frac{1}{j\omega C_1}, \tag{3.1}$$

where $\omega = 2\pi f$, and f is the frequency in Hertz (Hz). Moreover, $Z_t(f)$ is the equivalent impedance of the transformer T_1 for high-frequency. From Fig. 20, it is possible to evaluate the impedance at the port of the VNA instrument by using

$$Z_M(f) = \frac{Z_t(f)[Z_c(f) + Z_{pl}(f)]}{Z_t(f) + Z_c(f) + Z_{pl}(f)}. \tag{3.2}$$

A convenient way to obtain an measure of $Z_M(f)$ (i.e., $\widehat{Z}_M(f)$) is from the $\widehat{S}_{11}(f)$ scattering parameter [62, 176], where "$\widehat{\ }$" means that the VNA equipment can only

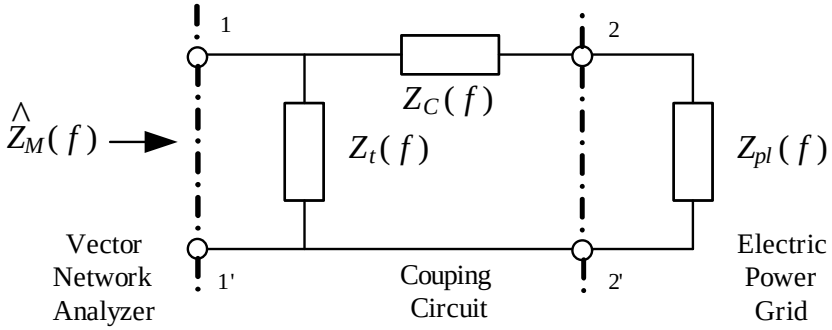

Figure 20: Equivalent circuit for measuring the access impedance of electric power grid.

provide an measure of the parameter. Based on the measure of the $S_{11}(f)$, the measure of the impedance $Z_M(f)$ is given by

$$\widehat{Z}_M(f) = Z_S \frac{1 + \widehat{S}_{11}(f)}{1 - \widehat{S}_{11}(f)}, \tag{3.3}$$

where $Z_s(f)$ is the internal impedance of the VNA instrument, which has typical value of 50 Ω, and $\widehat{S}_{11}(f)$ is the measure of the reflection scattering parameter at the input port of the VNA instrument. Note that $\widehat{Z}_M(f)$ is not the measure of access impedance of the electric power grid, see (3.2). A way to obtain $\widehat{Z}_{pl}(f)$ is by calibrating the VNA instrument together with the PLC coupling circuit and connection cables to reduce the coupling error between the VNA instrument and the electric power grid. After the calibration, the PLC coupling circuit is considered part of the VNA instrument and this new VNA instrument presents an internal impedance, which is expressed by

$$Z'_s(f) = Z_c(f) + \frac{Z_t(f)Z_s(f)}{Z_t(f) + Z_s(f)}. \tag{3.4}$$

In this sense, when we use the VNA instrument calibrated together with the PLC coupling circuit and connection cables, we can obtain an measure of the access impedance of the electric power grid by using

$$\widehat{Z}_{pl}(f) = Z'_s(f) \frac{1 + \widehat{S'}_{11}(f)}{1 - \widehat{S'}_{11}(f)}, \tag{3.5}$$

where $\widehat{S'}_{11}(f)$ is an measure of the reflection scattering parameter at the port of PLC coupling circuit, see $2 - 2'$ in Fig 20. This measurement strategy minimizes the distortion (error) introduced by the PLC coupling circuit. Thus, the measure of access impedance must be rewritten as

$$\widehat{Z}_{pl}(f) = Z_s(f) \frac{1 + \widehat{S'}_{11}(f)}{1 - \widehat{S'}_{11}(f)} + \epsilon(f), \tag{3.6}$$

where $|\epsilon(f)| \propto \left|Z_s(f) - Z_s^{'}(f)\right|$ denotes an approximation of the error introduced by the adopted strategy to indirectly measure the access impedance under the presence of PLC coupling circuit and connection cables.

It is important to highlight that each measure obtained with the VNA instrument consists of $\widehat{S}'_{11}[k] = \widehat{S}'_{11}(f)|_{f=k\Delta f}$, where $0 \leq k \leq K-1$ and $\Delta f \in \mathbb{R}^+$ is the VNA frequency resolution. Thus, the ℓ^{th} discrete version of a measure of the access impedance of the electric power grid at the point of connection can be measured by using

$$\widehat{Z}_{pl,\ell}\,[k] = (\widehat{Z}_{pl,\ell}\,(f) - \epsilon(f))|_{f=k\Delta f}, \tag{3.7}$$

$$= \widehat{R}_{pl,\ell}[k] + j\widehat{X}_{pl,\ell}[k] \tag{3.8}$$

$$= Z_s[k]\frac{1+\widehat{S}'_{11,\ell}[k]}{1-\widehat{S}'_{11,\ell}[k]}, \tag{3.9}$$

where $\widehat{Z}_{pl,\ell}$ is the ℓ^{th} measure of the access impedance given by (3.6) and $\widehat{S}'_{11,\ell}[k]$ is the ℓ^{th} measure of the scattering parameter for the k^{th} tone.

3.2 THE ACCESS IMPEDANCE MODELING PROCEDURE

It is well known that there is a lack of statistical models for the access impedance in electric power grid. To deal with this problem, this section outlines a simple and straightforward procedure to obtain a statistical model of the access impedance in the frequency domain, when a data set of measured access impedances is available. The proposed procedure applies when $A(f) = \{R_{pl}(f), X_{pl}(f)\}, \forall f \in \mathbb{R}$, is a random process in which the values of $A(f_1)$ and $A(f_2)$, for $f_1 \neq f_2$, $\forall f_1,\ f_2 \in \mathbb{R}$, are modeled with the same statistical distribution. Also, we assume that the values of the parameters of the chosen statistical distribution can be different for $A(f_1)$ and $A(f_2)$.

Now, let us assume that $S_f = \{\alpha_1(f), \cdots, \alpha_M(f)\}$, is a set of parameters associated with the chosen statistical distribution in which M is the number of parameters and $\alpha_i(f) \in \mathbb{R}$ is the waveform that models the parameter of chosen statistical distribution in the frequency domain. We can discretize $\alpha_i(f)$ as follows:

$$\alpha_i\,[k] = \alpha_i\,(f)\,|_{f=k\Delta f^*}\,, k = 0, 1, ..., K-1, \tag{3.10}$$

where $\Delta f^* = \min_i \Delta f_i^*$, in which

$$\Delta f_i^* = \max_{|R_{\alpha_i}(\Delta f_i)| \geq \beta |R_{\alpha_i}(0)|} \{\Delta f_i\}, \tag{3.11}$$

with

$$R_{\alpha_i}(\Delta f_i) = \int_{-\infty}^{\infty} \alpha_i(f)\alpha_i(f+\Delta f_i)\,df \tag{3.12}$$

and $0 \leq \beta \leq 1 \,|\, \beta \in \mathbb{R}$. Note that Δf^* is the minimum frequency bandwidth that guarantee the flatness of $\alpha_i(f)$ with reliability level of β. Therefore, $A(f)$ for $k\Delta f^* < f < (k+1)\Delta f^*$ can be modeled using the chosen distribution with a set of parameters $S_k = \{\alpha_1[k], \cdots, \alpha_M[k]\}$.

Such discretization assist us to perform numerical simulation and to obtain a concise model for $\alpha_i(f)$. Moreover, it is a very useful and effective approach to deal with discrete values of scattering parameters or access impedances, which is the type of information provided by a VNA instrument. In other words, this kind of discretization perfectly fits the scope of our work.

In this context, our aims is to model the access impedance of in-home, broadband and LV electric power grid based on L measures of $\widehat{Z}_{pl,\ell}[k]$, where $1 \leq \ell \leq L$ and $0 < k \leq K-1$. We assume that $\widehat{Z}_{pl}[k] = \widehat{R}_{pl}[k] + j\widehat{X}_{pl}[k]$, where $\widehat{R}_{pl}[k]$ and $\widehat{X}_{pl}[k]$ are random variables (r.v.s) for resistance and reactance components at the k^{th} tone and $\widehat{R}_{pl,\ell}[k]$ and $\widehat{X}_{pl,\ell}[k]$ are, respectively, the ℓ^{th} sample of these random variables. The proposed modeling procedure is organized into six steps, which are as follows:

- **Step 1:** Individually analyze the cumulative distribution function (CDF) of $\widehat{R}_{pl}[k]$ and $\widehat{X}_{pl}[k]$ r.v.s and remove the outliers.
- **Step 2:** Model the random variables $\widehat{R}_{pl}[k]$ and $\widehat{X}_{pl}[k]$, without outliers, using the statistical distribution that best model the most tones (one distribution for the resistance and another for the reactance). In order to select the best statistical distribution among the available ones, we suggest the use of the following evaluation criteria [180,181]: Akaike Information Criterion (AIC), Bayesian Information Criterion (BIC), Efficient Determination Criterion (EDC), and Log-Likelihood function. In other words, this step will yield $\widehat{\alpha}_i[k]$, where $\widehat{\alpha}_i[k]$ is the i^{th} parameter of the chosen statistical distribution at the k^{th} tone.
- **Step 3:** Fit $\widehat{\alpha}_i(k\Delta f^*)$ by using a polynomial approximation in order to obtain $\widehat{\alpha}_i(f)$. The use of polynomial approximation aims to provide a very simple representation of $\widehat{\alpha}_i(f)$. Due to the limitation of polynomial approximation to model $\widehat{\alpha}_i(f)$ in the whole frequency band, we suggest to divide the whole frequency band into several sub-bands and apply one polynomial approximation

for each frequency sub-band. If the number of sub-bands increases, then the polynomial approximation can offer better results. We point out that there is a compromise between performance and complexity by using this strategy. For instance, if the number of sub-bands is large, then we will need to use many polynomials. Note that, this step provides a first and rough model for the access impedance ($Z_{pl,1}(f)$) because it allows us to obtain $\widehat{\alpha}_i(f)$ from $\widehat{\alpha}_i[k] = \widehat{\alpha}_i(k\Delta f^*)$ by using the polynomial approximation as an interpolation technique.

- **Step 4:** It is important to highlight that $Z_{pl,1}[k] = Z_{pl,1}(k\Delta f^*)$ is uncorrelated. In order to insert correlation to it, filter $Z_{pl,1}[k]$ by using a low-pass filter. As a result, the model for access impedance with correlation is given by $Z_{pl,2}[k] = Z_{pl,1}[k] * w[k]$, where $*$ denotes the convolution operator and $w[k]$ is a low-pass filter, which is carefully chosen to minimize the mean square error between the magnitude of the autocorrelations of $Z_{pl,2}[k]$ and $\widehat{Z}_{pl}[k]$.

- **Step 5:** The model $Z_{pl,2}[k]$ does not perfectly fit the data set because there is some differences between $\overline{\widehat{Z}}_{pl}[k] = \mathbb{E}\{\widehat{Z}_{pl}[k]\} \cong \frac{1}{L}\sum_{\ell=0}^{L-1} \widehat{Z}_{pl,\ell}[k]$ and $\overline{Z}_{pl,2}[k] = \mathbb{E}\{Z_{pl,2}[k]\}$, where $\mathbb{E}\{\cdot\}$ is the expectation operator. In order to reduce these differences, we introduces a more refined model given by $Z_{pl}^{m}[k] = Z_{m}^{opt} Z_{pl,2}[k] + Z_{a}^{opt}$, where Z_{m}^{opt} and Z_{a}^{opt} are the optimal multiply and additive factors. In order to find these factors, we minimize the mean square error between $\overline{\widehat{Z}}_{pl}[k]$ and $\overline{Z}_{pl,2}[k]$. Therefore, these factors are given by

$$\{Z_{m}^{opt},\, Z_{a}^{opt}\} = \underset{Z_m,\, Z_a}{\operatorname{argmin}} \left\{ \sqrt{\sum_{k=0}^{K-1} |\overline{\widehat{Z}}_{pl}[k] - (Z_m \overline{Z}_{pl,2}[k] + Z_a)|^2} \right\}. \tag{3.13}$$

- **Step 6:** Finally, a continuous model for access impedance can be obtained by using an interpolation method on $Z_{pl}^{m}[k]$. Therefore, $Z_{pl}^{m}(f) = f(Z_{pl}^{m}[k])$, where $f(\cdot)$ denotes an interpolation function that individually applied to the resistive and reactive components of $Z_{pl}^{m}[k]$.

3.3 MEASUREMENT CAMPAIGN AND STATISTICAL ANALYSIS

In this Section, we perform a statistical analysis of the data set of measured access impedances, which was obtained with the measurement campaign, and discuss the obtained model by adopting the procedure suggested in Section 3.2.

Table 2: $P(A<x)$ for resistance and reactance components $A\in$\{resistance, reactance\}.

$P(A(f) < x)$	0.1	0.5	0.9	$\mathbb{E}\{A(f)\}$
Resistance (Ω)	11.64	38.75	127	58.98
Reactance (Ω)	-48.42	45.67	118.8	53.69

The measurement campaign was carried in three cities of Minas Gerais State, which are Juiz de Fora, Cataguases and Carandai. This measurement campaign includes 32 residences, two commercial stores, a telecommunications company facility and a farmer residence. All outlets were measured in each site. The measurements were performed in $L = 1.154$ single-phase outlets of these places. Each place has an area between 50 and 400 m^2. The access impedance of each outlet was measured by using the measurement setup discussed in Section 3.1 with the VNA instrument configured to operate in a frequency band of 2-500 MHz. It is important to emphasize that the use of VNA instrument does not allow us to obtain Δf^* as suggested in Section 3.2. Actually, the VNA instrument allow us to measure up to $K = 1001$ tones in the chosen frequency band. Due to this limitation of the VNA equipment, we use K=1001 and, as a consequence, $\Delta f = 498$ kHz.

Fig. 21 shows the CDF of the values of resistance and reactance of in-home electric power grid by considering the frequency band 2-500 MHz. Note that $P(A(f) < x)$ indicates the probability of $A(f)$ to be less than x, where $A(f) = \{R_{pl}(f), X_{pl}(f)\}$. In this figure, we note that resistance and reactance components show values between 0 and 1000 Ω and between -1000 Ω and 1000 Ω, respectively. We assume that the values outside of this interval have a low probability of occurrence and were considered outliers. Moreover, this plot shows that the access impedance has inductive behavior in most of the cases. Table 2 lists some points of these curves (i.e., x for $P(A(f) < x) = 0.1$, 0.5, 0.9) and the mean value. Note that, 50% of the values of the resistive and reactance components are below 38.75 Ω and 45.67 Ω, respectively. Also, Table 2 shows that 90% of the values of resistive components are below 127 Ω and above 11.64 Ω. For the reactance component, we note that 90% of the values are below 118.8 Ω and above -48.42 Ω.

In order to model the resistance r.v.s in each tone, we consider statistical distributions widely used in the literature, such as Lognormal, Exponential, Gamma, Inverse Gaussian, Logistic, Log-logistic, Nakagami, Normal, Weibull and t-location scale. On the other hand, to model the reactance, we consider just the Logistic, Normal and t-location scale distributions, since the others distributions do not support negative values. In order, to select the best distribution model, we use the evaluation criteria

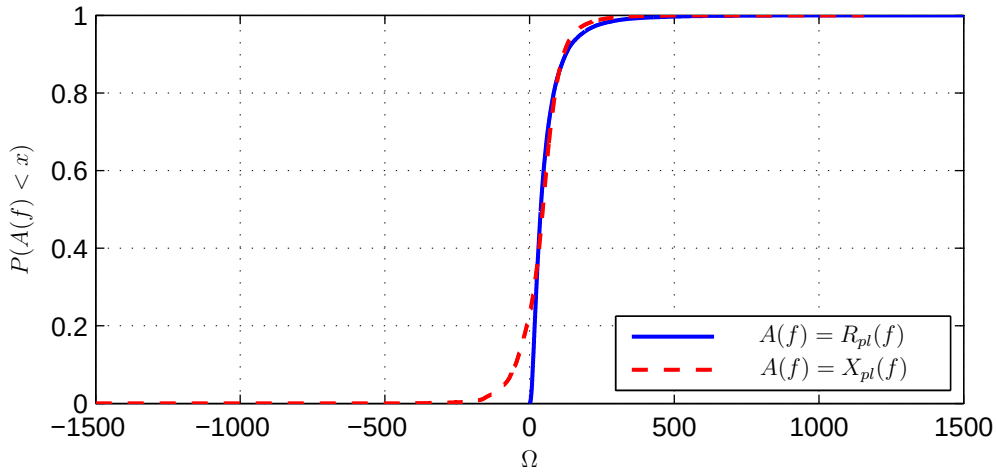

Figure 21: CDF of the resistance and reactance in the frequency band of 2-500 MHz.

Log-Likelihood, AIC, BIC and EDC to find the best distribution that could model the resistance and reactance r.v.s in the frequency domain.

Fig. 22(a) shows the percentage of frequencies that each distribution is the best one to model the resistance based on the evaluation criteria. Note that in 70% of the data set the resistance is better modeled by the Log-logistic distribution than with others distributions, which results in $\widehat{\alpha}_i(f)$ with $i = 1$ and 2, where $\widehat{\alpha}_1(f) = \mu(f)$ (log mean parameter) and $\widehat{\alpha}_2(f) = \sigma(f)$ (log scale parameter). Fig. 22(b) shows the resistance model for the tone equal to 50.3 MHz (*i.e.*, $f = 10^3\Delta f$). Note that the Log-logistic offers a good approximation in terms of shape and amplitude of the data histogram. At this frequency, the Log-logistic parameters are $\widehat{\mu}(10^3\Delta f) = 3.803$ and $\widehat{\sigma}(10^3\Delta f) = 0.623$.

Fig. 23(a) shows that in 100% of the data set the reactance is best modeled by the t-location scale distribution. Note that such statistical distribution has three parameters $\widehat{\alpha}_1(f) = \mu(f)$ (location parameter), $\widehat{\alpha}_2(f) = \sigma(f)$ (scale parameter) and $\widehat{\alpha}_3(f) = \nu(f)$ (shape parameter). Moreover, Fig. 23(b) exemplifies this choice for the tone equal to 50.3 MHz. As we can see, the t-location scale distribution offers a good approximation in terms of shape and amplitude of the data set histogram. For $k = 10^3$ ($k\Delta f = 50.3$ MHz), the t-location scale parameters are $\widehat{\mu}(10^3\Delta f) = 45.933$, $\widehat{\sigma}(10^3\Delta f) = 47.263$ and $\widehat{\nu}(10^3\Delta f) = 2.406$. We can note in Fig. 23(b) that the reactance at the aforementioned tone is more inductive than capacitive, which is something that occurs in other tones. In fact, this behavior is observed in all frequencies $2 \leq |f| \leq 500$ MHz.

Fitting $\widehat{\alpha}_i(k\Delta f)$ using a polynomial approximation, we obtain $\widehat{\alpha}_i(f)$. To do so, we

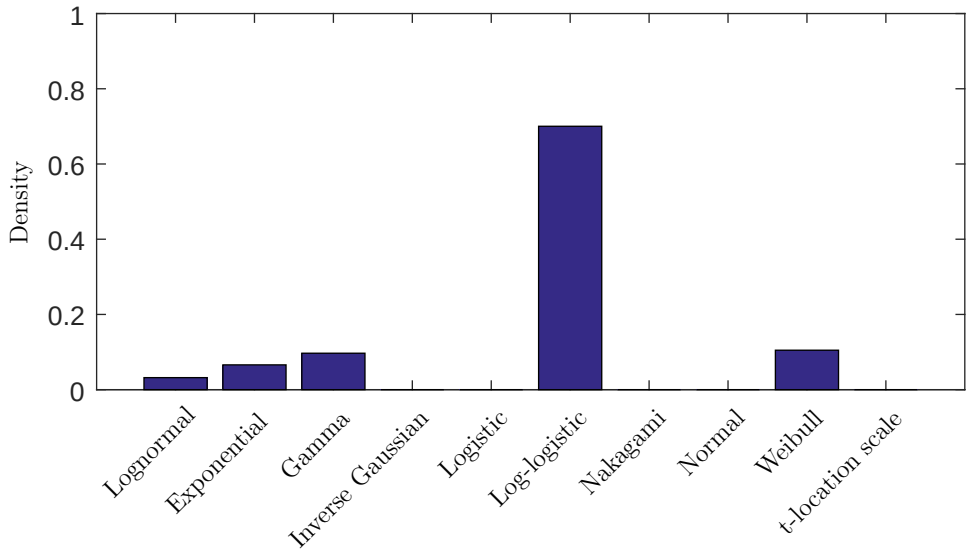

(a)

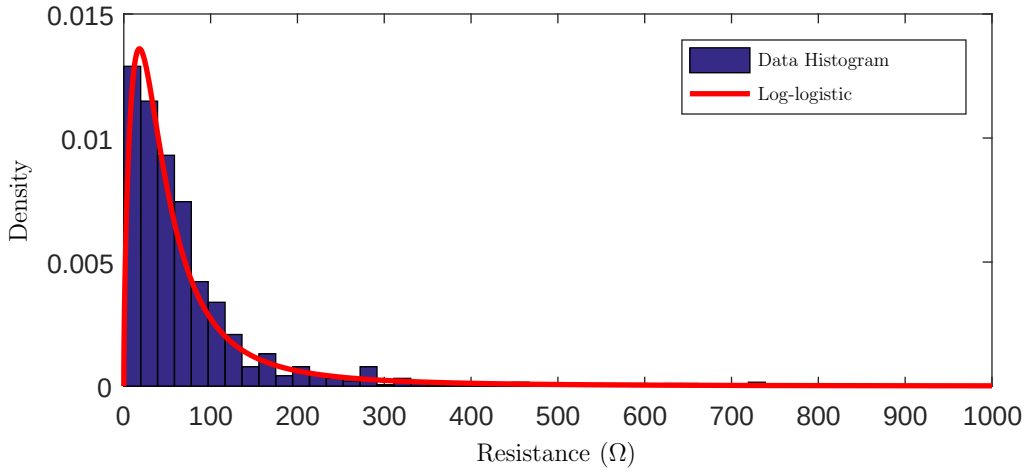

(b)

Figure 22: (a) Relative frequency that each statistical distribution is the best one to model the resistance and (b) Example of resistance modeling for $k = 10^3$ ($k\Delta f^*$= 50.3 MHz) using Log-logistic distribution.

divide the whole frequency band (2-500 MHz) into five sub-bands with bandwidth of approximately 100 MHz (e.g., 2-100 MHz, 100-200 MHz, 200-300 MHz, 300-400 MHz and 400-500 MHz) and fit $\widehat{\alpha}_i(k\Delta f)$ in each sub-band using a fifth order polynomial. As a result, we obtain $\widehat{\alpha}_i(f)= p_{i0} + p_{i1}f + p_{i2}f^2 + p_{i3}f^3 + p_{i4}f^4 + p_{i5}f^5$ for each sub-band, where $i = 1, 2$ for resistance and $i = 1, 2, 3$ for reactance. Table 3 lists all polynomial coefficients (without the index i for sake of simplicity) for modeling the parameters of the resistance component ($\widehat{\mu}(f)$ and $\widehat{\sigma}(f)$). Also, Figs. 24(a) and 24(b), show the obtained curves for $\widehat{\mu}(f)$ and $\widehat{\sigma}(f)$ by using the polynomials. As a result, by using these polynomials and the Log-logistic distribution, the first rough model of the resistance

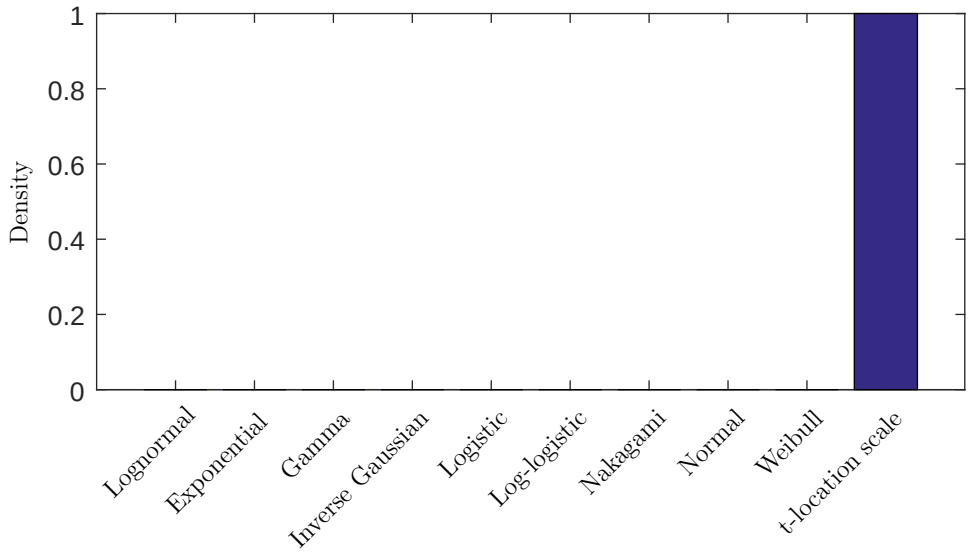

(a)

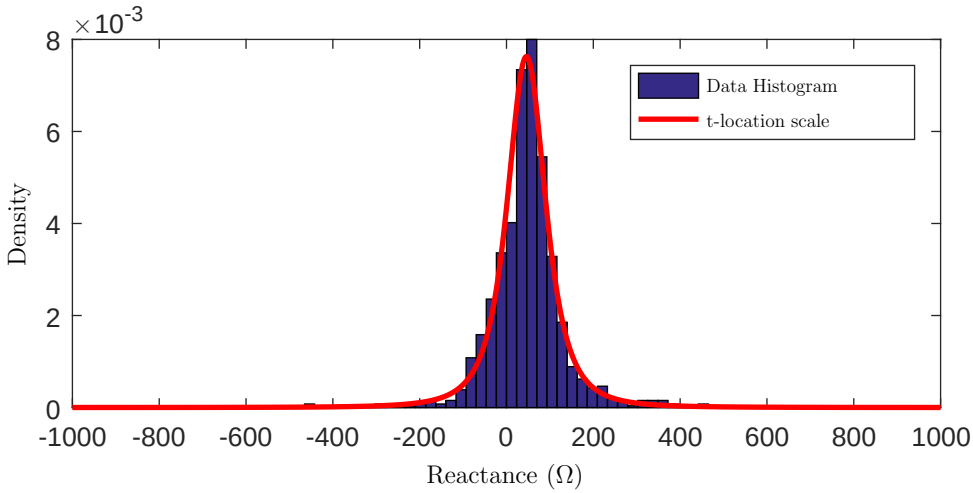

(b)

Figure 23: (a) Relative frequency that each statistical distribution is the best one to model the reactance (b) Example of reactance modeling for $k = 10^3$ ($k\Delta f^*$= 50.3 MHz) using the t-location scale distribution.

component, which is named $R_{pl,1}(f)$, is yielded.

Table 4 lists the polynomial coefficients for model the reactance by using the -location scale distribution, without the index i for sake of simplicity. Figs. 25(a), 25(b) and 25(c) show the curves that describes the parameters $\widehat{\mu}(f)$, $\widehat{\sigma}(f)$ and $\widehat{\nu}(f)$ of the t-location scale distribution when $2 \leq |f| \leq 500$ MHz. Therefore, using these polynomials and the t-location scale distribution, the first model of the reactance $X_{pl,1}(f)$ is obtained. As a result, the first rough model of the access impedance is given by $Z_{pl,1}(f) = R_{pl,1}(f) + jX_{pl,1}(f)$.

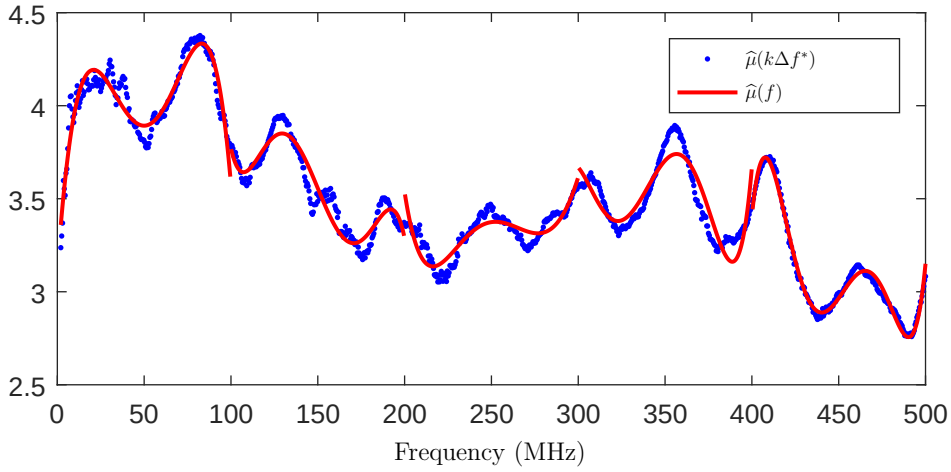

(a)

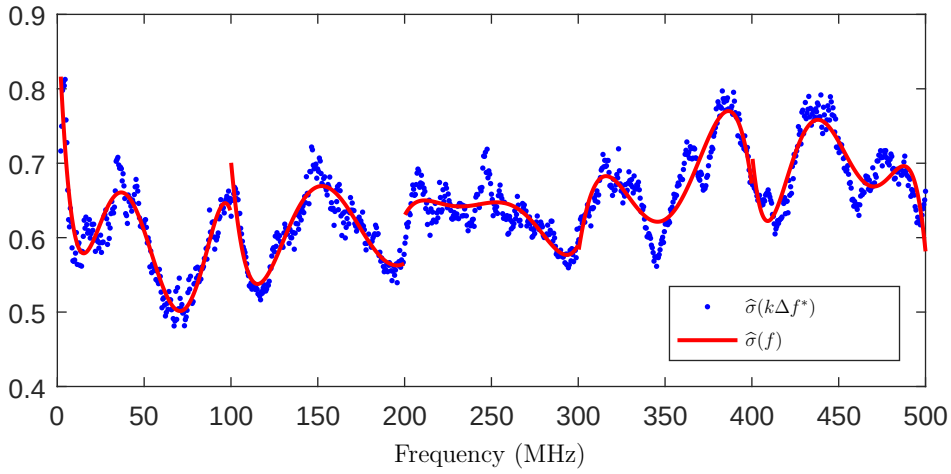

(b)

Figure 24: Parameters of a Log-logistic distribution used to model the resistance: (a) log mean and (b) log scale parameters.

Fig. 26 shows the magnitude of the access impedance autocorrelation for $\widehat{Z}_{pl}[k]$, $Z_{pl,1}[k]$ and $Z_{pl,2}[k]$, where the last one is obtained as described in the forth step of the procedure presented in Section 3.2 by using a low-pass digital filter expressed by

$$w[k] = e^{-\left|k-\frac{N-1}{2}\right|\frac{1}{\tau}} \tag{3.14}$$

in which this digital filter is an exponential window that is used to mimic the autocorrelation among samples of $Z_{pl,1}[k]$, $k = 0, 1, \cdots, N$, $\tau = 8.69N/2D$, $N = 21$, and $D = 79$. Note that this filter inserts correlation on $Z_{pl,1}[k]$ and the correlation curves of the filtered model ($Z_{pl,2}[k]$) and the data set ($Z_{pl,1}[k]$) are similar for sample shift from 0 up to 20 samples. It indicates that this access impedance model is valid in terms of autocorrelation for sample shift up to 20 samples.

By following the procedure described in the fifth step of the procedure outlined

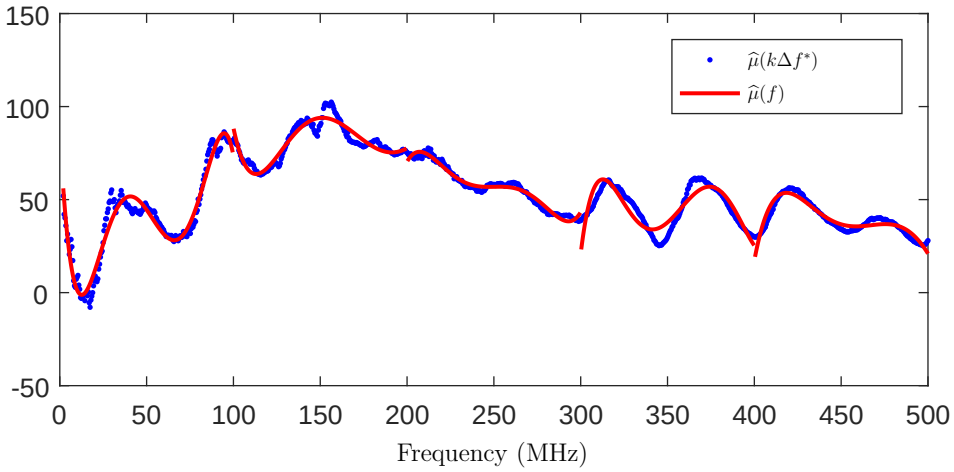

(a)

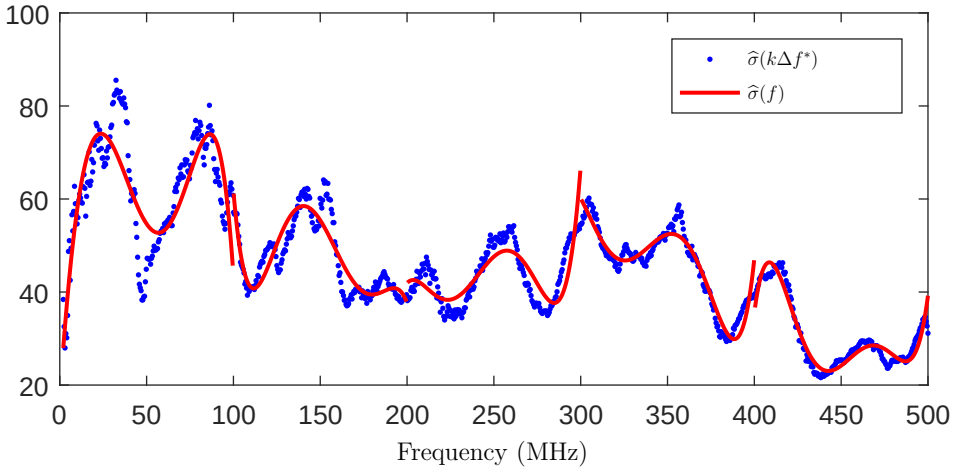

(b)

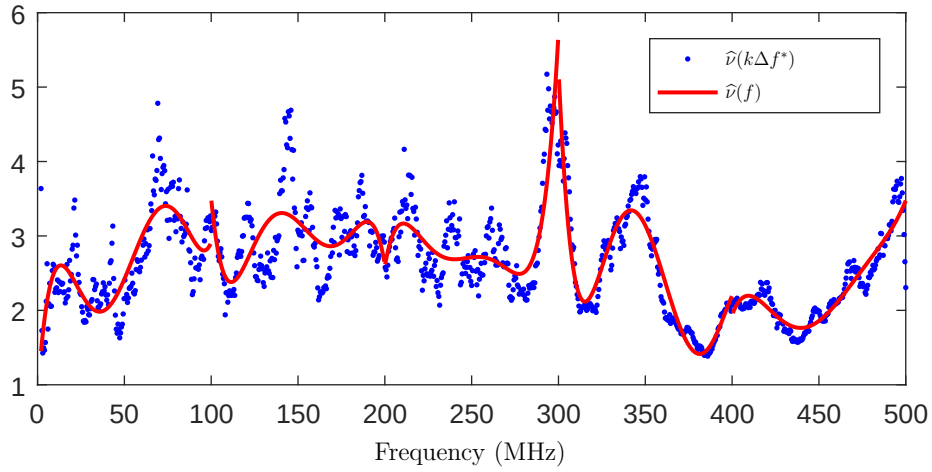

(c)

Figure 25: Parameters of a Log-logistic distribution used to model the reactance: (a) location, (b) scale and (c) shape parameters.

in Section 3.2 we found $Z_m^{opt} = 0.19$ and $Z_a^{opt} = -12 - j6$. In this sense, Fig. 27 shows the mean value of resistance and reactance components of $\widehat{Z}_{pl}[k]$, $Z_{pl,1}[k]$, and

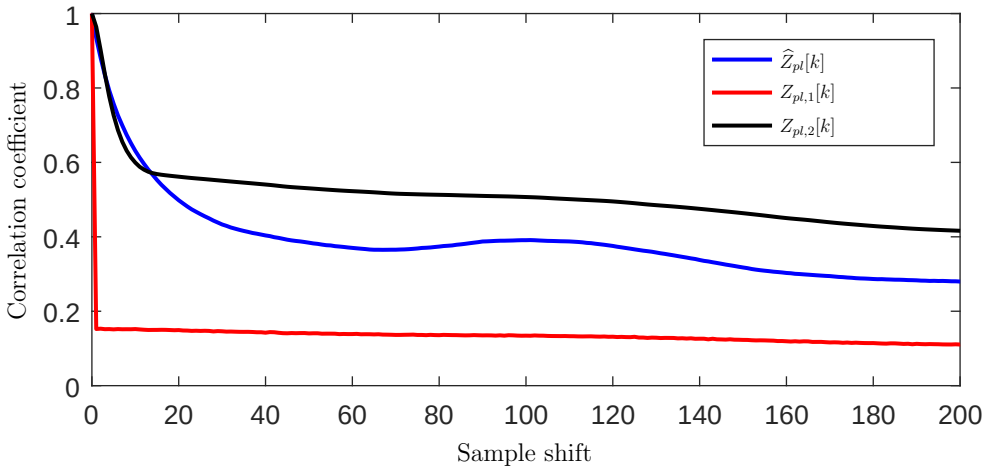

Figure 26: Magnitude of the access impedance autocorrelation for the data set ($\widehat{Z}_{pl}[k]$), the model before filtering ($Z_{pl,1}[k]$) and after filtering ($Z_{pl,2}[k]$).

$Z_{pl}^{m}[k]$. Note that $Z_{pl}^{m}[k]$ does not have offset in relation to $\widehat{Z}_{pl}[k]$. Therefore, $Z_{pl}^{m}[k]$ can be interpolated to obtain $Z_{pl}^{m}(f)$ and used to model the access impedance of in-home, broadband and LV electric power grid in the frequency band from 2 MHz up to 500 MHz.

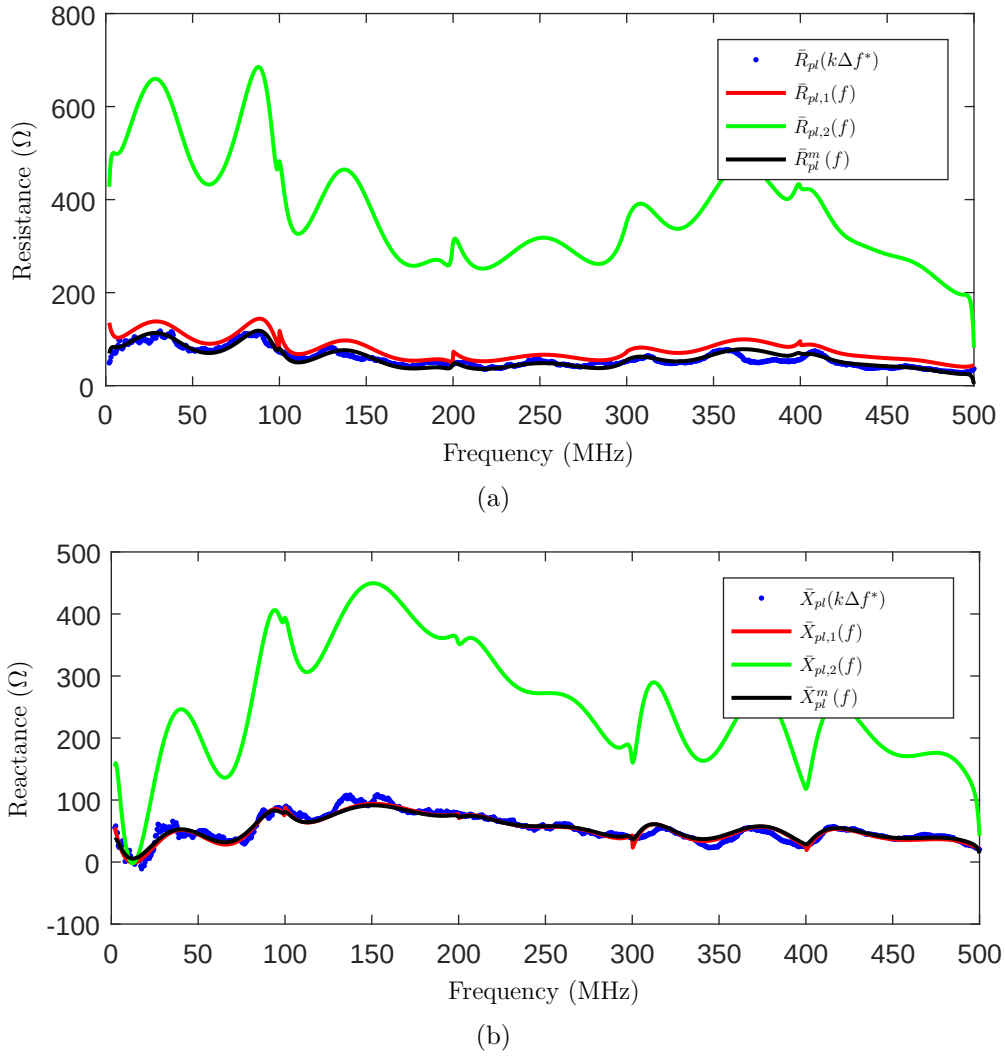

Figure 27: Mean value of resistance (a) and reactance (b) in different steps of the proposed procedure described in Section 3.2.

3.4 SUMMARY

This Chapter have discussed measurement, characterization and modeling the statistical analysis of the access impedance in-home of electric power grid. The statistical analysis was motivated by the fact that access impedance is time and frequency varying and affect the impedance matching between the PLC transceiver and electric power grid. In Chapter 5, we will exploit the discussed information to introduce adaptive PLC coupling circuit.

Table 3: Coefficients of the fifth degree polynomial for modeling the parameters of the resistance component.

Frequency Band (MHz)	Parameter	p_0	p_1	p_2	p_3	p_4	p_5
$2 < \|f\| \leq 100$	$\widehat{\mu}(f)$	-3.15×10^{-10}	-3.09×10^{-7}	7.22×10^{-5}	-5.06×10^{-3}	1.28×10^{-1}	3.12×10^{0}
	$\widehat{\sigma}(f)$	-3.07×10^{-9}	8.41×10^{-7}	-8.22×10^{-5}	3.44×10^{-3}	-5.85×10^{-2}	9.20×10^{-1}
$100 < \|f\| \leq 200$	$\widehat{\mu}(f)$	-5.89×10^{-9}	4.41×10^{-6}	-1.30×10^{-3}	1.88×10^{-1}	-1.34×10^{1}	3.78×10^{2}
	$\widehat{\sigma}(f)$	-5.50×10^{-10}	4.73×10^{-7}	-1.59×10^{-4}	2.63×10^{-2}	-2.12×10^{0}	6.74×10^{1}
$200 < \|f\| \leq 300$	$\widehat{\mu}(f)$	-1.19×10^{-9}	1.64×10^{-6}	-8.92×10^{-4}	2.40×10^{-1}	-3.19×10^{1}	1.69×10^{3}
	$\widehat{\sigma}(f)$	4.88×10^{-10}	-6.04×10^{-7}	2.97×10^{-4}	-7.29×10^{-2}	8.89×10^{0}	-4.31×10^{2}
$300 < \|f\| \leq 400$	$\widehat{\mu}(f)$	5.47×10^{-9}	-9.33×10^{-6}	6.34×10^{-3}	-2.15×10^{0}	3.63×10^{2}	-2.44×10^{4}
	$\widehat{\sigma}(f)$	-5.60×10^{-11}	3.33×10^{-8}	2.19×10^{-5}	-2.33×10^{-2}	6.77×10^{0}	-6.55×10^{2}
$400 < \|f\| \leq 500$	$\widehat{\mu}(f)$	1.03×10^{-8}	-2.33×10^{-5}	2.10×10^{-2}	-9.44×10^{0}	2.12×10^{3}	-1.90×10^{5}
	$\widehat{\sigma}(f)$	-2.24×10^{-9}	5.05×10^{-6}	-4.55×10^{-3}	2.05×10^{0}	-4.60×10^{2}	4.12×10^{4}

Table 4: Coefficients of the fifth degree polynomial for modeling the parameters of the reactance component.

Frequency Band (MHz)	Parameter	p_0	p_1	p_2	p_3	p_4	p_5
$2 < \|f\| \leq 100$	$\widehat{\mu}(f)$	-1.07×10^{-6}	2.85×10^{-4}	-2.72×10^{-2}	1.11×10^{0}	-1.71×10^{1}	8.6×10^{1}
	$\widehat{\sigma}(f)$	-1.49×10^{-7}	1.94×10^{-5}	5.49×10^{-4}	-1.51×10^{-1}	5.45×10^{0}	1.77×10^{1}
	$\widehat{\nu}(f)$	1.91×10^{-8}	-5.21×10^{-6}	5.05×10^{-4}	-2.05×10^{-2}	3.24×10^{-1}	8.82×10^{-1}
$100 < \|f\| \leq 200$	$\widehat{\mu}(f)$	1.02×10^{-4}	1.02×10^{-4}	-3.39×10^{-2}	5.51×10^{0}	-4.38×10^{2}	1.37×10^{4}
	$\widehat{\sigma}(f)$	-2.49×10^{-7}	1.94×10^{-4}	-5.98×10^{-2}	9.06×10^{0}	-6.75×10^{2}	1.98×10^{4}
	$\widehat{\nu}(f)$	-1.63×10^{-8}	1.25×10^{-5}	-3.76×10^{-3}	5.59×10^{-1}	-4.10×10^{1}	1.19×10^{3}
$200 < \|f\| \leq 300$	$\widehat{\mu}(f)$	1.98×10^{-7}	-2.48×10^{-4}	1.24×10^{-1}	-3.06×10^{1}	3.77×10^{3}	-1.85×10^{5}
	$\widehat{\sigma}(f)$	2.04×10^{-7}	-2.47×10^{-4}	1.19×10^{-1}	-2.85×10^{1}	3.40×10^{3}	-1.61×10^{5}
	$\widehat{\nu}(f)$	1.47×10^{-8}	-1.81×10^{-5}	8.85×10^{-3}	-2.16×10^{0}	2.62×10^{2}	-1.27×10^{4}
$300 < \|f\| \leq 400$	$\widehat{\mu}(f)$	3.72×10^{-7}	-6.66×10^{-4}	4.76×10^{-1}	1.69×10^{2}	3.01×10^{4}	-2.13×10^{6}
	$\widehat{\sigma}(f)$	1.61×10^{-7}	-2.73×10^{-4}	1.85×10^{-1}	-6.23×10^{1}	1.05×10^{4}	-7.02×10^{5}
	$\widehat{\nu}(f)$	-1.90×10^{-8}	3.43×10^{-5}	-2.47×10^{-2}	8.86×10^{0}	-1.58×10^{3}	1.13×10^{5}
$400 < \|f\| \leq 500$	$\widehat{\mu}(f)$	8.46×10^{-8}	-2.01×10^{-4}	1.90×10^{-1}	-8.93×10^{1}	2.10×10^{4}	-1.97×10^{6}
	$\widehat{\sigma}(f)$	2.64×10^{-7}	-5.97×10^{-4}	5.38×10^{-1}	-2.42×10^{2}	5.45×10^{4}	-4.90×10^{6}
	$\widehat{\nu}(f)$	3.95×10^{-9}	-9.02×10^{-6}	8.24×10^{-3}	-3.76×10^{0}	8.55×10^{2}	-7.77×10^{4}

4 DESIGN AND CHARACTERIZATION OF NON-ADAPTIVE CAPACITIVE COUPLER

According to Chapter 2, a PLC coupling circuit is a very important component of a PLC transceiver due to several reasons, such as prevention of to damages caused by mains signal and disturbances originated from the electric power grid and maximization of power transfer between the PLC transceiver and the electric power grid, among others. In spite of its importance, the majority of the contributions address superficially the design of PLC coupling circuits [44,140]. Maybe, the problem is the fact that PLC coupling circuits can be very different in accord with the classification introduced in Chapter 2. Paying attention to the low-voltage and in-home electric power grid, it is clear that the PLC coupling circuit without impedance matching adaptation has not been recognized as a relevant research problem by PLC community [96, 141] because the use of passive components can be easily and effectively used to design low-cost and simple PLC coupling circuits [48], which are demanded by the market. As a result, it is quite difficult to find in the literature designs of PLC coupling circuits to carry out researches in the PLC field by correctly and efficiently taking into account PLC signal injection and extraction into/from the electric power grid.

In order to overcome this problem, this chapter focuses on the design of capacitive, SISO and LV PLC coupling circuits for both broadband and narrowband applications. Broadband PLC deals with frequencies above 1.7 MHz, while narrowband PLC deals with frequencies bellow 500 kHz. In this Chapter, the following narrowband and broadband frequency bands are covered: 9 kHz-500 kHz, 1.7-50 MHz , 1.7-100 MHz and 1.7-500 MHz. Moreover, it discusses the prototypes of the designed PLC coupling circuits to work with the aforementioned frequency bands, which ones can be easily reproduced and used to interface with any PLC transceiver, data acquisition and waveform signal generation equipment suitable for LV electric power grid [2, 106, 142–144].

This Chapter is organized as follows: Section 3.1 focuses on the specification and design of PLC coupling circuits, while Section 3.2 addresses the prototypes of PLC coupling circuits and the results obtained by measuring their scattering parameters.

The Chapter ends with a Summary Section.

4.1 SPECIFICATION AND DESIGN

Almost all the characteristics that are to be sought in the design of a capacitive, SISO, and LV PLC coupling circuit has been discussed in Section 2. Essentially, narrowband (Fig. 28) and broadband (Fig. 29) PLC coupling circuits consist of four basic blocks, which are electrical protection, analog high-pass filter (C_{BLOCK} capacitor), galvanic isolation (RF transformer with 1:1 windings ratio), and analog low-pass filter (5^{th} order analog elliptic filter). The analog elliptic filter has a short transition frequency band, which makes it ideally suitable for dealing with analog-to-digital converters that operate close to the Nyquist sampling frequency or close to the critical sampling frequency. Furthermore, the ripple effect in the band-pass is distributed across both the band-pass and stop-band elliptic filters, making it an excellent candidate for being used in a PLC coupling circuits. Note that the ripple in the band-pass is not a relevant issue because it is small and a PLC transceiver applies equalization when the coherent digital modulation scheme. The capacitor presents a very high impedance to the 50/60 Hz mains signal and allows high-frequency signals to pass through it by offering very low impedance to high-frequency components. While the purpose of the transformer is to provide electrical isolation, the combination of the analog high-pass filter (C_{BLOCK}) and the analog low-pass filter compose a band-pass filter that eliminates high power mains signal and high-frequency signals, which are out of band of interest.

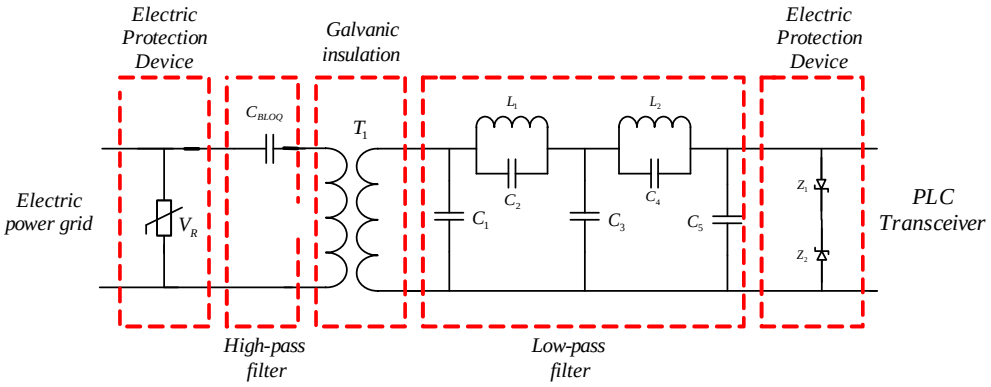

Figure 28: The block diagram of the narrowband, capacitive, SISO and LV PLC coupling circuit.

Narrowband PLC couplers are defined herein as those that allow the injection and the extraction of signals in the frequency range $|f| \leq 500$ kHz, following the IEEE 1901.2 Standard [145]. This standard contemplates narrowband data commu-

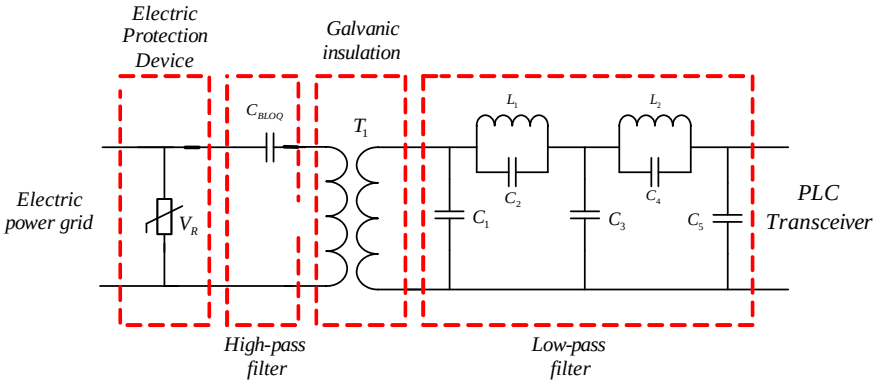

Figure 29: The block diagram of the broadband, capacitive, SISO and LV PLC coupling circuit.

nication (i.e., between 9kHz and 500 kHz) through electric power grids, supporting communications over LV (the line between transformer and meter, less than 1 kV), MV (1 kV up to 72 kV) and through LV/MV transformer. Data rates can be scalable up to 500 kbps, depending on the application requirements. This standard applies to data communication among equipment in the electric power grids (i.e., meter, transformers) and substations, electric vehicle and charging station, and home area networking communications scenarios. Lighting and solar panel are also potential uses of this standard. This standard defines detailed mechanisms for coexistence between different standards, ensuring that the desired data rates may be delivered and the coexistence may be correctly exploited.

Broadband PLC couplers are defined as those that allow the injection and extraction signals in the frequency range between fmin = 1.7 MHz and fmax = 500 MHz [139]. They allow PLC transceivers inject signals into the electric power grids by considering a large frequency bandwidth, consequently, data communication at high data-rates .are accomplished. Frequency bandwidths for broadband PLC coupler devices are 1.7-30 MHz in Europe, 1.7-50 MHz in Brazil, and 1.7-86 MHz in the USA. According to the Brazilian Telecommunication Regulatory Agency (ANATEL), the allowed frequency band for broadband PLC systems is between 1.705 and 50 MHz, see Resolution 527 of 8 April of Agência Nacional de Telecomunicações (ANATEL) [146].

When designing a prototype of a PLC coupling circuit, inductors, capacitors, protection components, connectors and PCB need to be carefully chosen for attaining performance that agrees with the target specification. In fact, the mains signal and the PLC signal work with a distinct voltage, currents, and frequencies and the design of a PLC coupling circuit that properly succeeds in dealing with these differences is of great interest.

In this context, to connect the PLC coupling circuit to the electric power grid, the chosen connector was the KRE connector. The KRE connector works with voltages levels as high as 250 V_{rms} and a maximum current of 15 A. The maximum wire size it handles is 12 AWG and makes use of plated-through holes (PTH). Dimensions in (mm) and the photo of the KRE connector is shown in Fig. 30.

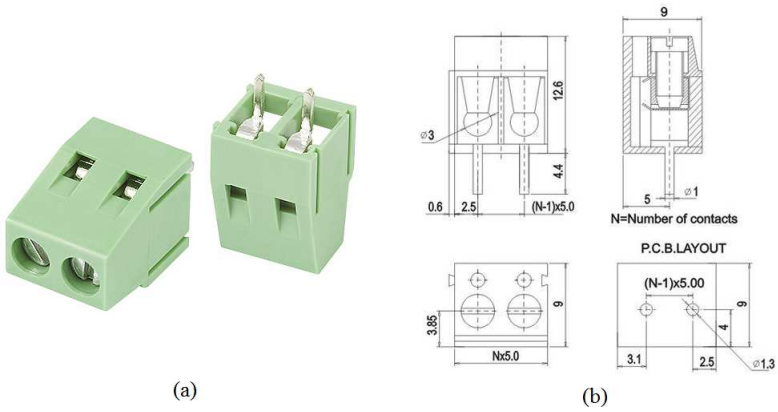

Figure 30: (a) Photo of the chosen KRE connector. (b) dimensions in (mm) of the chosen KRE connector.

Moreover, we have adopted (SubMiniature version A) SMA connectors, which are semi-precision coaxial RF connectors, which is applied to inject/extract signal to the PLC transceiver. In fact, SMA type of connector has aimed the use from DC to 18 GHz with an impedance equal to 50 Ω. A standard-polarity SMA female connector has a center sleeve surrounded by a barrel with outside threads. The pad dimensions in (mm) and the photo of the SMA connector is shown in Fig. 31.

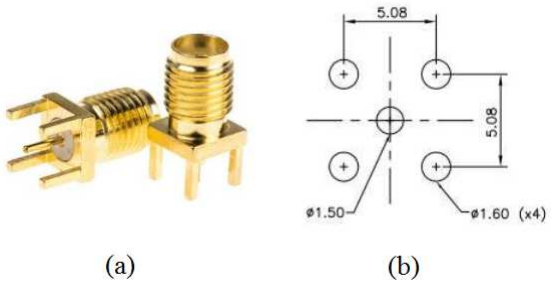

Figure 31: (a) Photo of the chosen SMA connector. (b) dimensions in (mm) of the chosen SMA connector.

Electrical protection is an essential part of a PLC coupling circuit. The effects of the surges, lightning, inductive switching, a fault in electrical installation and over-voltages can damage PLC transceivers if protection countermeasures are not considered. Protection diverts the surge currents to the ground and reduces the amplitude of the

transient over voltages to a safe level, thus protector the PLC transceivers from damage. However, as discussed in Sub-section 2.1.6, the protection components must be chosen so that they introduce as small as possible distortions into the transmitted/received signals by PLC transceivers [86]. In order to protect the PLC transceiver from surges, the SPD component is chosen and installed at the entrance of the PLC coupling circuit, between phase and neutral line after the KRE connector, see Figs. 28 and 29. Also, in narrowband PLC coupling circuit, Zener diodes must be installed to protect PLC transceiver against surges that were not heavily attenuated by the SPD component.

The SPD components chosen for the narrowband PLC coupling circuit prototype is the MOV with de clamped voltage of 250 V_{rms} and the Zener diode with voltage protection of 5.6 V_{cc}. For broadband PLC coupling circuit the chosen SPD is the GDT with the spark over-voltage of 420 V_{rms} [147]. Fig. 32 shows the photos of the SPD components used in the design of such PLC coupling circuits.

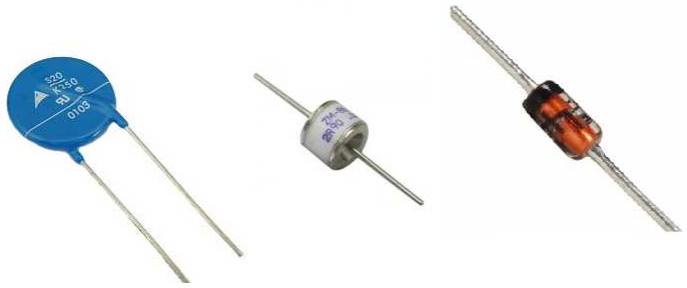

(a) (b) (c)

Figure 32: Photos of the chosen SPD components: (a) MOV, (b) GDT and (c) Zener diode.

The effectiveness of C_{BLOCK} capacitor for coupling PLC transceivers to the electric power grid are very important. In fact, the C_{BLOCK} capacitor is a most critical component of a PLC coupling circuit because it has two primary functions: to block the low-frequency mains signal (commonly 50 Hz or 60 Hz) and to offer low impedance to the PLC signal. For designing C_{BLOCK} capacitors for both narrowband and broadband we must pay attention to the SRF of the used capacitor to avoid significative distortion on the transmitted signal. In other words, one must ensure that the SRF is higher than the chosen maximum frequency of operation. A SMD ceramic capacitor component with size 1008 was adopted for both narrowband and broadband designs because its SRF is equal to 1 GHz. Also, this capacitor offers an isolation voltage of 1 kV [148]. Finally, but not the least, the values of the capacitor used in both narrowband and broadband PLC coupling circuits were specified in accord with the minimum frequency

of operation (9 kHz and 1.7 MHz) of the target PLC coupling circuits.

It is well established that RF transformers are often used to provide galvanic isolation between primary and secondary windings and impedance matching between the electric power grid and PLC transceiver [149], see Sub-section 2.1.3. In fact, the RF transformer must provide flat insertion loss and low return loss in the band of frequency of interest for both narrowband and broadband PLC coupling circuits. The RF transformer used in the proposed PLC coupling circuits have the transformation ratio equal to 1:1. In other words, the RF transformer does not change the impedance matching between PLC transceiver and the electric power grid. Therefore, the input impedance seen by the electric power grid is the input impedance of the designed analog low-pass filter which is located after the RF transformer. Note that the analog low-pass filter was designed to offer impedance equal to 50 Ω. Fig. 33 shows the photos of RF transformers used in the PLC coupling circuits. Actually, Fig. 33(a) shows the RF SMD transformer for the designed PLC coupling circuit covering the frequency band of 9-500 kHz, 1.7-50 MHz and 1.7-100 MHz, while Fig. 33(b) shows the RF transformer used to design PLC coupling circuit for the frequency bandwidth between 1.7 and 500 MHz. The RF transformers in Fig. 33(a) has flat insertion loss in the range of frequency 0.005-100 MHz with 500 V_{rms} inter-winding isolation, maximum of 1/4 Watt RF input power and 250 mA maximum current rating, see detail in [150]. On the other hand, the RF transformer in Fig. 33(b) has the maximum current rating equal to 30 mA, maximum of 1/4 Watt RF input power and flat insertion loss in the frequency band of 0.4-500 MHz, see [151].

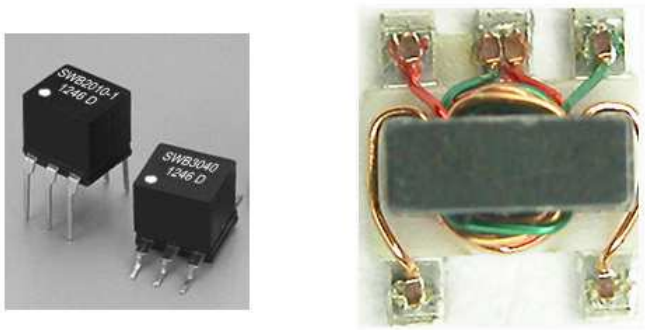

(a) (b)

Figure 33: Photos of chosen RF transformers: (a) frequency band of 0.005-100 MHz (b) frequency band of 0.4-500 MHz.

Due to the short transition bandwidth requirement, the chosen analog low-pass filter is elliptic. It is specified by requiring values for the band-pass ripple, stop-band

ripple and the sharpness of the transition bandwidth and it is obtained with a smaller number of inductors and capacitors compared to Butterworth and Chebyshev analog filters [152]. The elliptic analog low-pass filter was designed using the ADS software by imposing that input and output impedances are equal to 50 Ω [11].

Due to the high frequencies operation of broadband PLC coupling circuits, passive SMD components were chosen to design the analog low-pass filters because they have low resistance and inductance at the connection with the PCB and, as a consequence, unwanted RF radiation is minimized, better performance in high-frequency operation is obtained and small size prototypes are designed. Also, the choice of passive SMD components for prototyping the analog low-pass elliptic filter is mainly based on the SRF. In this context, the analog low-pass elliptic filter was implemented using inductors of high-quality factor efficiency and capacitors of high stability [153]. All inductors and capacitors components have a size of 1008 and SRF equal to 1 GHz. Fig. 34 illustrates typical SMD components used in the design of the analog low-pass elliptic filter.

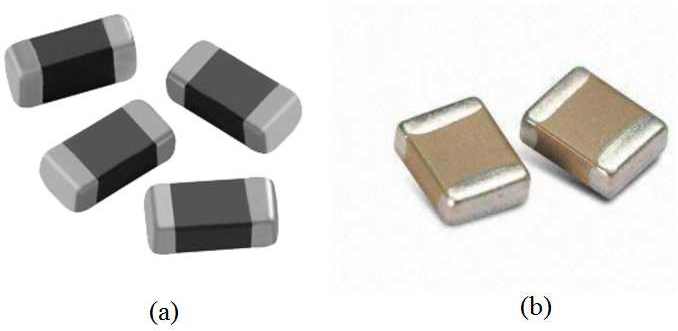

Figure 34: Photos of chosen SMD components with size of 1008: (a) inductor and (b) capacitor

Regarding the PCB for high-frequency signals, there are many aspects to consider such as skin effect, the impedance of tracks and ground planes. For a PCB with a ground plane layer adjacent to the signal layer, we have a well-defined impedance that is determined by the geometry of the track, the thickness of the board layer that separates the track from the ground plane, the dielectric constant (ε_r) material of PCB, and the frequency of the PLC signal. PCB transmission line consists of a single conductor track on one side of a dielectric substrate and a single ground plane on the other side. This allows the characteristic impedance of the line to be controlled by defining the dimensions in a single plane. By taking into account the chosen frequency

bands, we state that the track width w of a conductor in a PCB can be obtained with

$$w = \frac{7.48h}{e^{\left(Z_0 \frac{\sqrt{\varepsilon_r}+1.41}{87}\right)}} - 1.25T, \tag{4.1}$$

where h is the dielectric thickness, T is the track thickness, ε_r is the dielectric constant of the PCB and Z_0 is the characteristic impedance of the conductor. The narrowband and broadband PLC coupling circuits were designed using a PCB two-layer fiberglass with h=1.5 mm, T=0.1 mm, ε_r=6.0 and the characteristic impedance equal to 50 Ω. Thus, the track width that guarantees the characteristic impedance equal to 50 Ω is 2 mm.

A ground plane is often designed to cover most of the area of PCB which is not occupied by the track circuit. In a microstrip technique, there is a separate ground layer covering the entire board. This serves to facilitate the design of a PCB, allowing the designer to ground any component without having to run additional tracks and to provide an image plane for RF return currents created in the top layer and bottom layer. The ground plane also conducts the large return currents from many components without significant voltage drops, ensuring that the ground connection of all the components is at the same reference potential. In the PCB design, the length of tracks must be designed as short as possible, in an effort to reduce the additional inductance, power losses, low attenuation, and signal reflections to keep the characteristic impedance of them in 50 Ω and the small dimensions of a PCB. In this work, the tracks of PCB were designed with the bend of 45° to ensure less inductance in the connections among components and to minimize impedance mismatching [154]. The design of PCB was carried out by using the Altium software [155]. All prototypes of PCB were designed using the fiberglass material as a substrate.

In order to measure the insertion loss and return loss of the narrowband and broadband capacitive, SISO and LV PLC coupling circuit, the VNA instrument is used to measure the scattering parameters with the reference impedance of 50 Ω. The chosen VNA instrument is the Agilent E5061B [156].

4.2 PROTOTYPES OF PLC COUPLERS

This section describes, the prototypes of capacitive, SISO and LV PLC coupling circuits. As it was discussed in the introduction of this Chapter, these prototypes work in the following frequency bands:

- narrowband: 9 kHz-500 kHz.
- broadband: 1.7 MHz-50 MHz.
- broadband: 1.7 MHz-100 MHz.
- broadband: 1.7 MHz-500 MHz.

This Sub-section is organized as follows: Sub-section 4.2.1 focuses on the prototype of narrowband PLC coupling circuit and the Sub-sections 4.2.2, 4.2.3 and 4.2.4 discusses the prototype of broadband PLC coupling circuits in the frequency bands of 1.7-50 MHz, 1.7-100 MHz and 1.7-500 MHz, respectively.

4.2.1 NARROWBAND PLC COUPLER 9 KHZ TO 500 KHZ

The schematic of the narrowband, capacitive, SISO and LV coupling circuit (9-500 kHz) designed with the ADS software is shown in Fig. 35. It covers four essential parts: protection, analog high-pass filter, galvanic isolation and analog low-pass filter. According to this figure, the first stage of protection is constituted by MOV device (V_{R1}) which is placed before the C_{BLOCK} capacitor and is directly connected to the electric power grid. The second stage of electric protection is composed of Zener diodes (Z_1 and Z_2) placed after the analog low-pass filter. Note that, J_1 denotes the KRE connector used to connect the PLC coupling circuit to the outlet of the electric power grid, with a power cable, while J_2 is a typical RF SMA connector, which is used to connect a PLC transceiver or equipment to the PLC coupling circuit. The capacitor C_6 is the blocking capacitor (C_{BLOCK}) that works as an analog high-pass filter, which is connected in series with the RF transformer T_1. The RF transformer (T_1) used is the WB1010-PCL component, see [150]. The capacitors C_1 to C_5 and inductors L_1 and L_2 constitutes the analog low-pass filter. Tab. 5 presents the adopted specifications to design the narrowband and analog low-pass elliptic filter, while Tab. 6 lists the values of components obtained by using ADS software.

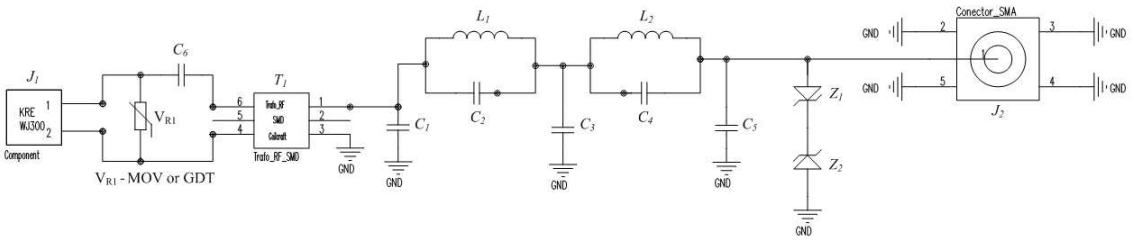

Figure 35: Schematic of the narrowband, capacitive, SISO and LV PLC coupling circuit.

Table 5: Specifications of the narrowband analog low-pass filter.

Description	Value
Input impedance Z_{in}	50 Ω
Output impedance Z_{out}	50 Ω
Type of filter	Elliptic
Passband ripple	0.5 dB
Stopband attenuation	40 dB
Cut-off frequency (f_c)	500 kHz
Maximum insertion loss	-15 dB

Table 6: Details of components used in the prototype of the PLC coupling circuit.

Component	Value	Maximum Voltage (V)	Maximum current (mA)	Frequency band (MHz)
V_{R1}		250 V_{rms}		
Zener diode		5.6 V_{cc}	7.2	35
T_1	WB1010-PCL	500 V_{cc}		0.005-100
C_{BLOQ}	330 nF	1k V_{rms}		0-900
C_1	10 nF	50 V_{rms}		0-900
C_2	6,8 nF	50 V_{rms}		0-900
C_3	2,2 nF	50 V_{rms}		0-900
C_4	15 nF	50 V_{rms}		0-900
C_5	10 nF	50 V_{rms}		0-900
L_1	10 μH		150	0-20
L_2	15 μH		120	0-15

The top and bottom of the PCB of the narrowband, capacitive, SISO and LV PLC coupling circuit (9 kHz to 500 kHz), which was designed in Altium Software, are shown in Fig. 36. Note that this PCB was designed following the microstrip technique discussed in Section 4.1. The two-layer fiberglass PCB was made up of solder mask which is a thin lacquer-like layer of polymer that is usually applied to the copper tracks of PCB for protection against oxidation and to prevent solder bridges from forming between closely spaced solder pads. The pad of RF transformer T_1 was designed to solder both SMD or PTH and the capacitors C_1 to C_6 and inductors L_1 and L_2 was designed for pad size 1008. The bottom and top layers of the designed PCB are shown in Fig. 36(a) and Fig. 36(b) respectively, while the prototype of this narrowband PLC coupling circuit is shown in Fig.37.

Fig. 38 shows the insertion loss ($S_{21}(f)$ scattering parameter) magnitudes and return loss ($S_{11}(f)$ and $S_{22}(f)$ scattering parameters) of the prototyped PLC coupling circuit. The insertion loss ($S_{21}(f)$ scattering parameter) was omitted, because $S_{21}(f)$=$S_{21}(f)$. This equality appears due to the fact that the access impedance of the VNA equipment is equal to 50 Ω. Note that, the insertion loss will be equal to the sum

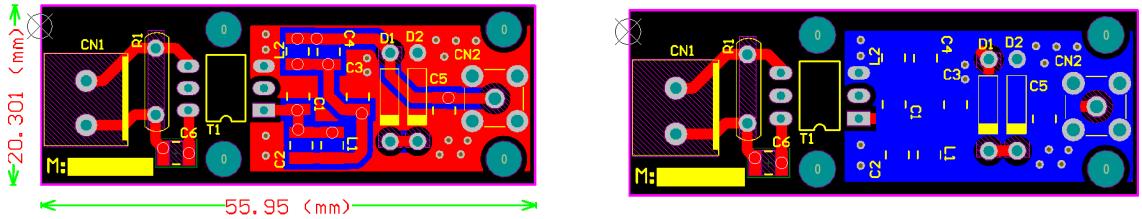

(a) Top layer plane (b) Bottom layer plane

Figure 36: The PCB of the narrowband PLC coupling circuit.

(a) Top layer plane (b) Bottom layer plane

Figure 37: The prototype of the narrowband capacitive, SISO and LV PLC coupling circuit.

of three loss factors. One is the loss due to the impedance mismatching at the PLC coupling circuit input, the second is due to the impedance mismatching at the PLC coupling circuit output and the third is due to the dissipative loss associated with each reactive characteristic of the components used in the PLC coupling circuit.

Regarding Fig. 38, we note that the magnitude of the insertion loss, $S_{21}(f)$, varies between 0 and -5 dB in the frequency band of 9-500 kHz. The measured cut-off frequency, the point at which the insertion loss $S_{21}(f)$ drops with a slope of -6 dB, is 528 kHz. The magnitude of return loss, $S_{11}(f)$, exhibits several ripples in the reflection coefficients between -6 dB in the frequency of 200 kHz and -10.5 dB in the frequency of 12 kHz. Moreover, for the magnitude of return loss, $S_{22}(f)$, the reflection coefficients fluctuates between -6 dB in the frequency of 200 kHz and -22 dB in the frequency of 390 kHz. In the stop-band, 40 dB of attenuation was measured which satisfies the design specifications listed in Tab. 6. Regarding the rejection of the mains signal, an attenuation of 50 dB is attained using the C_{BLOCK} capacitor.

4.2.2 BROADBAND PLC COUPLER 1.7 MHZ TO 50 MHZ

This Sub-section aims to give a comprehensive analysis of broadband, capacitive, SISO and LV PLC coupling circuit (1.7 MHz to 50 MHz). The schematic of the PLC coupling circuit designed in the ADS software is shown in Fig. 39. According to this figure, the first stage of protection is constituted by the GDT device (V_{R1}),

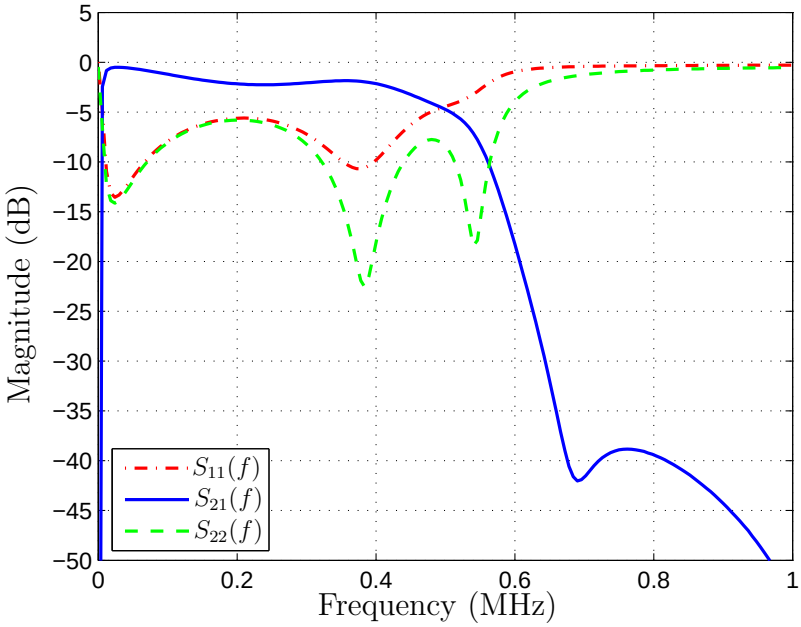

Figure 38: Insertion loss and return loss of the PLC coupling circuit prototype.

with suppression voltage of 420 V_{rms}, which is placed before the C_{BLOCK} capacitor and directly connected to the electric power grid [147]. However, for PLC coupling circuit with the frequencies above 30 MHz the capacitance and impedance values of MOV, transient voltage suppressor (TVS) and Zener diode severely impact on the insertion loss $S_{21}(f)$ scattering parameter, and should be avoided by all means, as discussed in Sub-section 2.1.6. The RF transformer T_1, connectors J_1 and J_2, capacitors C_1 to C_5, inductors L_1, L_2 and C_{BLOCK} are the same components discussed in Sub-section 4.2.1. Tab. 7 lists the used specification to design the broadband analog and low-pass elliptic filter. The values of components designed using ADS Software are listed in Tab. 8.

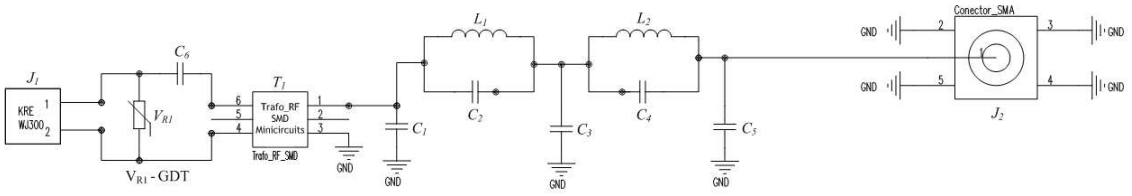

Figure 39: Schematic of the electronic circuit of the broadband, capacitive, SISO and LV PLC coupling circuit.

The top and bottom of the two-layer fiber glass PCB shown in Fig. 40 follows the same design discussed in the Sub-section 4.2.1 using the microstrip technique designed in Altium software. However, as the frequency increases the complexity of the design of PCB increases (i.e., skin depth is frequency-dependent; at lower frequencies, the RF current will use more of the cross-sectional area of a track than at higher frequencies).

Table 7: Specifications of the broadband analog low-pass filter.

Description	Value
Input impedance Z_{in}	50 Ω
Output impedance Z_{out}	50 Ω
Type of filter	Elliptic
Passband ripple	0.5 dB
Stopband attenuation	40 dB
Cut-off frequency (f_c)	50 MHz
Maximum insertion loss	-15 dB

Table 8: Details of components used in the prototype of the PLC coupling circuit.

Component	Value	Maximum Voltage (V)	Maximum current (mA)	Frequency band (MHz)
V_{R1}		420 V_{rms}		
T_1	WB1010-PCL	500 V_{cc}		0.005-100
C_{BLOQ}	1.5 nF	1k V_{rms}		0-900
C_1	100 pF	50 V_{rms}		0-2600
C_2	10 pF	50 V_{rms}		0-8000
C_3	130 pF	50 V_{rms}		0-2200
C_4	33 pF	50 V_{rms}		0-3000
C_5	82 pF	50 V_{rms}		0-2900
L_1	180 nH		620	0-750
L_2	150 nH		800	0-800

To prevent such effects, the design of the PCB was carried out to reduce power loss and to keep the impedance of the transmission line of the PCB equal to 50 Ω. The prototype of the broadband PLC coupling circuit is shown in Fig.41.

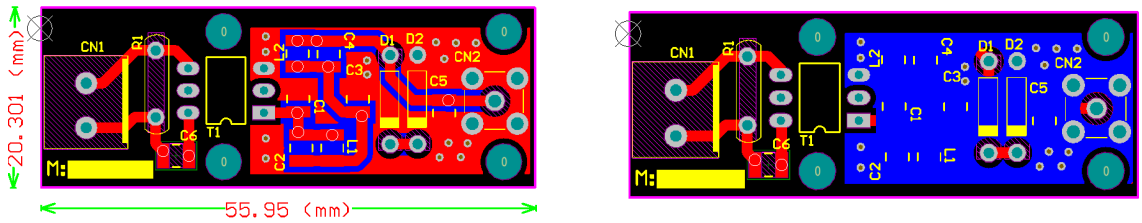

(a) Top layer plane (b) Bottom layer plane

Figure 40: The PCB of the broadband PLC coupling circuit.

Fig. 42 shows insertion loss, $S_{21}(f)$, and return loss, $S_{11}(f)$ and $S_{22}(f)$. The magnitude of the insertion loss $S_{21}(f)$ scattering parameters, exhibits a ripple varying between 0 and -2 dB in the frequency band of 1.7-48 MHz and in the frequency band of 48-50 MHz the cutback of insertion loss is -5 dB. Beyond the cut-off frequency of 50 MHz, we see a relatively sharp roll-off, slightly faster near the cut-off frequency, where the insertion loss drops with a slope of -6 dB, measured at the frequency of

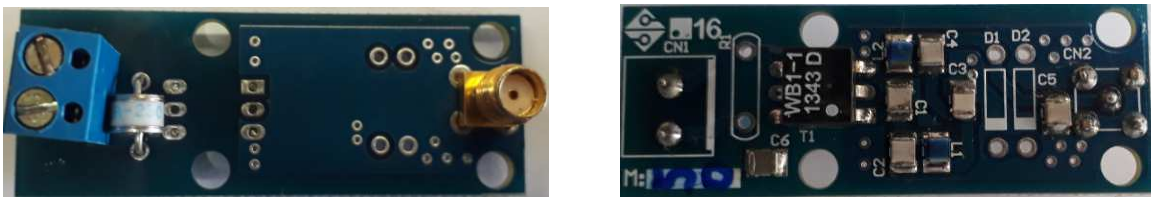

(a) Top layer plane (b) Bottom layer plane

Figure 41: The prototype of the broadband capacitive, SISO and LV PLC coupling circuit.

50.25 MHz. The magnitude of return loss, $S_{11}(f)$, fluctuates between -6 dB in the frequency of 2.5 MHz and -25 dB in the frequency of 46 MHz. Moreover, for the magnitude of $S_{22}(f)$ return loss fluctuates between -6 dB in the frequency of 1.7 MHz and -29 dB in the frequency of 32 MHz. We also observe that the magnitude of $S_{11}(f)$ and $S_{22}(f)$ scattering parameters approach to 0 dB in the stop-band, meaning that the incoming signal is reflected back. In the stop-band, the designed minimum attenuation of 40 dB is measured satisfying the design specifications for the stop-band. Regarding the rejection of the mains signal, an attenuation of 50 dB is attained using the C_{BLOCK} capacitor.

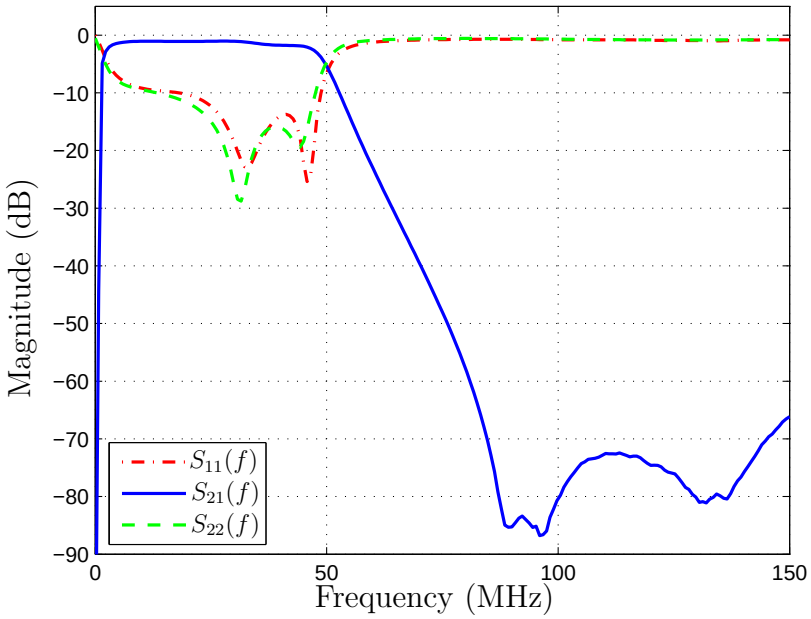

Figure 42: Insertion loss and return loss of the PLC coupling circuit prototype.

4.2.3 BROADBAND PLC COUPLER 1.7 MHZ TO 100 MHZ

The broadband, capacitive, SISO and LV PLC coupling circuit (1.7-100 MHz) was designed following the same design discussed in Section 4.1. The design of schematic

and PCB of the PLC coupling circuit, RF transformer, protection component, the components of analog low-pass elliptic filter and C_{BLOCK} capacitor are the same discussed in the Sub-section 4.2.2. Tab. 9 lists the used specification of the analog broadband low-pass elliptic filter and Tab. 10 lists the values of all components designed in the analog low-pass fifth order elliptic filter and C_{BLOCK} capacitor designed using ADS Software.

Table 9: Specifications of the broadband analog low-pass filter.

Description	Value
Input impedance Z_{in}	50 Ω
Output impedance Z_{out}	50 Ω
Type of filter	Elliptic
Passband ripple	0.5 dB
Stopband attenuation	40 dB
Cut-off frequency (f_c)	100 MHz
Maximum insertion loss	-15 dB

Table 10: Details of components used in the prototype of the PLC coupling circuit.

Component	Value	Maximum Voltage (V)	Maximum current (mA)	Frequency band (MHz)
V_{R1}		420 V_{rms}		
T_1	WB1010-PCL	500 V_{cc}		0.005-100
C_{BLOQ}	1.5 nF	1k V_{rms}		0-900
C_1	47 pF	50 V_{rms}		0-3800
C_2	5.6 pF	50 V_{rms}		0-10000
C_3	62 pF	50 V_{rms}		0-3500
C_4	15 pF	50 V_{rms}		0-7000
C_5	47 pF	50 V_{rms}		0-3500
L_1	91 nH		1000	0-750
L_2	68 nH		1300	0-800

The top and bottom of the two-layer fiber glass PCB shown in Fig. 43 follows the same design discussed in the Sub-section 4.2.2 using the microstrip technique designed in Altium software. The prototype of the broadband PLC coupling circuit is shown in Fig. 44.

Fig. 45 shows insertion loss magnitudes and return loss magnitudes. As can be seen, the curve magnitude of the insertion loss varies between 0 and -2 dB in the frequency band of 1.7-96 MHz and in the frequency band of 96-100 MHz the cutback of insertion loss is equal to -5 dB. A slope of -6 dB was measured in the frequency of 101 MHz of the insertion loss magnitude. The return loss fluctuates between -6 dB in the frequency of 2 MHz and -32 dB in the frequency of 62 MHz. Moreover, for the

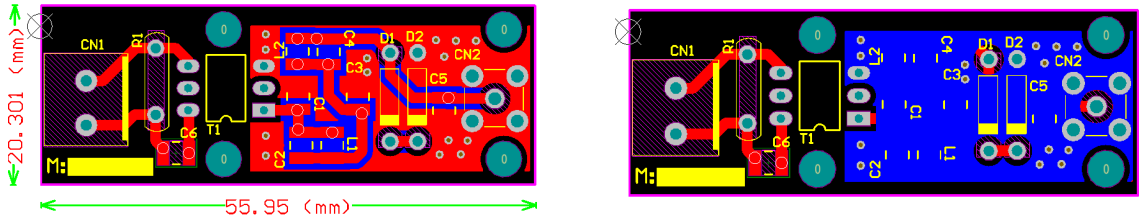

(a) Top layer plane (b) Bottom layer plane

Figure 43: The PCB of the broadband PLC coupling circuit.

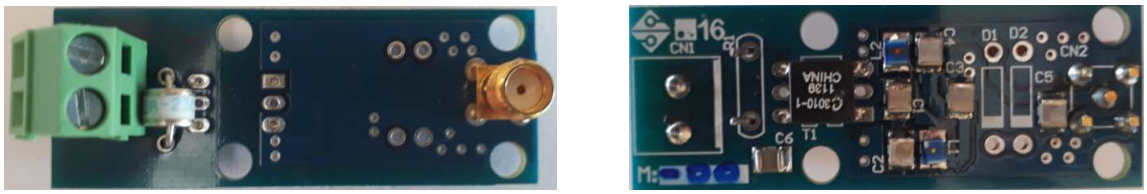

(a) Top layer plane (b) Bottom layer plane

Figure 44: The prototype of the broadband capacitive, SISO and LV PLC coupling circuit.

magnitude of return loss fluctuates between -6 dB in the frequency of 1.7 MHz and -18 dB in the frequency of 85 MHz. In the stop-band, the minimum attenuation of 40 dB is measured satisfying the design specifications in the stop-band. The rejection of the mains signal attenuation of 50 dB is attained using the C_{BLOCK} capacitor.

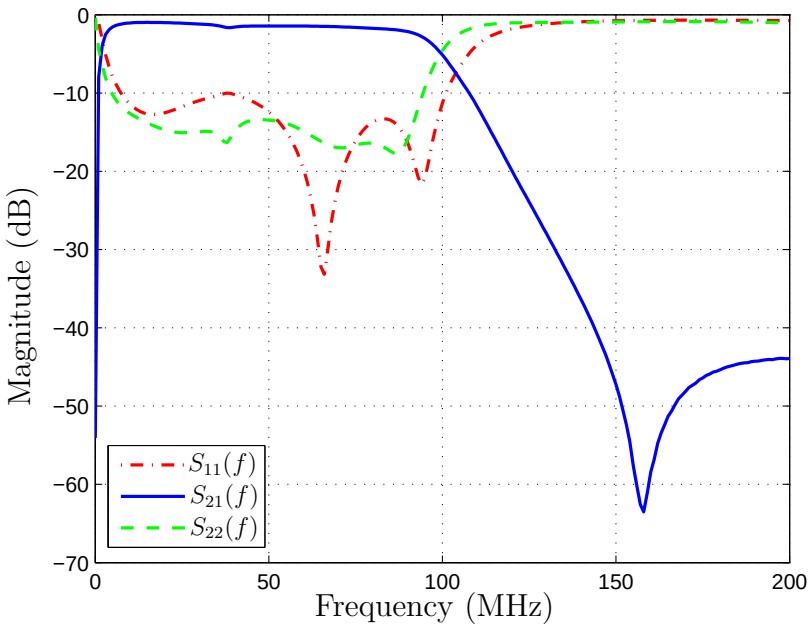

Figure 45: Insertion loss and return loss of the PLC coupling circuit prototype.

4.2.4 BROADBAND PLC COUPLER 1.7 MHZ TO 500 MHZ

The focus of this Sub-section is to analyze the broadband, capacitive, SISO and LV PLC coupling circuit (1.7-500 MHz) which was designed according to the Section 4.1. The schematic of the coupling circuit, protection component, and the components of the analog low-pass elliptic filter and C_{BLOCK} are the same discussed in the Sub-section 4.2.2. The two-layer fiberglass PCB designed for the PLC coupling circuit of 1.7-500 MHz is shown in Fig. 46. As can be seen, the RF transformer T_1 has a different pad of the RF transformer T_1 used in the frequency band of 9-500 kHz, 1.7-50 MHz and 1.7-100 MHz. The RF transformer used is a TC1-1TX+ component, see [151], because it covers the frequency band of 0.4-500 MHz. Tab. 11 lists the specification of the analog broadband low-pass elliptic filter. The values of components, C_{BLOCK} (C_6) and analog low-pass fifth order elliptic filter, listed in Tab. 12 was designed by ADS Software. The prototype of the broadband PLC coupling circuit is shown in Fig.47.

Table 11: Specifications of the broadband analog low-pass filter.

Description	Value
Input impedance Z_{in}	50 Ω
Output impedance Z_{out}	50 Ω
Type of filter	Elliptic
Passband ripple	0.5 dB
Stopband attenuation	40 dB
Cut-off frequency (f_c)	500 MHz
Maximum insertion loss	15 dB

Table 12: Details of components used in the prototype of the PLC coupling circuit.

Component	Value	Maximum Voltage (V)	Maximum current (mA)	Frequency band (MHz)
V_{R1}		420 V_{rms}		
T_1	TC1-1TX+	500 V_{cc}		0.4-500
C_{BLOQ}	1.5 nF	1k V_{rms}		0-900
C_1	6.2 pF	50 V_{rms}		0-10000
C_2	3.3 pF	50 V_{rms}		0-11000
C_3	8.2 pF	50 V_{rms}		0-850
C_4	1.2 pF	50 V_{rms}		0-11000
C_5	5.6 pF	50 V_{rms}		0-10000
L_1	12 nH		1000	0-3300
L_2	15 nH		1000	0-2500

Fig. 48 shows the magnitude of insertion loss and return loss. Note that the magnitude of the insertion loss varies between 0 and -5 dB in the frequency band

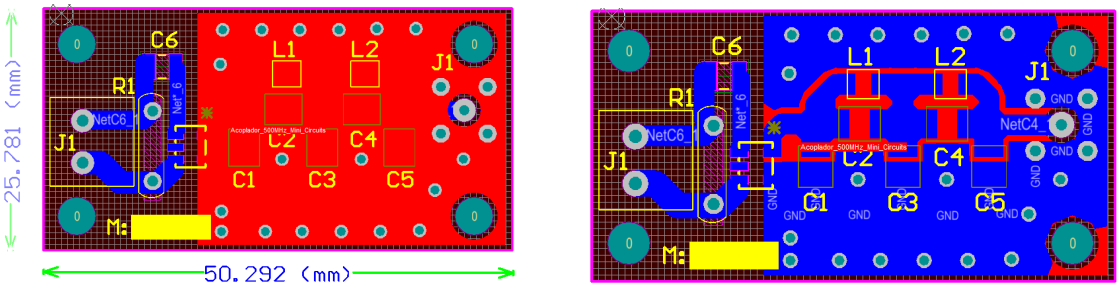

(a) Top layer plane (b) Bottom layer plane

Figure 46: The PCB of the broadband PLC coupling circuit.

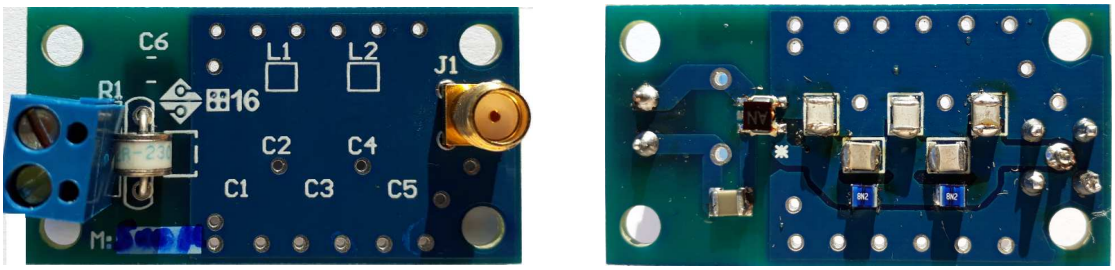

(a) Top layer plane (b) Bottom layer plane

Figure 47: The prototype of the broadband capacitive, SISO and LV PLC coupling circuit.

of 1.7-500 MHz. Moreover, we see that the effects of trace characteristic impedance, skin effect and dielectric losses begin to dominate the overall amplitude attenuation of signals at frequencies above 100 MHz. As may be seen, the insertion loss associated with PLC coupling circuit up to 500 MHz is higher than its counter part related to PLC coupling circuits designed up to 100 MHz. These discrepancies are attributed to the non-ideal behavior of the microstrip as well as of the inductance of the tracks. Fig. 48 depicts the cut-off frequency, the point of $S_{21}(f)$, drops with a slope of -6 dB, measured in the frequency of 520 MHz. The magnitude of return loss fluctuates between -6 dB in the frequency range of 220-460 MHz and -25 dB in the frequency of 15 MHz. Moreover, for the magnitude of return loss fluctuates between -7 dB in the frequency band of 300-500 MHz and in the frequency of 55 MHz, -40 dB. In the stop-band, the results obtained are compatible with the specification of Tab. 12, which is a minimum attenuation of 40 dB. Regarding the rejection of the mains signal, an attenuation of 50 dB is attained using the C_{BLOCK} capacitor.

4.3 SUMMARY

In this Chapter, we have designed and characterized a narrowband and broadband, capacitive, SISO and LV PLC coupling circuit. The design of appropriate PLC coupling

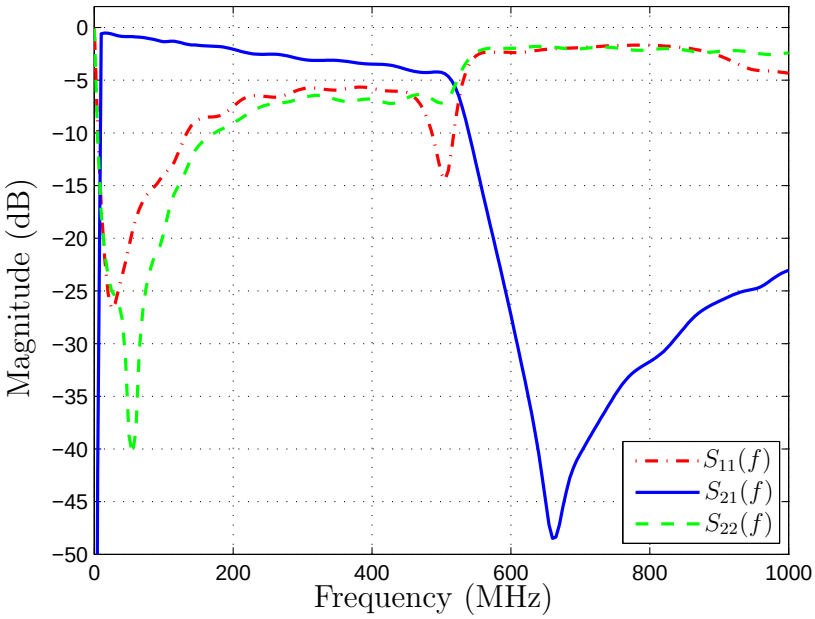

Figure 48: Insertion loss and return loss of the PLC coupling circuit prototype.

circuits is detailed and the scattering parameters of the developed PLC coupling circuits was measured and analyzed. From the outcomes of this investigation, it is possible to conclude that the PLC coupling circuits added to the microstrip technique applied to design the PLC coupling circuit with frequencies of up to 500 MHz, can offer with satisfactory results.

On the basis of the promising findings presented in this Chapter after a deep analysis of the prototypes PLC coupling circuits for the frequency bands of 9-500 kHz, 1.7-50 MHz, 1.7-100 MHz and 1.7-500 MHz. This Chapter presents a discussion of some of the key issues facing a design of PLC coupling circuits and the results obtained indicate that the PLC coupling circuits have a flat frequency response within the band-pass and attenuation greater than 40 dB and 50 dB in rejection band.

In the next section, the impedance characterization of the electric power grid line will be investigated, which is closely linked to the themes discussed in this Chapter.

5 ADAPTIVE PLC COUPLING CIRCUIT

In a typical data communication system, transmitter output and the receiver input impedances are designed to a fixed value according to a given line impedance value. Previous studies indicate that the access impedances of the electric power grid are continuously changing and depending on time, frequency and location mainly to dynamic of loads. It exhibits high-frequency selectivity, when we look at the frequency bandwidth adopted by narrowband and broadband PLC systems and, as a consequence, it is rather difficult to accomplish the impedance matching completely [182, 183]. In such scenario, impedance matching between PLC transceivers and electric power grid play an important role in improving maintaining appropriate signal strength at the point of connection with the electric power grid and, as a consequence, the reliability and/or high data rate of a PLC system [68,184]. The dynamics of access impedance at the point of connection to the electric power grid have always been recognized one of the weaknesses of PLC systems. Aiming to improve the impedance matching between the PLC transceiver and the electric power grid, this Chapter introduces an adaptive PLC coupling circuit for impedance matching.

Current researches focus on methods to minimize the impedance mismatching between the electric power grid and PLC transceivers [10,62,185]. Since the impedance variation of the electric power grid mainly depends on the loads connected to it, we can hardly be controlled this variation. For instance, the PLC coupling circuits presented in Chapter 4, present an optimum performance only in the frequency which the electric power grid impedance and the PLC coupling circuit designed impedance are equal, in this case, 50 Ω. Variations on network topology combined with unknown cable and load impedances, difficult the impedance matching using PLC coupling circuits with fixed input/output impedance. Several publications have appeared in recent years choosing the RF transformers turns winding ratio of 1:J, adapting, the PLC transceiver impedance to be roughly equal to a chosen known electric power grid impedance [4,186]. In [187], the authors proposed a two different PLC coupling circuits, incorporating a 4:1 and 2:1 winding ratio for permanent connection between PLC transceiver and the

electric power grid, to match the impedance between them. As reported by [144] the use of different couplers for different electric power grid conditions can result in substantial transmission gains.

The adaptive PLC coupling circuit proposed in [63, 188] for impedance matching has problems of size, cost, and performance. Other methods are proposed to adapt the PLC transceivers using a microcontroller to control the gain of a power amplifier monitoring the current injected into the electric power grid. The transmission power of the injected signal is monitored by a circuit, controlled by Fuzzy Logic, based algorithm and the impedance of the PLC coupling circuit is adapted dynamically by tuning the inductor and RF transformer of the PLC coupling circuit [189]. Moreover, [67] discussed a voltage controllable inductance circuit, which is composed of an operational amplifier, applied to the introduced PLC coupling circuit which impedance matching is achieved using the voltage controllable inductance circuit. In [190], the authors emphasized the benefits of active inductors over tapped transformer and a digital variable capacitor which can be controlled by a microcontroller. Transformerless impedance matching circuit combined with capacitor banks and active inductor topologies were proposed in [191].

One important performance aspect is the bandwidth of the broadband impedance matching. The Smith chart gives a good match at a single frequency, but often a broadband design is required. The Bode-Fano criterion [192] relates the quality of the match to the bandwidth network. This criterion shows that a perfect match is only possible if we assume very narrow frequency bandwidth or a single frequency. A broadband impedance matching with cascaded L-Networks curves can be achieved by cascading more sections of filters with additional intermediate impedances, creating smaller impedance ratios, and correspondingly lower Q factor for each section of filtering. However, it depends both on the load resistance and impedance of the electric power grid that is time and frequency varying. Consequently, the PLC coupling circuit needs an adaptation in the cascade L-Networks every time that the electric power grid impedance changes to keep maximum power transfer [10]. In [64], was proposed an adaptive impedance matching which automatically matches the impedance, changing the tap of the RF transformers. It is controlled by a microcontroller using a feedback circuit which measures the reflected power of the signal injected by a transmitter of the PLC transceiver into the electric power grid.

Several publications have appeared in recent years discussing the hardness of electric power grid for data communications including multiple reflections, interferences,

noise and time-varying access impedance of the electric power grid. In such scenario, the impedance matching between PLC transceivers can be pursued designing an adaptive PLC coupling circuit. In this regards, different from the aforementioned works, this Chapter addresses an adaptive, broadband, capacitive and LV PLC coupling circuit in the frequency bands of 2-50 MHz, 2-100 MHz and 2-500 MHz, from now on called adaptive matching circuit, in which the input impedance is designed based on measurement of the access impedance of the electric power grid, which was discussed in Chapter 3. Therefore, this Chapter presents and evaluate a design of the adaptive matching circuit which can adjust the impedance between PLC transceiver and electric power grid by switching among different impedance matching circuits (analog and low-pass filter).

The remainder of this Chapter is organized as follows: Section 5.1 formulates the matching impedance problem related to PLC systems; Section 5.2 discusses the proposed adaptive broadband, capacitive, SISO, LV PLC coupling circuit; Section 5.3 outlines the implementation of the adaptive broadband, capacitive, SISO, LV PLC coupling circuit; and implementation and experimental results are presented in Section 5.4.

5.1 PROBLEM FORMULATION

Several practical questions arise when dealing with impedance matching in narrowband and broadband PLC coupling circuits. The electric power grid differs considerably in topology structure and physical properties from conventional media such as twisted pair and coaxial cable. We can use the theory applied to a two-wire transmission line to adopt two-port ABCD matrices for modeling the signal propagation and to analyze electric power grid impedance [193, 194]. Fig. 49 shows a model based on ABCD matrix that can be used to analyze the impedance matching problem in a PLC system, which is composed of PLC transceivers and the electric power grid. This model emphasizes that PLC transmitter, PLC receiver and electric power grid are the time-varying system. Also, due to the fact that the coherence time of in-home and LV is lower than 600 μs [53], then we can assume that during this time interval, the electric power grid are time-invariant system and, as a consequence, these grid can be modeled by ABCD matrix. To be more precise, if t$\in$[0, T_c) , in which T_c is the coherence time, then ABCD matrix does not change. According to Fig. 49, we have

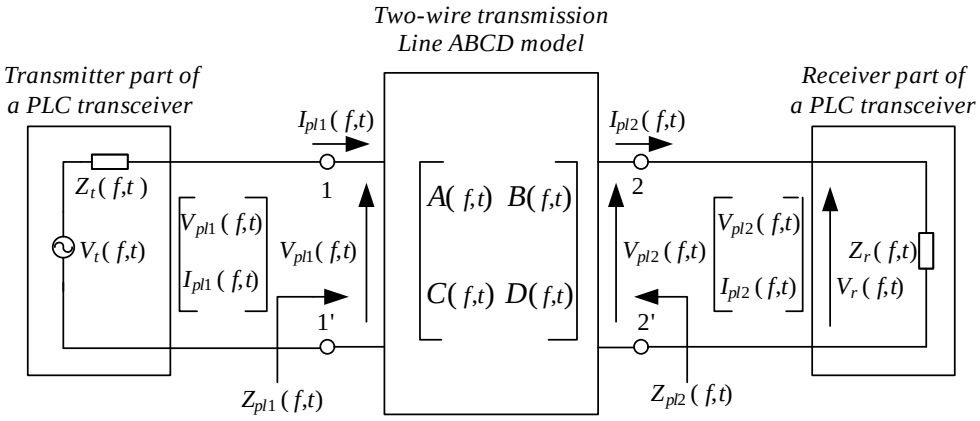

Figure 49: Two-port ABCD time varying matrix model of a PLC system.

$$\begin{bmatrix} V_{pl1}(f,t) \\ I_{pl1}(f,t) \end{bmatrix} = \begin{bmatrix} A(f,t) & B(f,t) \\ C(f,t) & D(f,t) \end{bmatrix} \begin{bmatrix} V_{pl2}(f,t) \\ I_{pl2}(f,t) \end{bmatrix}. \tag{5.1}$$

Note that $V_t(f,t)$ is the voltage source with $Z_t(f,t)$ internal impedance; $V_{pl1}(f,t)$ and $I_{pl1}(f,t)$ are respectively the voltage and current at the input port of the electric power grid; $V_{pl2}(f,t)$ and $I_{pl2}(f,t)$ are the voltage and current at the output port of the electric power grid, respectively; $V_r(f,t) = V_{pl2}(f,t)$ is the voltage in the input port of the PLC transceiver; $Z_r(f,t)$ is the impedance in the input port of the PLC transceiver; and $Z_{pl1}(f,t)$ and $Z_{pl2}(f,t)$ are the access impedance at the input and output port of the electric power grid. Note that $V_{pl1}(f,t)$ can be obtained with $V_{pl1}(f,t) = V_t(f,t) - Z_t(f,t)I_{pl1}(f,t)$ which is the voltage at the input port of the two-port ABCD of the electric power grid. The voltage $V_r(f,t)$ at the receiver of the PLC transceiver, which has an impedance $Z_r(f,t)$ is

$$V_r(f,t) = V_{pl2}(f,t) = Z_r(f,t)I_{pl2}(f,t). \tag{5.2}$$

The relations between the input and output ports of the two-wire transmission line, showed in Fig 49 can be obtained using

$$\begin{aligned} V_{pl1}(f,t) &= A(f,t)\,V_{pl2}(f,t) + B(f,t)\,I_{pl2}(f,t) \\ I_{pl1}(f,t) &= C(f,t)\,V_{pl2}(f,t) + D(f,t)\,I_{pl2}(f,t). \end{aligned} \tag{5.3}$$

It means that two-port network can be written in function of the input impedance parameters, $Z_{pl1}(f,t)$, of the electric power grid and can be obtained with ABCD matrix, see (5.1). As a result,

$$Z_{pl1}(f,t) = \frac{V_{pl1}(f,t)}{I_{pl1}(f,t)} = \frac{A(f,t)\,Z_r(f,t) + B(f,t)}{C(f,t)\,Z_r(f,t) + D(f,t)}. \tag{5.4}$$

It means that the input access impedance parameter of the electric power grid depends of the input impedance $Z_r(f,t)$ of the PLC transceiver and the ABCD parameters of the electric power grid [195]. Thus, we can conclude that to maximize the power delivered by the transmitter to the receiver, the PLC coupling circuit must be designed to precisely match the impedance of the input and output ports of the two-wire transmission line, which is modeled as a ABCD time varying matrix, with the $Z_t(f,t)$ and $Z_r(f,t)$ impedances.

The concepts of impedance matching and ABCD matrix can assist the understanding of problems related to the impedance matching between the electric power grid and a PLC transceiver. In the model showed in Fig. 49, $Z_{pl1}(f,t)$ represents the impedance of the electric power grid seen by the transmitter of PLC transceiver which could be matched with the impedance $Z_t(f,t)$. $Z_{pl2}(f,t)$ is the electric power grid impedance seen by the $Z_r(f,t)$ impedance of the PLC transceiver. However, if $Z_t(f,t)$ are equal to $Z_{pl1}(f,t)$ and the $Z_r(f,t)$ equal to $Z_{pl2}(f,t)$ the maximum power transfer occur between PLC transceivers.

However, since the access impedance of electric power grid is continuously changing depending on time and location, it is very difficult to match perfectly the impedance if $Z_r(f,t)$ and $Z_t(f,t)$ are not designed by addressing time variable t. Based on this scenario, it is clear that to match the impedance between PLC transceivers and the electric power grid, we need to design an adaptive PLC coupling circuit that is capable of detecting variation in the impedance of electric power grid and dynamically adjust the impedance of the coupling circuit. Note that Chapter 4 assumes that $Z_r(f,t)=Z_r(f)$, $\forall t\in\mathbb{R}$ and $Z_t(f,t)=Z_t(f)$, $\forall t\in\mathbb{R}$. In other words, Chapter 4 does not take into account the time-varying behavior of access impedances.

5.2 THE PROPOSED ADAPTIVE IMPEDANCE MATCHING CIRCUIT

Based on the fact that the design of impedance matching circuits for large frequency band and the design of dynamics components may very complicated issues. This Section presents a proposal that is simple to be accomplished. The main idea is to use the concept of "divide to conquer". Based on this concept, several impedance matching circuits are designed and dynamically chosen to provide the best matching between PLC transceiver and the electric power grid. To illustrate it, the block diagram of the proposed adaptive PLC coupling circuit, is shown in Fig. 50.

This adaptive PLC coupling circuit proposes an approach which is able to choose a matching circuit (analog filter) among J available matching circuit (analog filters) by controlling both Switch 1 and Switch 2 blocks. Each analog filter has a different input impedance, enabling J different matchings with the electric power grid. If the $J \longrightarrow \infty$, then the proposed Bank of impedance matching circuits tends to correctly perform the matching between the electric power grid and PLC transceivers. However, it may result in a very expensive solution. Therefore, a careful choice of J may result in a reasonable trade-off between performance and complexity. The left-hand side of the block diagram is composed of the interface with the electric power grid.

Note that the control block in the block diagram is very important because it is responsible for choosing which impedance matching circuit has to be applied. In this regard, the sensing of the signal at the output of Bank of Switches is of paramount important as well as the design of the control algorithm responsible for making a decision.

It is important to emphasize that the proposed adaptive PLC coupling circuit can be effective if the following issues are correctly addressed:

- Number of impedance matching circuits: the choice of J will dictate the complexity. For practical reason, J must be lower than 5.
- Switches: the correct specification of switches are very important because they can remarkable influence the overall performance.
- Impedance matching circuits: it is very important to choose analog filters that are reflectionless, in other words, they do not reflect signals in their stop bands back to the source. Also, the analog filter must be capable of matching with a pre-specified set of impedance values covering a wide frequency bandwidth, which in this work, is equal to 50, 100 and 500 MHz.
- The choice of impedances matchings must be representative of the electric power grid, otherwise it will not be efficient.

According to Fig. 50 the analog filter which best impedance matching between the PLC transceiver and the electric power grid is performed by the control block. The control block is composed of a logarithmic amplifier which measures the strength of the signal received and a microcontroller which analyzes the signal from the logarithmic amplifier at the ADC input port. The logarithmic amplifier is used because applications

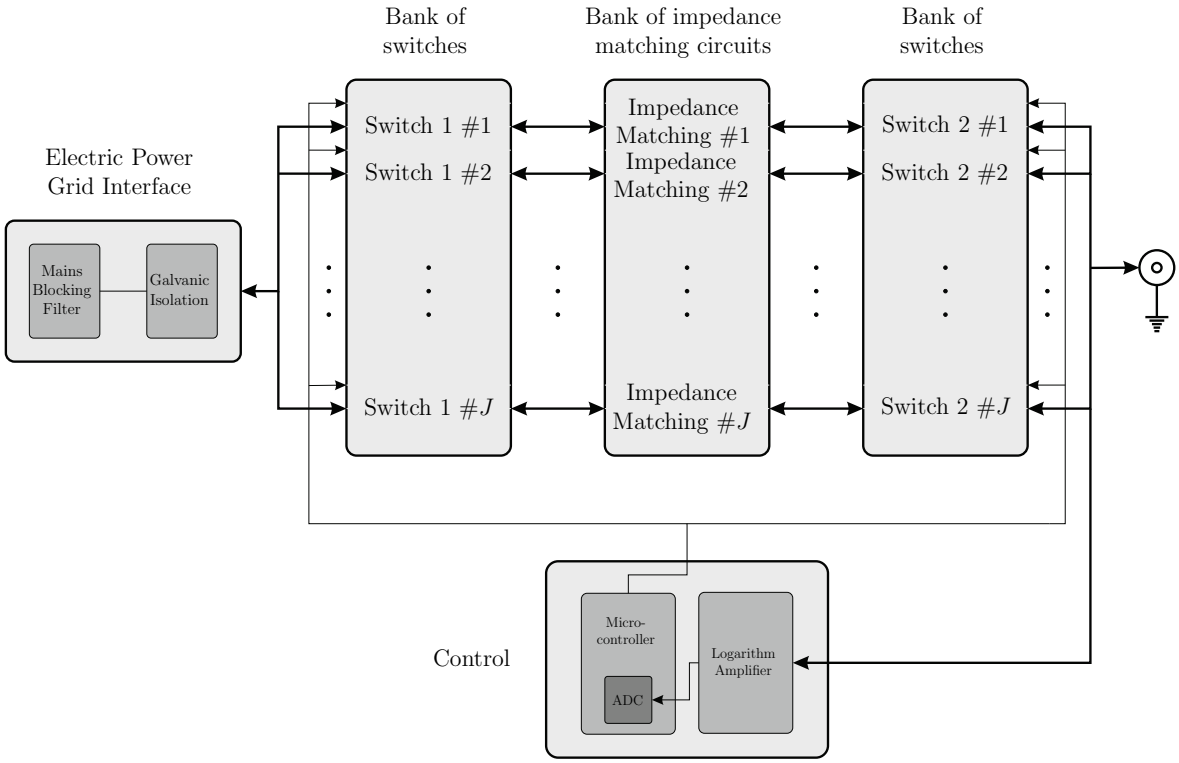

Figure 50: Block diagram of the proposed adaptive PLC coupling circuit.

involving signals with a very large frequency band may offer difficulties in concurrently dealing with both large amplitude and small amplitude signals. For such circumstances, the dynamic range can be compressed by logarithmic conversion (large amplitude) and (small amplitude). The output is a voltage scaled 25 mV/dB, generated by a current of nominally 2 μA/dB through an internal 12.5 kΩ resistor. This voltage varies from 0.25 V at an input of -74 dBm up to 2.5 V for an input of +16 dBm. The essential purpose of the logarithmic amplifier, in this adaptive PLC coupling circuit, is to amplify and compresses a signal of wide dynamic range to its decibel equivalent voltage and provide a reference voltage level to the ADC input port of the microcontroller. The microcontroller is able to analyze which bank of impedance matching, from (1 to J) delivers the higher voltage level and chose, from the general purpose input/output (GPIO) pin, which switches (Switch 1#1 to Switch 1#J and Switch 2#1 to Switch 2#J) will be used to connect the PLC transceiver to the electric power grid. Details about each component of the proposal are presented in Subsection 5.2.1 - 5.2.3.

5.2.1 BANK OF SWITCHES

The switch is a component which route signals between two circuits. It must have their small size, low power consumption, low insertion loss and high off-state isolation.

When the switch-on state is selected, the switch connects the input port of a signal to the output port and in the switch-off state, the switch offers a high impedance to the signal.

Some important parameters must be considered to specify RF switches suitable for the application. One of the important parameters is the transition time that measures the speed which the position of switches can be toggled. Switching rate represents the time for toggling from one state to another. The RF power handling is another measure which informs how efficiently a switch bypasses the signal. The RF switch must be matched in its both ports with the impedance of its preceding and succeeding stages. The cut-off frequency shows the maximum frequency operation that can be routed through it with acceptable loss. Particular attention must be paid to the insertion loss of a switch. Another important concern is the isolation of a switch which is specified when there is no signal transmission or indicates a very small coupling between the input port and an output port. The impedance of the switch during signal transmission (switch-on state) is important because it would result in the attenuation of the signal.

5.2.2 BANK OF IMPEDANCE MATCHERS

The main objective of the bank of filters is to provide or yield impedance matching and filtering the undesirable signals from the electric power grid, while at the same time it must be an economical solution. Before specifying the impedance values for each analog and low-pass irregular filter of the bank of impedance matching is necessary to know the electric power grid impedance values. The design of analog and low-pass irregular filter impedance matching circuits for broadband PLC coupling circuit is also discussed in Appendix A. The bank of impedance matching circuits is constituted by analog and low-pass irregular filters [196], each one matching the impedance between the electric power grid and PLC transceiver for a given specific value. The analog and low-pass filters are designed in such a way that the input impedance is used to provide impedance matching with the electric power grid. Each analog and low-pass filter of the bank of impedance matching circuits is selected by the switches (Switch 1 #1 to Switch 1 #J). The output impedance of the analog and low-pass filters, connected with the (Switch 2 #1 to Switch 2 #J), is fixed in 50 Ω to provide impedance matching with the PLC transceiver.

The low-pass analog filter of each adaptive PLC coupling circuit may be understood as a filter that adjusts its impedance with the access impedance of the electric power

grid in order to maximize the power transfer between PLC transceivers and the electric power grid. In the analog low-pass filter design, the choice of the input impedance of the analog irregular and Chebyshev filters are in accord with to the impedances values obtained in the measurement campaign, discussed in Chapter 3. In the design of the analog low-pass filter, two analog irregular filters was designed with input and output impedance ratio of 1:2 (25 to 50 Ω) and 2:1 (100 to 50 Ω). The analog low-pass Chebyshev filter was designed with the impedance ratio of 1:1 (50 to 50 Ω).

The choice of the 4^{th} order analog and low-pass irregular filters for the ratio of 1:2 and 2:1, for wideband impedance matching, allows simpler structures for the impedance matching of unequal resistances, some voltage gain and good attenuation at high-frequency. The analog filter with the ratio 1:1 was designed using Chebyshev structure even order, due to the first element of the filter be an inductor that will be used to absorb the reactance component of the electric power grid. The values of the reactance components in the Chebyshev filter presents values near to the values measured of the access impedance of electric power grid.

5.2.3 CONTROL

The flowchart in Fig. 51 illustrates the algorithm that is adopted in the control block. The start point of the algorithm, when the PLC coupling circuit is switch on, consist of switching the J impedance matching circuits and measure the mean voltage level that is sampled by the ADC input port for each circuit, which represents the strength of signal provided by PLC transceiver. The mean voltage level is given by

$$V_{mean} = \frac{1}{M} \sum_{n=0}^{M-1} V_{ADC}\,[n] \tag{5.5}$$

where $V_{ADC}[n]$ is the n^{th} sample of acquired signal and M is the number of samples. For the sake of simplicity, from now on, the mean voltage level will be mentioned only as a voltage level. The signal strength at the output of each impedance matching circuit is memorized and the best circuit is defined as the one that has the largest voltage level at the output of one of the switches belonging to Bank of Switches 2. After that, the microcontroller selects the best circuit (analog low-pass filter). After this first step, the microcontroller keeps checking the voltage level read by the ADC. If the voltage level drops significantly compared with the memorized best voltage level, the searching process for the best impedance matching circuit starts again and we return to the start point. Furthermore, periodic searches are done, returning to the start point, to ensure

that the current impedance matching circuit is still the best.

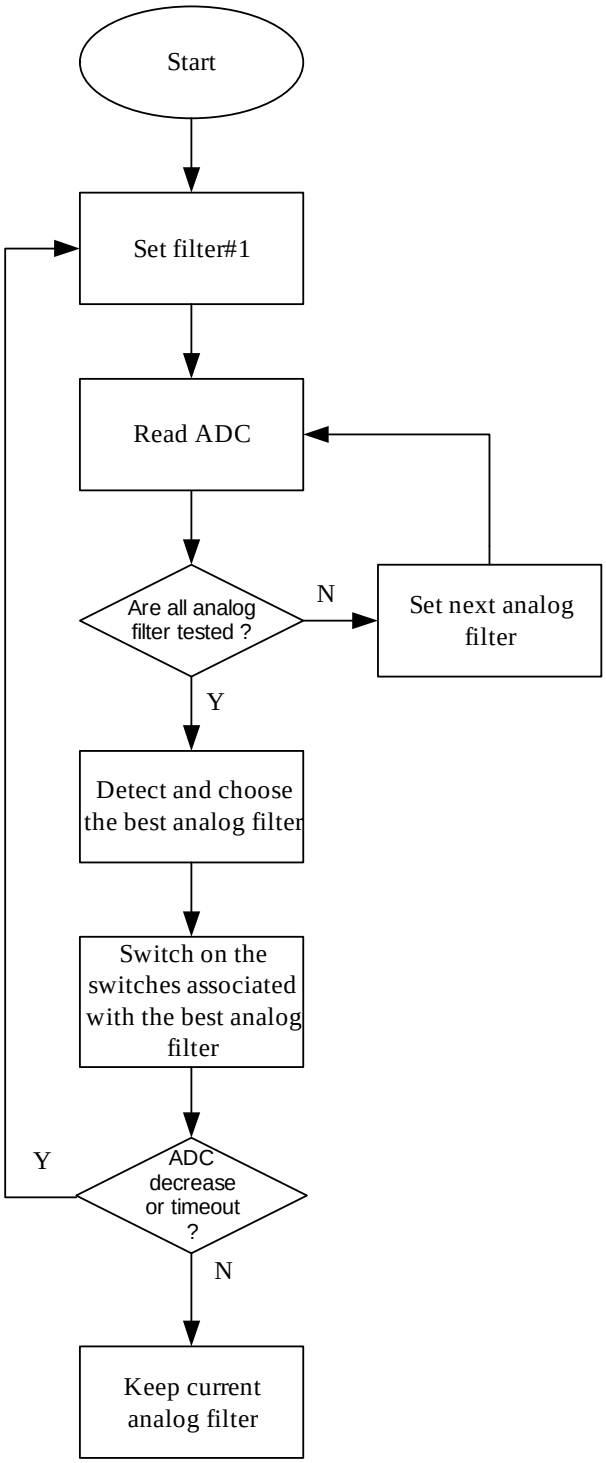

Figure 51: Flowchart of the impedance matching control algorithm in the control block.

5.3 PROTOTYPE OF THE PROPOSED ADAPTIVE PLC COUPLING CIRCUIT

Fig. 52 shows the schematic of the proposed adaptive PLC coupling circuit for operating in frequency bands of 1.7-50 MHz, 1.7-100 MHz and 1.7-500 MHz. The characteristics of the components KRE connector J_1, protection component VR_1, RF transformer T_1, C_{BLOCK} capacitor C_1, SMA connector J_2 and the capacitors C_2 to C_9 and inductors L_1 to L_8 are the same components as discussed in Chapter 4. The chosen RF Transformer T_1 covers the frequency band of 0.4-500 MHz, see [151].

In order to choose the number of analog filters with different input impedance to be implemented in the adaptive PLC coupling circuit, the results present in Chapter 3 must be taken into account. As depicted in Fig. 21, 90% of the input resistance values measured are between 25 Ω and 100 Ω, and mean value equal to 50 Ω. Due to that, three analog filters (J=3) are implemented with the aforementioned input resistance values. It is important to mention that the output impedance of the analog filters must be matched at 50 Ω with the PLC transceivers. In order to maintain the input and output impedance ratio of the analog irregular and Chebyshev filters, matching with the access impedance of electric power grid, we chose to maintain a ratio of 1:2, 1:1 and 2:1, respectively. Moreover, the choice of this input and output resistance ratio must keep the bandwidth of the PLC coupling circuits according with the frequency bands 2-50 MHz, 2-100 MHz and 2-500 MHz.

In the schematic of Fig. 52, the components SW_{1-1}, L_1, L_2, C_2, C_3, and SW_{2-1} are parts of 4^{th} order analog and low-pass irregular filter whose input impedance is 25 Ω and the output impedance equal to 50 Ω. The components SW_{1-2}, L_3, L_4, L_5, C_4, C_5 and SW_{2-1} constitute the 5^{th} order Chebyshev analog and low-pass filter with input and output impedance equal to 50 Ω and the analog filter composed of the components SW_{1-3}, L_6, L_7, C_6, C_7 and SW_{2-3} are parts of the 4^{th} order analog and low-pass irregular filter designed with input impedance equal to 100 Ω and output impedance equal to 50 Ω. Tabs. 13, 14 and 15 list the components used in this implementation.

The chosen connectors CN_1 and CN_2 connect the microcontroller device in the PCB and these connectors are a board to board connectors single row type, which is the plastic base or mounting plate to which the contacts are attached. Box header connectors feature a header which completely surrounds its contacts, whereas a pin headers contacts are exposed. Fig. 53 shows the photo and dimensions pad in (mm) of the chosen board connector.

Table 13: Details of components used in the prototype of adaptive the PLC coupling circuit in the frequency band of 1.7-50 MHz.

Component	Value	Maximum Voltage (V)	Maximum current (mA)	Frequency band (MHz)
VR_1		250 V_{rms}		
T_1	TC1-1TX+	500 V_{cc}		0.4-500
C_{BLOCK}	1.5 nF	1k V_{rms}		0-900
L_1	100 nH		250	0-1250
L_2	220 nH		400	0-1400
L_3	270 nH		200	0-900
L_4	390 nH		100	0-900
L_5	270 nH		200	0-1200
L_6	470 nH		80	0-600
L_7	220 nH		250	0-1200
C_2	180 pF	350 V_{rms}		0-2000
C_3	82 pF	212 V_{rms}		0-1900
C_4	180 pF	350 V_{rms}		0-2000
C_5	82 pF	350 V_{rms}		0-2000
C_6	39 pF	350 V_{rms}		0-4000
C_7	82 pF	350 V_{rms}		0-2000

Table 14: Details of components used in the prototype of adaptive the PLC coupling circuit in the frequency band of 1.7-100 MHz.

Component	Value	Maximum Voltage (V)	Maximum current (mA)	Frequency band (MHz)
VR_1		250 V_{rms}		
T_1	TC1-1TX+	500 V_{cc}		0.4-500
C_{BLOCK}	1.5 nF	1k V_{rms}		0-900
L_1	56 nH		600	0-1900
L_2	120 nH		300	0-1300
L_3	120 nH		300	0-1300
L_4	180 nH		250	0-1250
L_5	120 nH		300	0-1300
L_6	220 nH		250	0-1200
L_7	100 nH		400	0-1400
C_2	82 pF	350 V_{rms}		0-2000
C_3	39 pF	350 V_{rms}		0-1900
C_4	39 pF	350 V_{rms}		0-2000
C_5	39 pF	350 V_{rms}		0-2000
C_6	22 pF	350 V_{rms}		0-4000
C_7	47 pF	350 V_{rms}		0-2000

Table 15: Details of components used in the prototype of adaptive the PLC coupling circuit in the frequency band of 1.7-500 MHz.

Component	Value	Maximum Voltage (V)	Maximum current (mA)	Frequency band (MHz)
VR_1		250 V_{rms}		
T_1	TC1-1TX+	500 V_{cc}		0.4-500
C_{BLOCK}	1.5 nF	1k V_{rms}		0-900
L_1	10 nH		700	0-4800
L_2	22 nH		700	0-3000
L_3	27 nH		600	0-2800
L_4	39 nH		600	0-1200
L_5	27 nH		600	0-2800
L_6	39 nH		600	0-1200
L_7	18 nH		400	0-1400
C_2	18 pF	350 V_{rms}		0-2000
C_3	8.2 pF	350 V_{rms}		0-1900
C_4	6.8 pF	350 V_{rms}		0-2000
C_5	6.8 pF	350 V_{rms}		0-2000
C_6	3.9 pF	350 V_{rms}		0-4000
C_7	10 pF	350 V_{rms}		0-2000

To accomplish the objective to manage the analog filter switching of the analog filter, there is a microcontroller a ADC and power supply. The microcontroller chosen is the ESP-8266 [197]. The microcontroller is attached to the connectors CN_1 and CN_2 and the pins 2 and 6 of connector CN_1 and 2 of CN_2 are used to connect the microcontroller and the PCB to the same ground potential. The pin 5 of CN_1 and CN_2 provides a power supply (3.3 Vcc) to the logarithmic amplifier and the pin 15 of the connector CN_1, which is the ADC input port, receives the voltage level read from the logarithm amplifier. The output pins 8, 13 and 14 of the connector CN_2 are used to switch the filters. One output port switches two switches at the same time, connecting the input port (connector J_1) to the output port (connector J_2) of the adaptive PLC coupling circuit. The resistors R_1 to R_3 are used to limit the current through LED_1 to LED_3, which show the chosen analog filter. The resistors R_4 to R_6 are used to put the ports of the switch in a low logic level and, of course, to avoid the switch from being triggered when it is not in operation.

Fig. 54 shows the schematic of the chosen logarithm amplifier (AD 8307) [198] used to detect the strength signal from the PLC transceiver. The components C_8, C_9 and the inductor L_8 comprises a narrowband analog filter designed to detect the frequency of the maximum gain of the analog and low-pass irregular and Chebyshev analog filter calculated by $(f_x/1.6376)$, where f_c is the cut-off frequency. As mentioned

in Appendix A, the proposed bandwidth of the analog and low-pass filter was expanded to 1.6376 rad/s because the ratio between R_S and R_L designed to 1:2 or 2:1. Thus, the center frequency of the band-pass analog filter 1 rad/s is designed by $f_x/1.6376$.

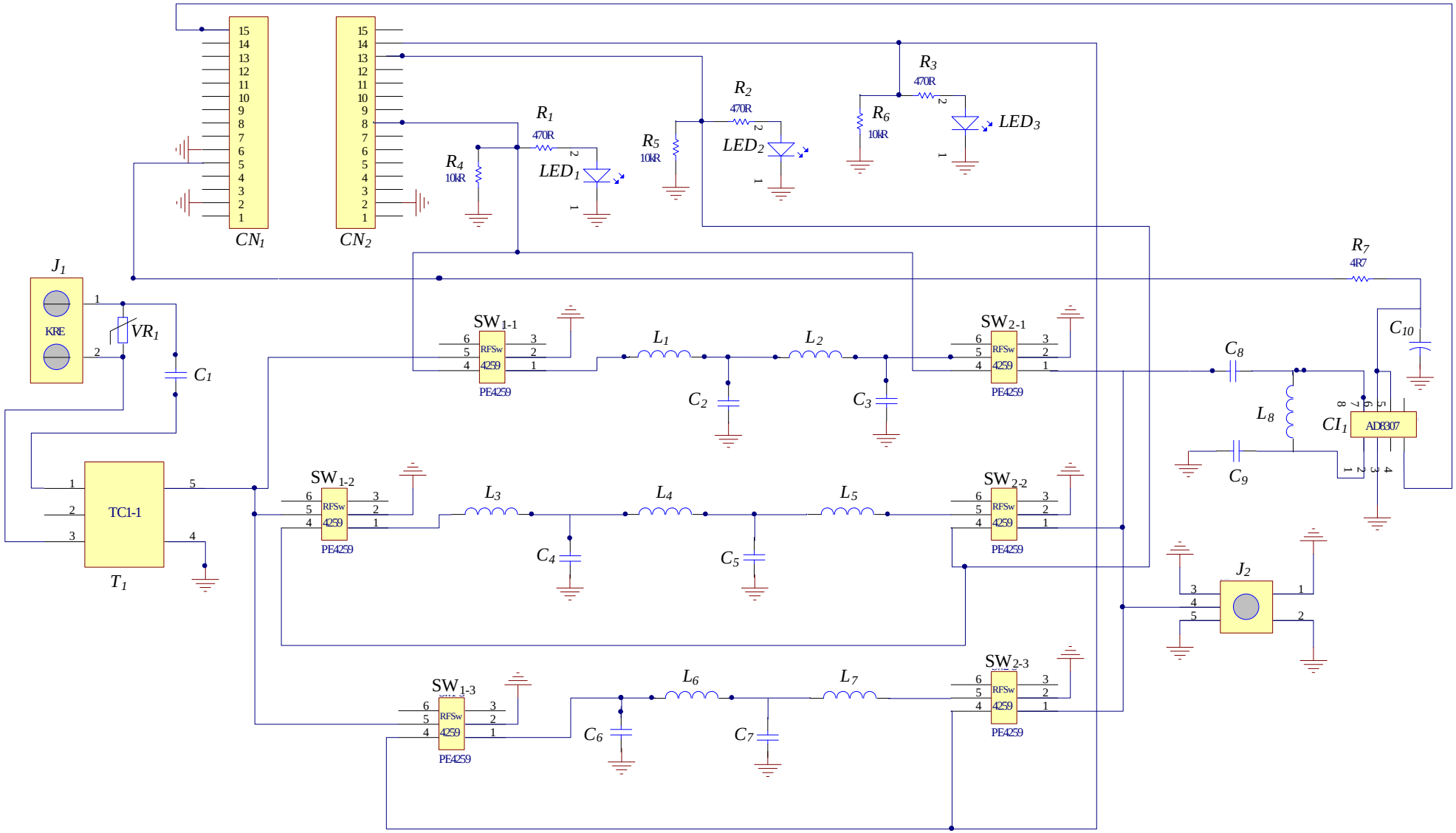

Figure 52: Schematic of the adaptive broadband, capacitive, SISO and LV PLC coupling circuit with J=3.

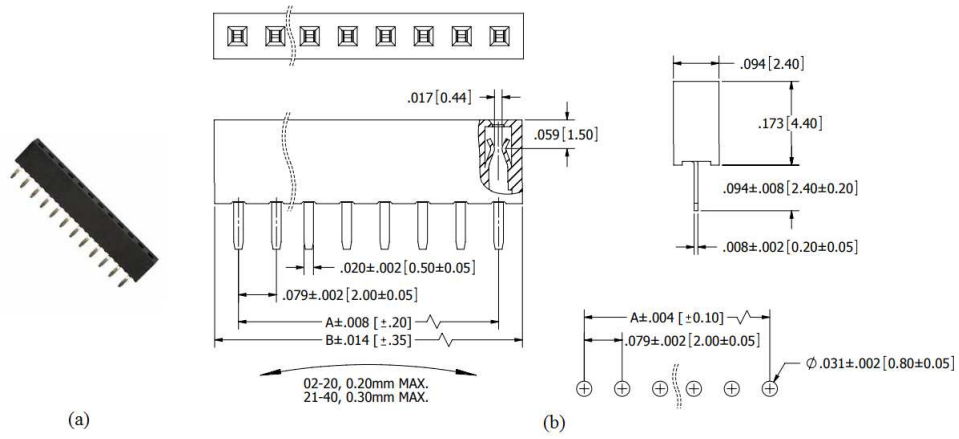

Figure 53: (a) Photo of chosen board connector. (b) dimensions in (mm) of the chosen board connector.

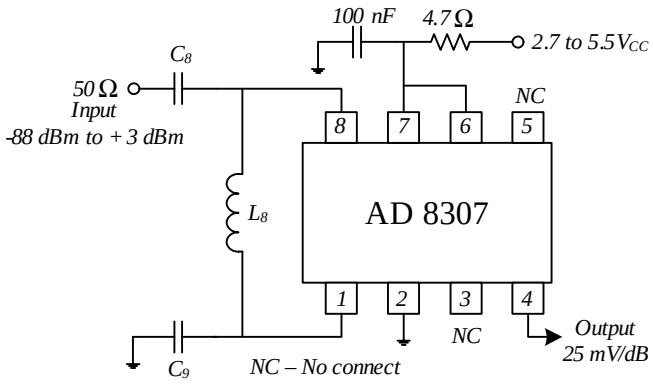

Figure 54: Schematic of the chosen logarithm amplifier AD 8307.

As can be seen in the datasheet of the manufacturer [198], there is a table that provides set of values of C_8, C_9 and L_8 for a variety of center frequencies. However, the values of the table suggested in datasheet do not include the frequencies designed for the adaptive PLC coupling circuit for the chosen bands. To solve this problem, the design of these band-pass analog filter was carried out using the ADS software. As an example, the designed band-pass analog filter for the 50 MHz adaptive PLC coupling circuit, the center frequency of the band-pass analog filter should be designed for 50 MHz/1.6376 = 30.53 MHz. Fig. 55 shows the designed band-pass analog filter for the frequency of 30.53 MHz, where Fig. 55(a) shows the schematic circuit and C_8, C_9 and L_8 are the band-pass analog filter components. Note that C_{11}, C_{12} and Term2 simulate the input impedance of AD 8307. The Term1 is the impedance of the output of the analog and low-pass filter of the adaptive PLC coupling circuit. Fig. 55(b) shows the window of the tune parameters where the values of C_8, C_9 and L_8 are obtained sliding the values of these components in the window Tune parameters. To design the best insertion loss and return loss, the goals (OptimGoal1 and OptimGoal2) is shown in Fig. 55(a) with the minimum value of -45 dB for the return loss and the maximum value of 0.5 dB for the insertion loss. Finally, Fig. 55(c) shows the value of the insertion loss (m2 = -0.005 dB) and return loss (m1 = -29.767 dB) obtained for the desired frequency. Tab. 16 summarizes all values of C_8, C_9 and L_8 components for the frequency bands 1.7-50 MHz, 1.7-100 MHz and 1.7-500 MHz.

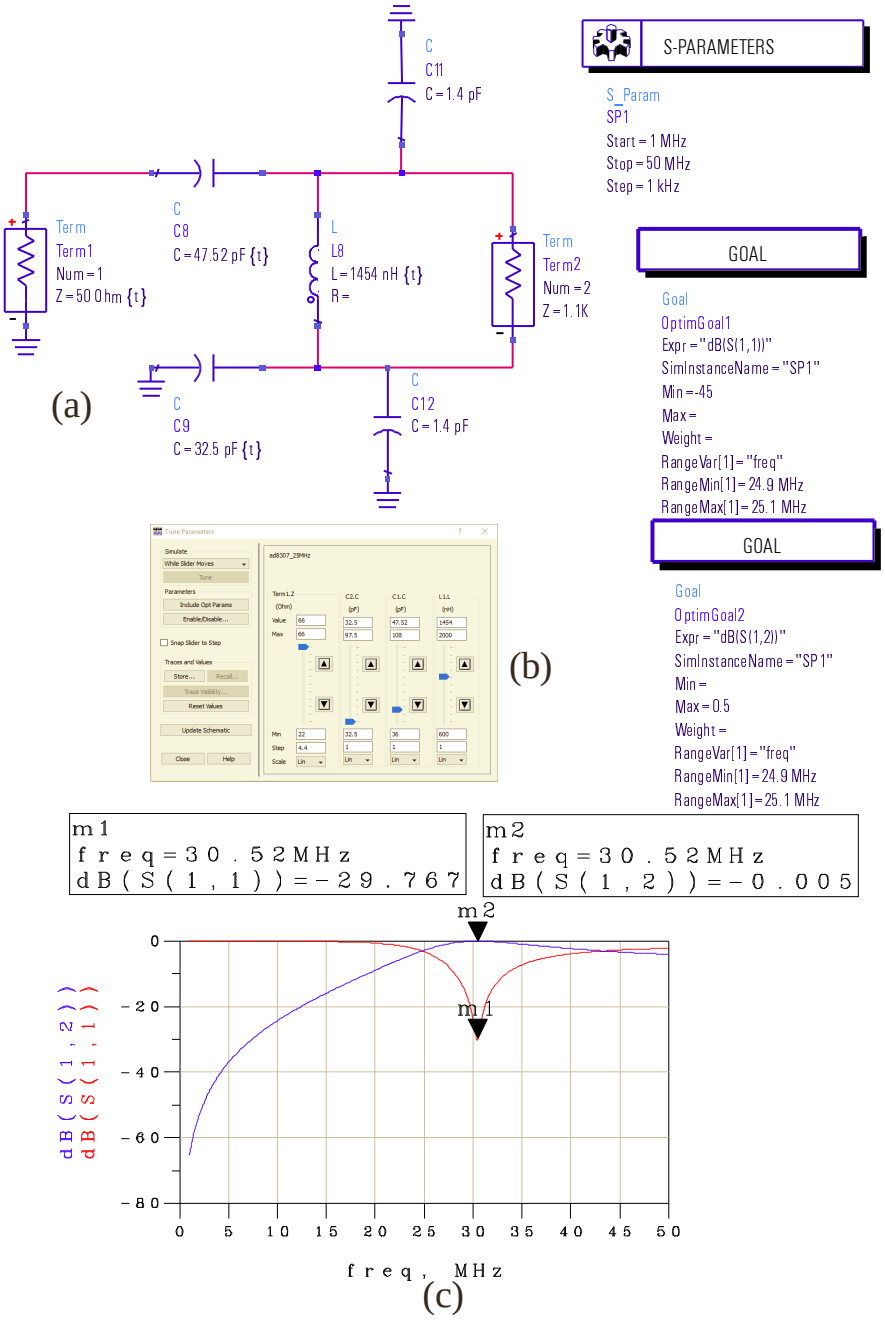

Figure 55: Design of analog band-pass filter in the input port of AD 8307. (a) Schematic of band-pass analog filter. (b) Tune Parameters of the analog band-pass filter (c) The insertion loss (dB(S(1,1))) and the return loss (dB(S(1,2))) of the analog band-pass filter.

Table 16: Details of band-pass analog filter components used in input port of AD 8307.

Frequency band (MHz)	Center frequency (MHz)	C_8 (pF)	C_9 (pF)	L_8 (nH)
2-50	30.53	47	33	1500
2-100	61.07	33	27	680
2-500	305.32	4.7	6.2	82

Fig. 54 shows the photo and dimensions pad of the AD 8307, which is SMD. Note that the dimensions are in inches and millimeters.

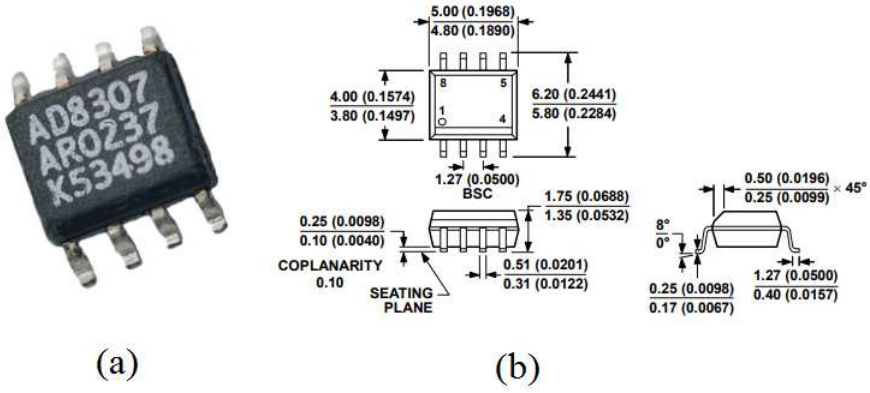

Figure 56: (a) Photo of chosen AD 8307. (b) dimensions in (mm) of the chosen AD 8307.

Due to the broad frequency band of operation, from DC through 3.0 GHz, the switch PE 4239 [199] was chosen in the design of the adaptive PLC coupling circuit. This switch is a SMD component single pole and double throw (SPDT or 1:2) to route signals from one input to two output paths. On the other hand, it has low insertion loss 0.7 dB at 1 GHz. This switch integrates on board CMOS control logic with a low-voltage CMOS-compatible control interface that can be controlled using either single-pin or complementary control inputs. It is well established that the switch was designed using the complementary pin control mode which allows the switch to operate using complementary control pin $CTRL$ (pin 4). In this operation mode, the switch does not need a power supply, the supply is driven by the 3.3 Vcc control logic from the microcontroller. Using a nominal 3.3 Vcc power supply voltage, a typical maximum input power 30 dBm can be injected at the ports 1 and 8. Actually, Fig. 57 shows the schematic diagram of the switch where the pins RF_1 and RF_2 are the output ports and the port RF_C is the common port where the signal is injected and switched for the RF_1 port according to the voltage level command $CTRL$. In other words, the voltage level of 3.3 Vcc in the $CTRL$ ports connects the input port RF_C to the output port RF_1.

As showed in Fig. 52, in the switches (SW_{1-1}) to (SW_{2-3}), the pin 5 is the common port $CTRL$ and the pin 1 is the RF_1 output port. The pin 4 is the $CTRL$ port which is controlled by the microcontroller output ports. Note that two switches are controlled by one output port of the microcontroller connecting the analog and low-pass irregular filter to the T_1 RF transformer, connector J_2, and only two switches are activating in each time, i.e, SW_{1-1} and SW_{2-1} are both used together. Fig. 58 shows the photo and

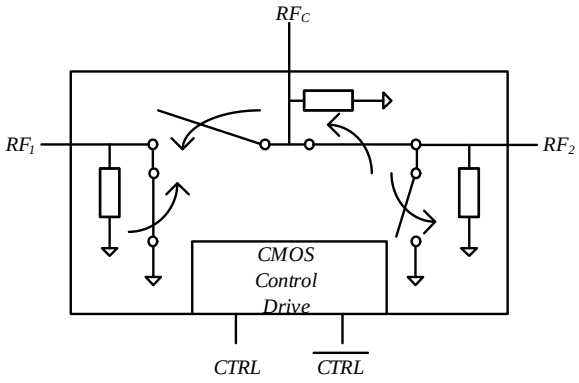

Figure 57: Schematic diagram of the RF Switch PE 4239.

dimensions pad of the SMD AD 8307. Note that the dimensions showed in inches and millimeters.

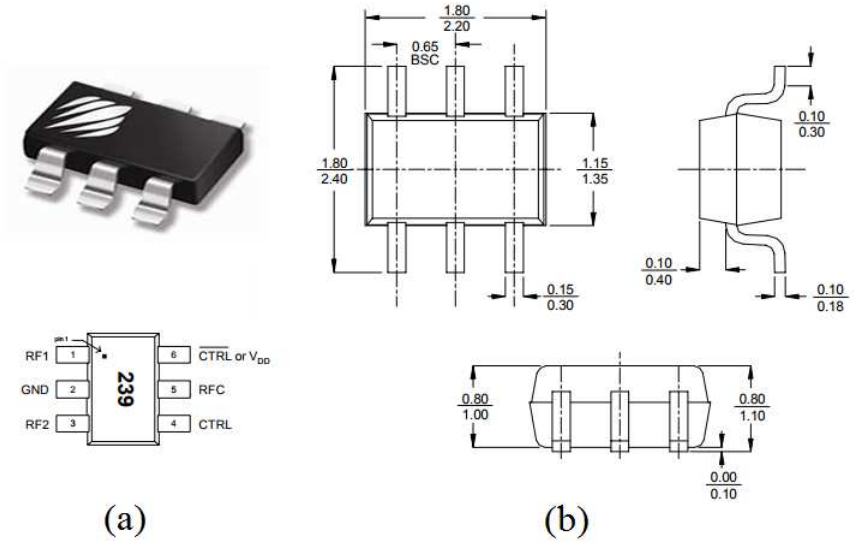

Figure 58: (a) Photo and pin configuration of chosen PE 4239. (b) dimensions in (mm) of the chosen PE 4239.

One of the most important parts of the adaptive PLC coupling circuit is the microcontroller ESP-8266. The microcontroller has various features and we can choose the exact peripheral to fit a particular system necessity. For the proposed adaptive PLC coupling circuit the ADC and GPIO ports are used to switch the analog irregular and Chebyshev low-pass analog filter, see Fig. 52. The ESP8266 has a single ADC channel available which its input voltage range is from 0 to 1.0 V_{DC}. It has a 10-bit precision and uses a successive-approximation-register (SAR) technique that operates by using a binary search algorithm. The analog input is tracked by the SAR ADC, then sampled and held during the conversion. The sampled input is compared to the value of an internal DAC, which adjusts in binary increments and attempts to get as close as

possible to the sampled value. The photo of Fig. 59 shows the microcontroller module which is connected to the connectors CN_1 and CN_2 as showed in Fig. 52. Moreover, Fig. 59 shows the pin definition of the microcontroller module. The pins are used in the design of PLC coupling circuit is the pin A0 which is the input port of the ADC, pins D1 (GPIO5), D2 (GPIO4)and D5 (GPIO14) ports used to switch the analog and low-pass filter by the switch. The 3.3 V pins are used for power supply to the logarithm amplifier.

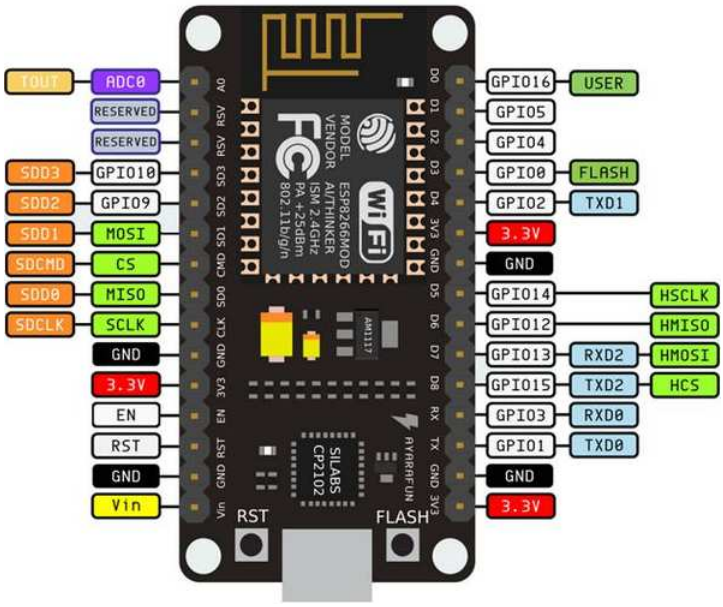

Figure 59: Pin configuration of chosen ESP 8266.

The top and bottom (layers view) of the two-layer fiber glass PCB of the adaptive PLC coupling circuit for the frequency bands 1.7-50 MHz, 1.7-100 MHz and 1.7-500 MHz, which was designed in Altium Software, are shown in Fig. 60(a) and (b), respectively. Note that this PCB was designed following the microstrip technique discussed in Section 4. The photo of a prototype of this adaptive PLC coupling circuit is shown in Fig. 61.

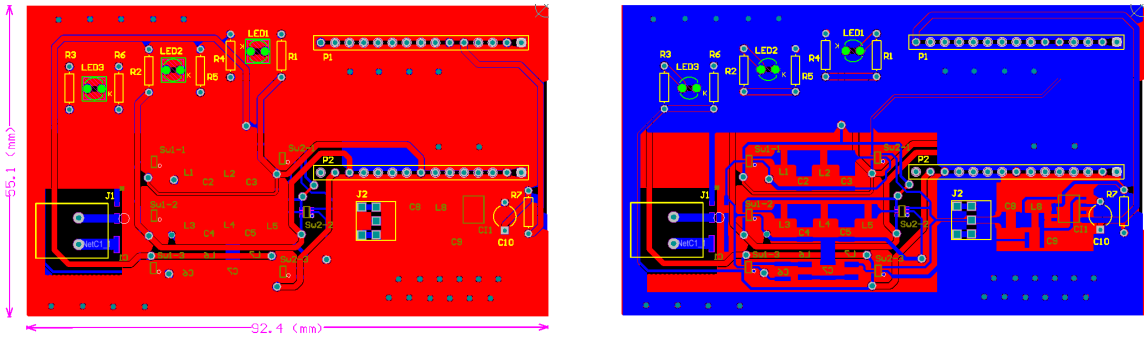

(a) Top layer plane (b) Bottom layer plane

Figure 60: The PCB of the adaptive, broadband, capacitive, SISO and LV PLC coupling circuit.

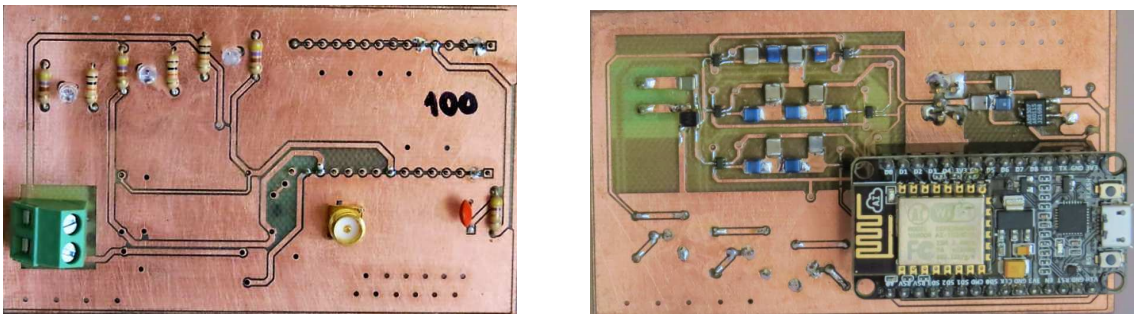

(a) Top layer plane (b) Bottom layer plane

Figure 61: The prototype of the adaptive, broadband, capacitive, SISO and LV PLC coupling circuit.

5.4 RESULTS

This Section addresses performance analyses of the proposed adaptive PLC coupling circuit that operates in the bands frequency 2-50 MHz, 2-100 MHz and 2-500 MHz. Moreover, it compares the results with the broadband, capacitive, SISO and LV PLC coupling circuit discussed in Chapter 4, non-adaptive which we name PLC coupling circuit. The measurements presented in this Section were obtained in the laboratory communication (LABCOM) of the Juiz de Fora Federal University. The equipment used in the measurements was the vectorial network analyzer, spectrum and power meter N9912A Agilent, whose frequency range is between 2 MHz and 4 GHz [200]. For this purpose, the scattering parameters $S_{11}(f,t)$, $S_{21}(f,t)$ of the adaptive PLC coupling circuits are compared with those obtained with the non-adaptive PLC coupling circuit, which has input and output impedances equal to 50 Ω, see Chapter 4. $S_{21}(f,t)$ transmission and $S_{11}(f,t)$ reflections parameters are obtained in terms of impedance of 50 Ω of the VNA instrument [45].

A typical experimental setup for measuring scattering parameters is shown in Fig. 62. In the test arrangement, the device under test will constitute the electric power grid and the adaptive PLC coupling circuits we wish to measure. The curves obtained in the measurement of the scattering parameters, between the PLC coupling circuits, were performed in an electric power grid with a voltage of 127 V_{rms} with a transmission line of 15 m in length constituted by two parallel wires with 2.5 mm in diameter.

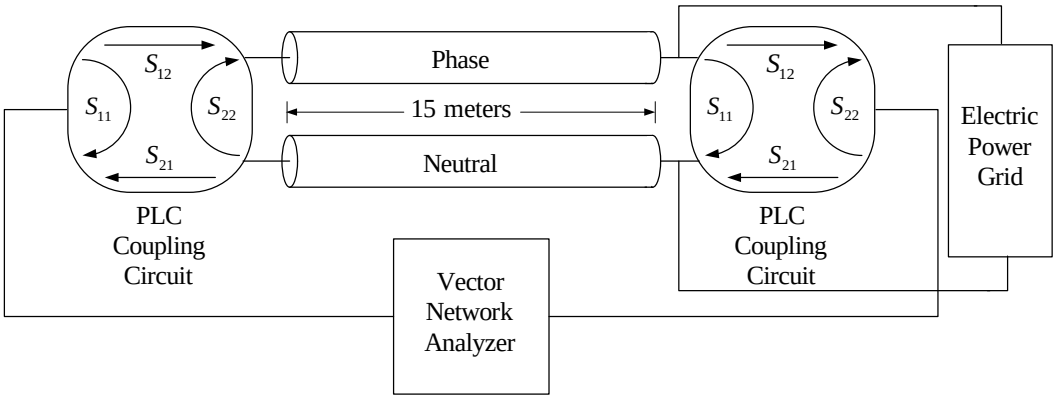

Figure 62: Scattering parameters measurement.

Tab. 17, presents the adopted specifications to design the irregular and Chebyshev analog and low-pass filter with input impedances Z_{in} equal to 25 Ω, 50 Ω or 100 Ω, where f_c is the cut-off frequency 50 MHz, 100 MHz or 500 MHz.

Finally, but not least, Sub-section 5.4.1 discusses the measurement of the scattering parameters of the adaptive PLC coupling circuit (2-50 MHz), while Sub-section 5.4.2 and 5.4.3 will evaluate the measurement of the of the scattering parameters of the adaptive PLC coupling circuit considering the frequency bands equal to (2-100 MHz) and (2-500 MHz), respectively. The same procedure for measuring the scattering parameters will be adopted for adaptive PLC coupling circuit (2-500 MHz) in Sub-section 5.4.3.

Table 17: Specification of adaptive and analog and low-pass filter.

Description	Value
Input impedance Z_{in}	Z_{in} (Ω)
Output impedance Z_{out}	50 Ω
Type of analog filter	Lowpass Irregular
Passband ripple	0.5 dB
Stopband attenuation	40 dB
Cut-off frequency	f_c (MHz)
Maximum insertion loss	-15 dB

5.4.1 ADAPTIVE BROADBAND, CAPACITIVE, SISO AND LV PLC COUPLING CIRCUIT (2-50 MHZ)

In this Sub-section, the results obtained from the measurements of the $S_{11}(f,t)$ and $S_{21}(f,t)$ parameters in electric power grid (127 V_{rms}, 60 Hz) are analyzed. The measurement was realized using two setups. The first one is composed of two PLC coupling circuit with input and output impedance equal to 50 Ω (designed as an elliptic analog filter), which will be called from now on as PLC coupling circuit 50 Ω, connected on both sides of the electric power grid. The second setup is composed of a PLC coupling circuit 50 Ω, such as the used in the first step setup, connected in one side of the electric power grid and an adaptive PLC coupling circuit (designed as analog irregular filter and Chebyshev analog filter) connected on the other side, which has its input and output impedance equal to 25 Ω, 50 Ω and 100 Ω. Fig. 62 illustrates the setup configuration.

Fig. 63 depicts the measurements of the $S_{21}(f,t)$ scattering parameter comparing the both setups. The green line is the measurement acquired using the first setup aforementioned. The red, blue and magenta lines are the measurements obtained using the second setup with the input and output impedance of the adaptive PLC coupling circuit equal to 25 Ω, 50 Ω and 100 Ω, respectively.

Note that the behavior of the magnitude of the $S_{21}(f,t)$ parameter up to 30 MHz is very similar and their values vary between -8.5 and -15 dB. Analyzing the frequency from 30 MHz up to 50 MHz the non-adaptive PLC coupling circuit 50 Ω presents the lower attenuation (green line). Beyond the cut-off frequency of 50 MHz, we see a relatively sharp roll-off varying between -20 (red line) and -25 dB (magenta line). At the stop-band, the designed minimum attenuation of 40 dB is achieved, in the best case, at 58 MHz by the PLC coupling circuit 50 Ω (green line), and, in the worst case, at 62 MHz by the adaptive PLC coupling circuit with the input impedance of 25 Ω.

Fig. 64 compares two adaptive PLC coupling circuits connected to the electric power grid with the same impedance. The $S_{21}(f,t)$ scattering parameters of two adaptive PLC coupling circuits both connected with an impedance of 25 Ω (red line), 50 Ω (blue line) and 100 Ω (magenta line). The adaptive PLC coupling circuits which impedance is equal to 25 Ω and 100 Ω are designed with irregular analog filter and the adaptive PLC coupling circuits both are designed with Chebyshev analog filter. The green line is the $S_{21}(f,t)$ parameter of non-adaptive PLC coupling circuit 50 Ω which is plotted in the Fig. 64 to compare the performance with the adaptive PLC coupling

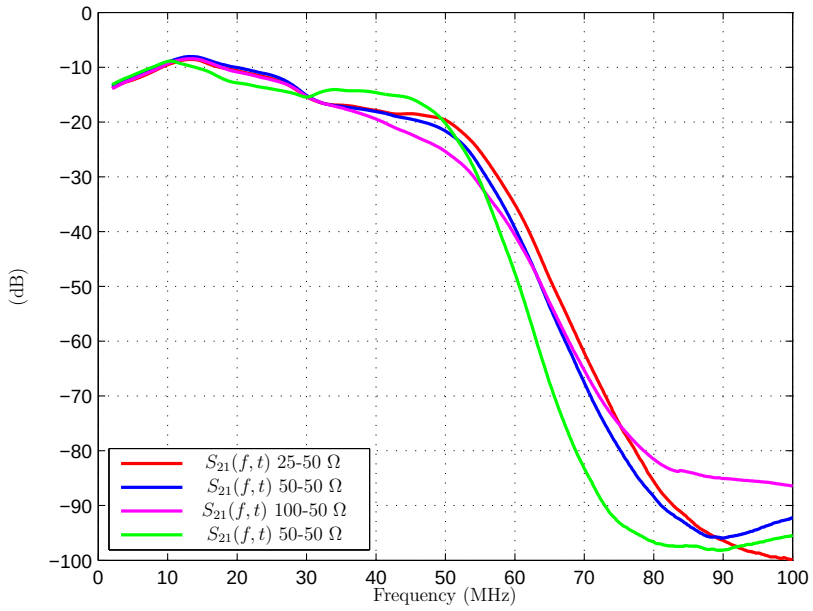

Figure 63: Magnitude of $S_{21}(f,t)$ scattering parameters comparing non-adaptive PLC coupling circuit 50 Ω with adaptive PLC coupling circuit 2-50 MHz.

circuits. Note that in the frequencies between 2 MHz and 15 MHz the behavior is very similar; however, in the frequency between 15 MHz and 40 MHz the adaptive PLC coupling circuits with impedances equal to 100 Ω and 50 Ω has a better insertion loss varying between 1 and 3 dB. For the frequency between 42 MHz and 50 MHz the non-adaptive PLC coupling circuit 50 Ω has the insertion loss with lower attenuation. As can be seen in Fig. 64, the non-adaptive PLC coupling circuit 50 Ω, designed with 5^{th} order elliptic analog filter, has a better attenuation in the stop-band frequency.

As we can see in Fig. 65, the magnitude of $S_{11}(f,t)$ return loss scattering parameter presents a similar response for all couplers analyzed. The ripples in the reflection coefficients vary between -2.5 dB in the frequency of 15 MHz and -35 dB in the frequency of 50 MHz. We also observe that the adaptive PLC coupling circuit with the input impedance of 50 Ω presents the best impedance matching in the frequency of 30.5 MHz, which is the frequency that the analog filter was designed to obtain the best impedance matching (50 MHz/1.6376).

Fig. 66, shows the magnitude of $S_{11}(f,t)$ return loss scattering parameter and compares two adaptive PLC coupling circuits connected to the electric power grid with the same impedance. The $S_{11}(f,t)$ scattering parameters of two adaptive PLC coupling circuits both connected with an impedance of 25 Ω (red line), 50 Ω (blue line) and 100 Ω (magenta line). The green line is the $S_{11}(f,t)$ parameter of non-adaptive PLC coupling

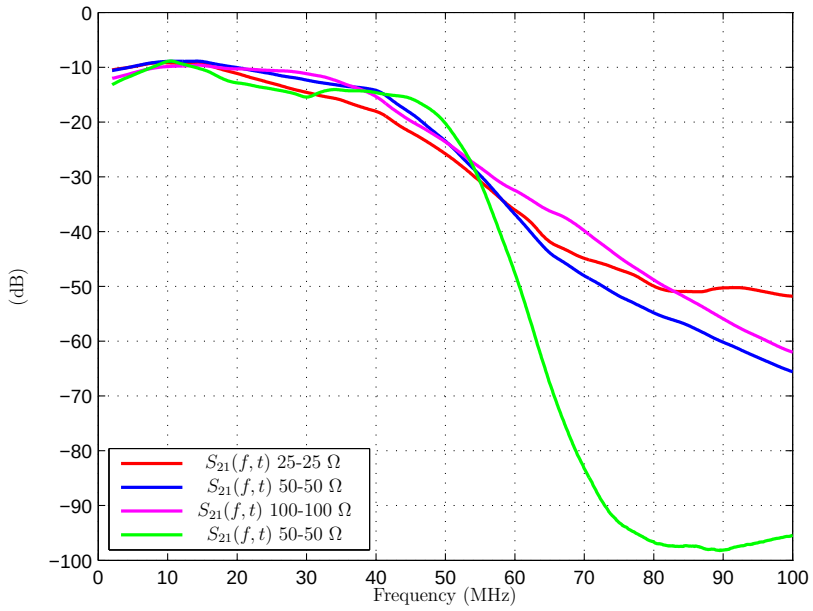

Figure 64: Magnitude of $S_{21}(f,t)$ scattering parameters comparing adaptive PLC coupling circuit with adaptive PLC coupling circuit and non-adaptive PLC coupling circuit 50 Ω in the frequency band of 2-50 MHz.

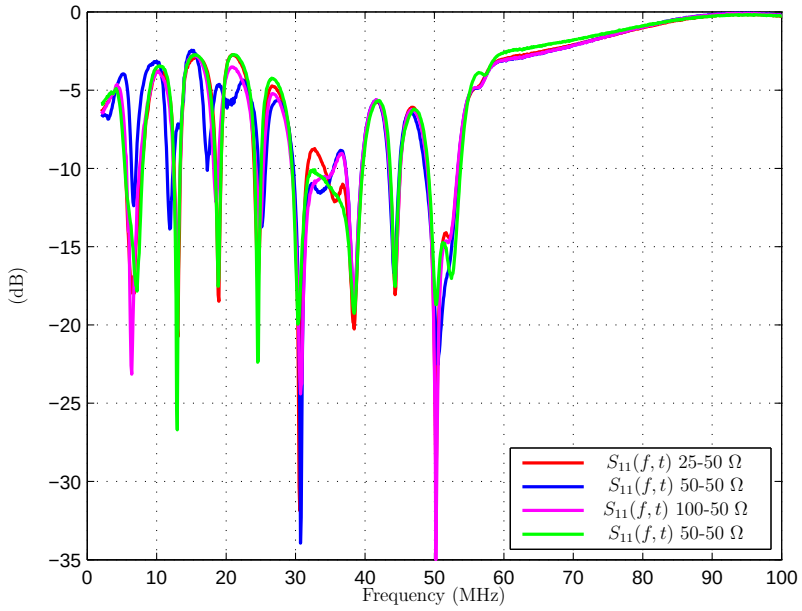

Figure 65: Magnitude of $S_{11}(f,t)$ scattering parameters comparing non-adaptive PLC coupling circuit 50 Ω with adaptive PLC coupling circuit 2-50 MHz.

circuit 50 Ω. As can be seen the behavior of the $S_{11}(f,t)$ is very similar in both Fig. 65 and 66. For the impedances 25 Ω and 50 Ω, $S_{11}(f,t)$ parameter shows the worse impedance matching in the frequency between 3 MHz and 12 MHz. The adaptive PLC

coupling circuits both matched in 100 Ω shows the best impedance matching in the whole frequency band.

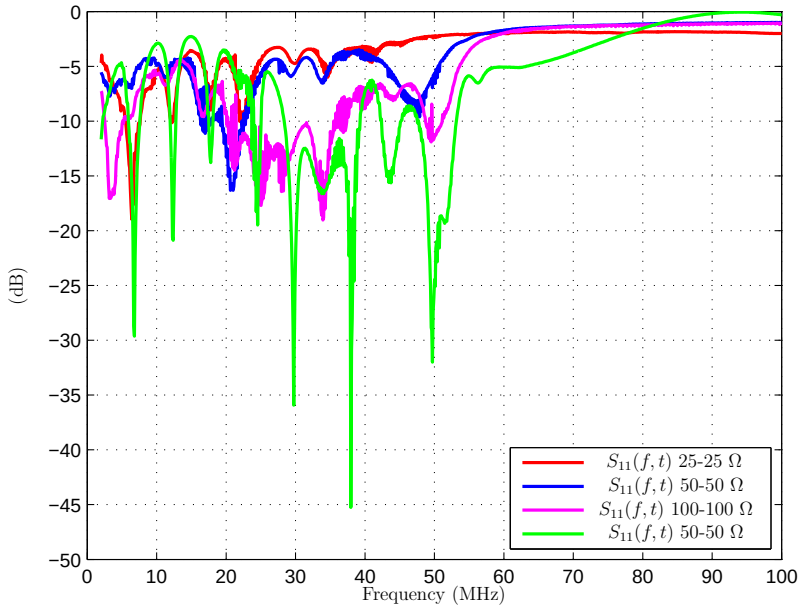

Figure 66: Magnitude of $S_{11}(f,t)$ scattering parameters comparing adaptive PLC coupling circuit with adaptive PLC coupling circuit and non-adaptive PLC coupling circuit 50 Ω in the frequency band of 2-50 MHz.

5.4.2 ADAPTIVE BROADBAND, CAPACITIVE, SISO AND LV PLC COUPLING CIRCUIT (2-100 MHZ)

This Sub-section aims to give a comprehensive analysis of impedance matching of the adaptive PLC coupling circuit in the frequency band of 2-100 MHz. The setup of measurements are the same as discussed in Sub-section 5.4.1 and shown in Fig. 62.

Fig. 67 shows the $S_{21}(f,t)$ insertion loss scattering parameter of the adaptive PLC coupling circuit with input impedance equal to 25 Ω presents worse attenuation curve (red line) and the others PLC coupling circuits have similar curves. The non-adaptive PLC coupling circuit 50 Ω (green line) has the best insertion loss varying between -16 dB in the frequency of 22 MHz and -35 dB in the frequency of 100 MHz. The designed minimum attenuation at the stop-band of 40 dB is measured in 102 MHz for non-adaptive PLC coupling circuit 50 Ω. At the cut-off frequency of 100 MHz, we see a sharp roll-off varying between -30 and -39 dB and the adaptive PLC coupling circuit Chebyshev analog filter with input impedance equal to 50 Ω presents the lowest attenuation. Note that the values of insertion loss increase comparing with the non-

adaptive PLC coupling circuits 50 Ω 2-50 MHz and the inductive behavior of the electric power grid is present after 50 MHz.

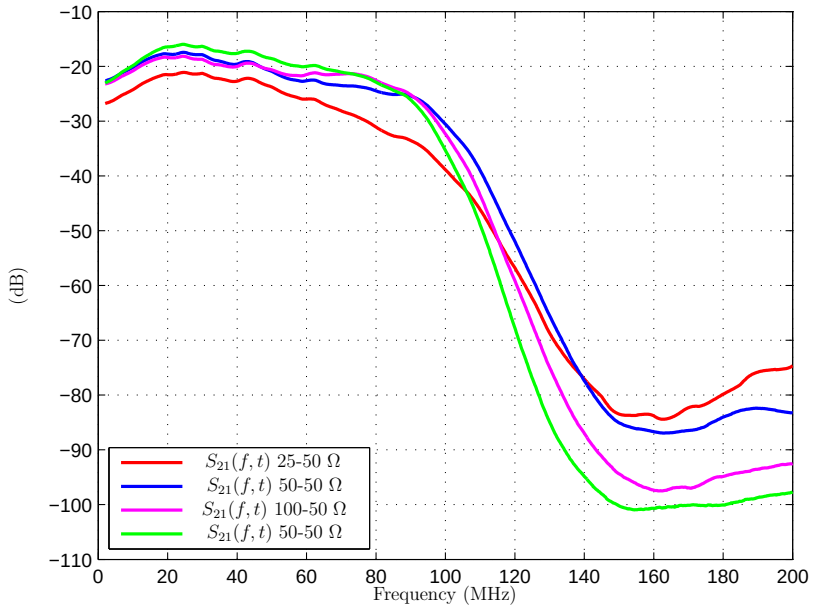

Figure 67: Magnitude of $S_{21}(f,t)$ scattering parameters comparing non-adaptive PLC coupling circuit 50 Ω with adaptive PLC coupling circuit 2-100 MHz.

Fig. 68 follows the same analysis of the Fig. 64 and compares the adaptive PLC coupling circuit and PLC coupling circuit 50 Ω. The results on Fig. 68 are compared with the Fig. 67 where we can see that the adaptive PLC coupling circuits with impedance 50 Ω and 100 Ω has the best insertion loss compared with PLC coupling circuit 50 Ω and adaptive PLC coupling circuit 25 Ω in the whole frequency band. Moreover, the PLC coupling circuit 50 Ω, which analog and low-pass filter was designed with 5^{th} order elliptic analog filter, has a better attenuation in the stop-band frequency.

The magnitude of return loss, $S_{11}(f,t)$ scattering parameter, exhibits ripples in the reflection coefficients with the similar response for all couplers analyzed. The ripples vary between -2 dB in the frequency of 22 MHz and -42 dB in the frequency of 98 MHz. We also observe that the adaptive PLC coupling circuit with input impedance equal to 100 Ω has the best impedance matching showing the best magnitude reflection parameter $S_{11}(f,t)$ in the whole frequency band. In the frequency of 61 MHz, where the analog filter was designed to obtain the best impedance matching (100 MHz/1.6376), the adaptive PLC coupling circuit, designed as Chebyshev analog filter, with input impedance equal to 50 Ω has the best impedance matching.

Fig. 70, shows the magnitude of $S_{11}(f,t)$ return loss scattering parameter and

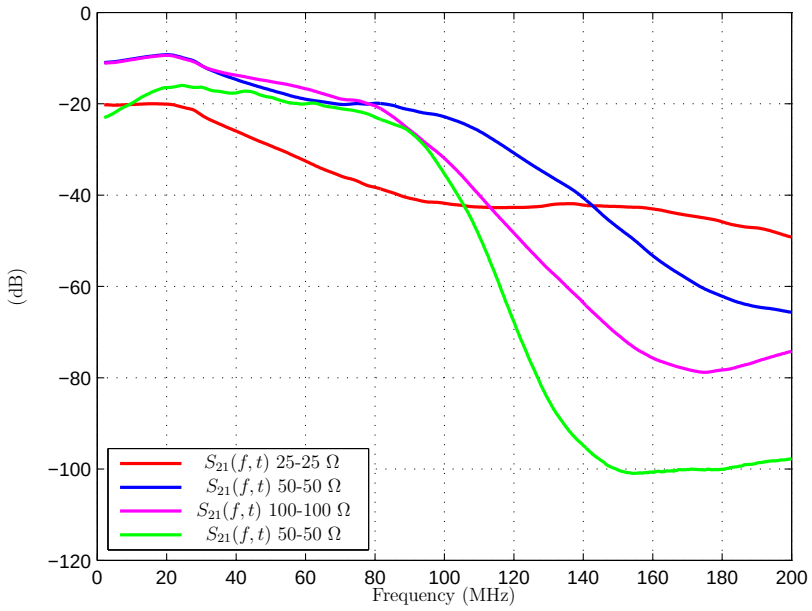

Figure 68: Magnitude of $S_{21}(f,t)$ scattering parameters comparing adaptive PLC coupling circuit with adaptive PLC coupling circuit and non-adaptive PLC coupling circuit 50 Ω in the frequency band of 2-100 MHz.

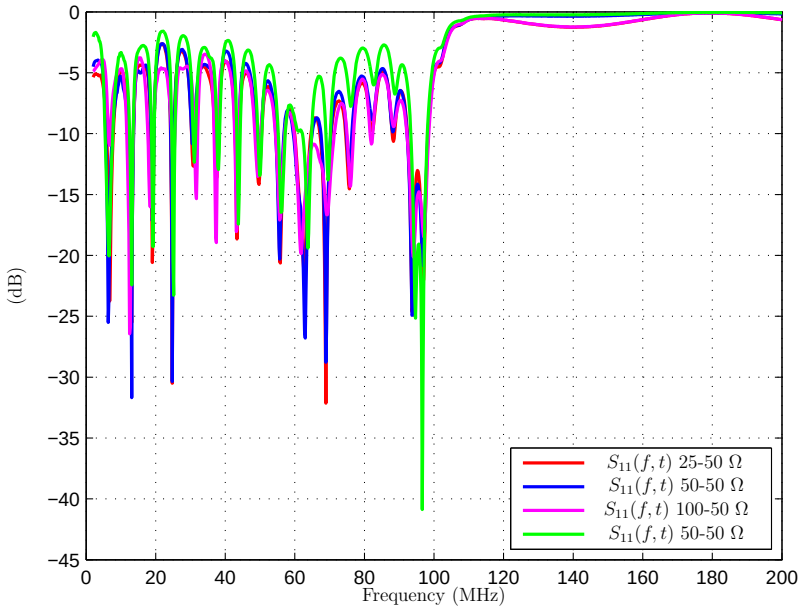

Figure 69: Magnitude of $S_{11}(f,t)$ scattering parameters comparing non-adaptive PLC coupling circuit 50 Ω with adaptive PLC coupling circuit 2-100 MHz.

compares two adaptive PLC coupling circuits connected to the electric power grid with the same impedance follows the same analysis of the Fig. 66 and compares the adaptive PLC coupling circuit and non-adaptive PLC coupling circuit 50 Ω. The

$S_{11}(f,t)$ scattering parameters of two adaptive PLC coupling circuits both connected with an impedance of 100 Ω (magenta line) presents the best impedance matching in the frequency band 2 MHz until 82 MHz. However, adaptive PLC coupling circuit $S_{11}(f,t)$ 50 Ω (blue line) has the best impedance matching in the frequency between 82 MHz until 100 MHz.

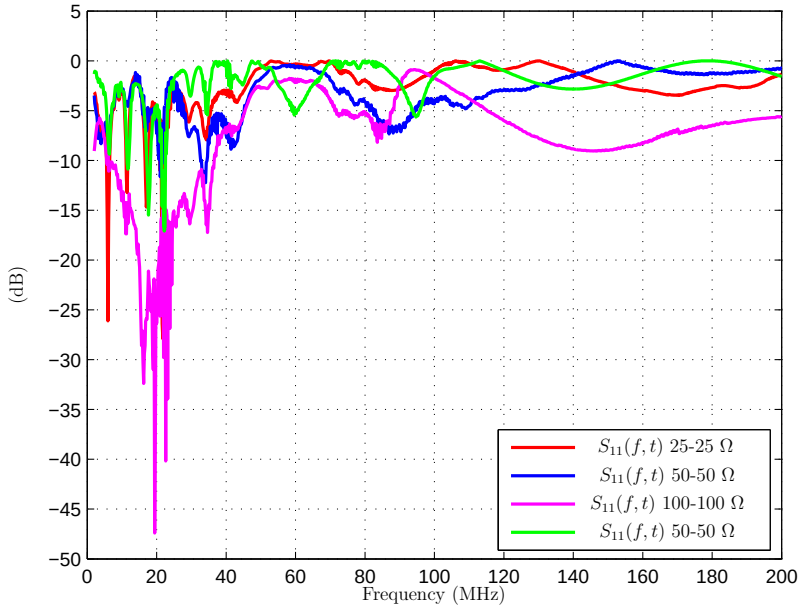

Figure 70: Magnitude of $S_{11}(f,t)$ scattering parameters comparing adaptive PLC coupling circuit with adaptive PLC coupling circuit and non-adaptive PLC coupling circuit 50 Ω in the frequency band of 2-100 MHz.

5.4.3 ADAPTIVE BROADBAND, CAPACITIVE, SISO AND LV PLC COUPLING CIRCUIT (2-500 MHZ)

This Sub-section aims to give a comprehensive analysis of impedance matching of the adaptive PLC coupling circuit in the frequency band of 2-500 MHz. The setup of measurements are the same as discussed in Sub-section 5.4.1 and shown in Fig. 62.

Fig. 71 shows $S_{21}(f,t)$ scattering parameter where the green line is the non-adaptive PLC coupling circuit 50 Ω has the best insertion loss varying between -15 dB in the frequency of 2 MHz and -45 dB in the frequency of 500 MHz. The adaptive PLC coupling circuits with input impedance equal to 25 and 50 Ω (red line and blue line respectively) presents worse attenuation after the whole frequency band. The designed minimum attenuation at the stop-band of 40 dB varies between 350 MHz, for the adaptive PLC coupling circuit designed with the input impedance of 25 Ω and 485 MHz for the PLC coupling circuit 50 Ω. The best magnitude insertion loss is obtained by

PLC coupling circuit 50 Ω in the frequency band between 2-500 MHz. We can see that the inductive behavior of the electric power grid causes several attenuations in this frequency band. At the cut-off frequency of 500 MHz, we see a sharp roll-off varying between -45 and -65 dB and the non-adaptive PLC coupling circuit 50 Ω presents the lowest attenuation.

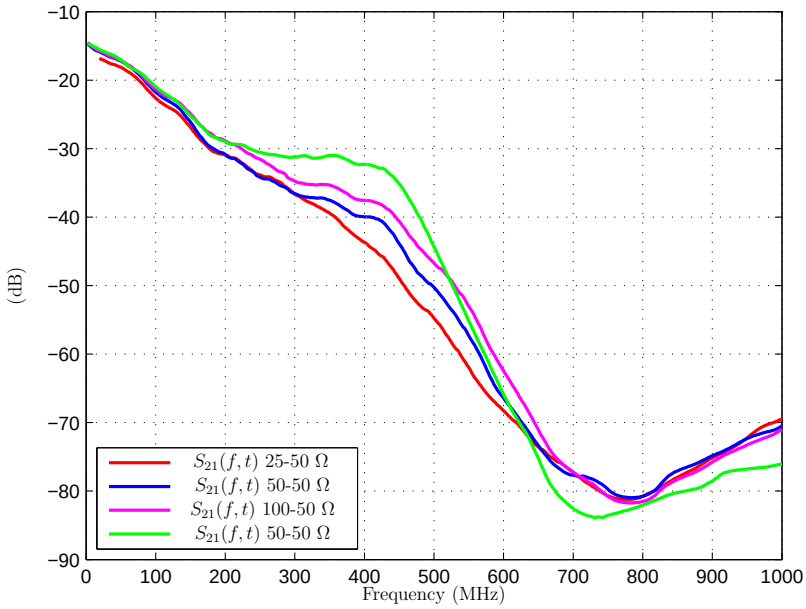

Figure 71: Magnitude of $S_{21}(f,t)$ scattering parameters comparing non-adaptive PLC coupling circuit 50 Ω with adaptive PLC coupling circuit 2-500 MHz.

Fig. 72 compares the adaptive PLC coupling circuit and non-adaptive PLC coupling circuit 50 Ω following the same analysis of the Fig. 64. The results on Fig. 72 are compared with the Fig. 67 where we can see that the adaptive PLC coupling circuits with impedance 50 Ω has the best insertion loss compared with the all adaptive PLC coupling circuit. The Figs. 71 and 72, shows that in both cases the non-adaptive PLC coupling circuit 50 Ω has the best insertion loss, the adaptive PLC coupling circuit with input impedance equal to 100 Ω has the second best results, and adaptive PLC coupling circuit with input impedance with 25 and 50 Ω has the worse results.

Interestingly results can be observed analyzing the magnitude of return loss, $S_{11}(f,t)$ scattering parameter. In both Figs. 73 and 74, the best impedance matching is obtained by the adaptive PLC coupling circuit with the input impedance of 50 Ω, which analog low-pass filter was designed with Chebyshev analog filter. The adaptive PLC coupling circuit with input impedance equal to 25 Ω shows the worse impedance matching and the results of the adaptive PLC coupling circuit with input impedance equal to 100 Ω

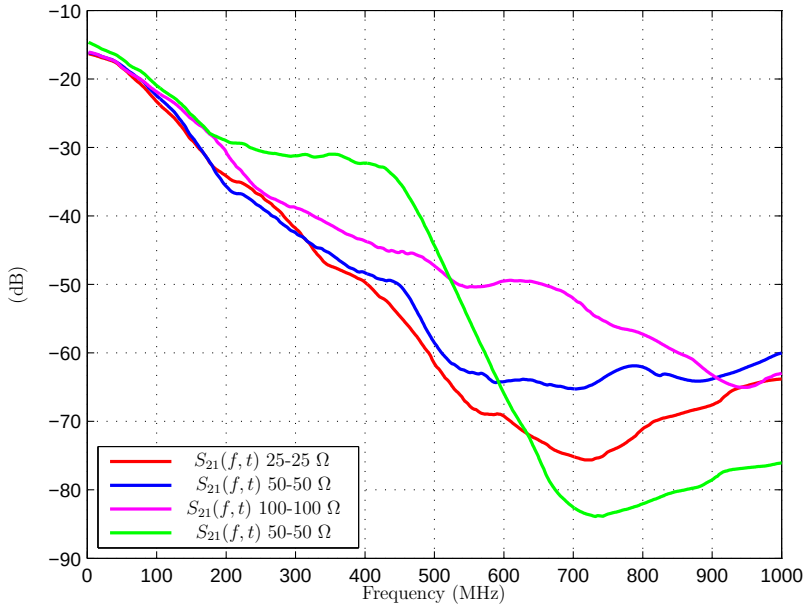

Figure 72: Magnitude of $S_{21}(f,t)$ scattering parameters comparing adaptive PLC coupling circuit with adaptive PLC coupling circuit and non-adaptive PLC coupling circuit 50 Ω in the frequency band of 2-500 MHz.

presents the impedance matching results near to the adaptive PLC coupling circuit with the input impedance of 50 Ω.

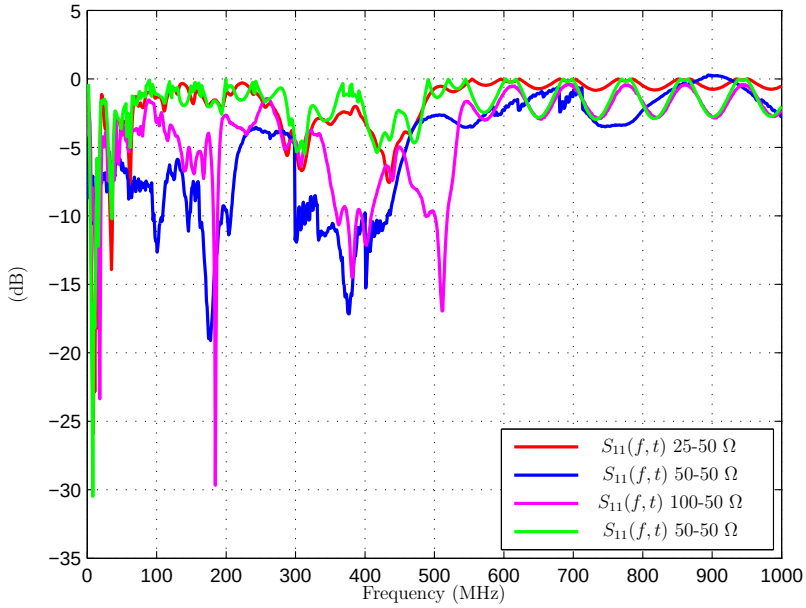

Figure 73: Magnitude of $S_{11}(f,t)$ scattering parameters comparing non-adaptive PLC coupling circuit 50 Ω with adaptive PLC coupling circuit.

Analyzing the $S_{21}(f,t)$ scattering parameter in all frequency bands, we note that

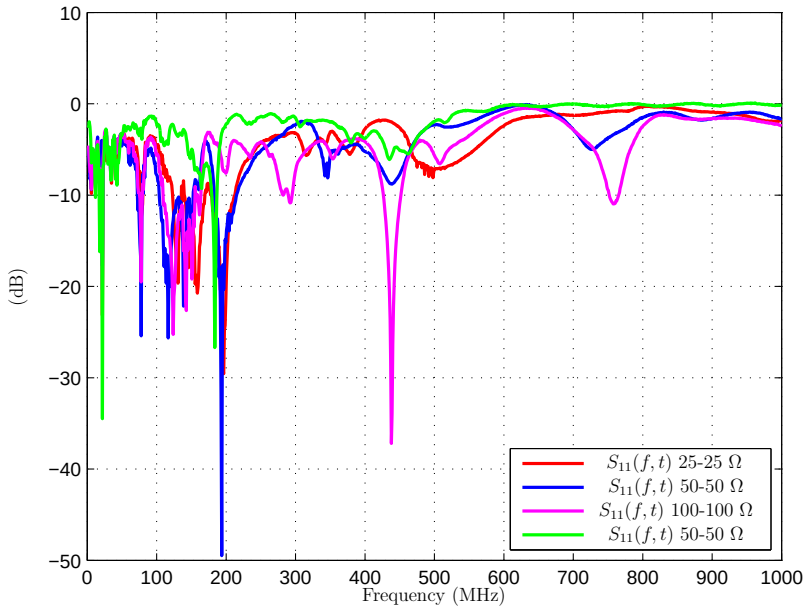

Figure 74: Magnitude of $S_{11}(f,t)$ scattering parameters comparing adaptive PLC coupling circuit with adaptive PLC coupling circuit and non-adaptive PLC coupling circuit 50 Ω in the frequency band of 2-500 MHz.

if the frequency band increase the attenuation increase due to the inductive behavior. With the increase of the bandwidth of the PLC coupling circuits we note that the curves of the S_{21} scattering parameters have values more distant from each other and the adaptive PLC coupling circuit with input impedance equal to 25 Ω has the worse insertion loss curves in all frequency bands.

The results of $S_{11}(f,t)$ scattering parameter shows that in the frequency band 2-50 MHz the values of the curves are very close and the PLC coupling circuits designed for the frequency bands of 2-50 MHz and 2-100 MHz shows a better impedance matching comparing with the other PLC coupling circuit. However, for the PLC coupling circuits in the frequency band 2-500 MHz, the analysis and simulation indicate that the non-adaptive PLC coupling circuit 50 Ω connected to the adaptive PLC coupling circuit 50 Ω presents the best impedance matching. The adaptive PLC coupling circuit with input impedance equal to 25 Ω shows the worse impedance matching in all analyzes and we conclude that the values of the resistance component of the access impedance of the electric power grid are between 50 Ω and 100 Ω.

The apparatus used to characterize the S_{11} and S_{21} scattering parameters with non-adaptive and adaptive PLC coupling circuits were described in this Chapter. In details, the measurement has shown the behavior of PLC coupling circuit scattering parame-

ters connected to the LV electric power grid. Important information has been noted concerning attenuation and reactive behavior of access impedance in the frequency band of 2-500 MHz. Moreover, the obtained results about S_{11} scattering parameter have shown it is possible to perform impedance matching between a PLC transceiver and the electric power grids using an adaptive PLC coupling circuit; however, the impedance matching between two adaptive PLC coupling circuits may be a difficult task to be accomplished because coordination between them is demanded.

Also, it is important to highlight that this is the first measurement of S_{11} and S_{21} scattering parameters proposed for non-adaptive and adaptive PLC coupling circuit on Brazilian electric power grid in the frequency band of 2-500 MHz.

5.5 SUMMARY

This Chapter has presented a design and analysis of adaptive PLC coupling circuits. The proposed adaptive PLC coupling circuits was designed with input impedance matching of 25 Ω, 50 Ω and 100 Ω, according to the statistical analyzes exhibit in Chapter 3. The numerical results showed that improvements in terms of impedance matching may be accomplished by using the proposed adaptive PLC coupling circuit.

6 CONCLUSION

Due to the fast increasing of LV narrowband and broadband PLC applications over the past decades, important issues in this matter needs to be further investigated, such as coupling circuits. In this regard, this thesis proposed the design of a capacitive, SISO and LV non-adaptive and adaptive PLC coupling circuits. The specification and design of such PLC coupling circuit prototypes are proposed measuring their scattering parameters and the performance of this PLC coupling circuits connecting to the electric power grid is analyzed. Furthermore, this dissertation proposes the design of an adaptive PLC coupling circuit with previous acknowledgment of the access impedance discussed in Chapter 3.

Chapter 2 has addressed a review on the use of PLC coupling circuits to enable data communications over AC and DC voltages. The review showed that the introduction of PLC coupling circuits to connect PLC transceivers to electric power grid could be used to minimize both signal distortion and insertion loss to improve PLC systems performance. In this regard, we isolated the key issues related to the design of a PLC coupler, such as the PCB design showing that electrical characteristics of the PCB cause significant impact on the coupling performance. We discussed the importance of insertion and return loss to characterize the PLC coupling circuits and quantify the distortion introduced by the PLC coupling circuits. We presented the block diagram of a coupling circuit, which is composed of an electric power protection device, a high-pass filter, a galvanic isolation and a low-pass filter. The protection stage has its main function in the clamp as much as possible the current and voltage surges. The high-pass filter, composed only of a capacitor is responsible for blocking the high power mains signal and enables the high-frequency transceiver's signal pass without being attenuated. A RF transformer provides galvanic isolation and, finally, a low-pass filter, composed of capacitor and inductors, is responsible for delimitates the cut-off frequency. Therefore, particular attention must be paid to the SRF of the components chosen, especially at high frequencies to avoid distortion in the frequency response. Furthermore, we provided a classification of PLC couplers based on the type of physical

coupling (capacitive, inductive, resistive and antenna). We point out that, regardless of electric power grid to be AC or DC, the inductive and capacitive PLC coupling circuit can be classified according to their voltage level as HV, MV and LV. The frequency bands allocated in PLC systems can be classified as narrowband and broadband and the PLC coupling circuits must be designed according to the chosen frequency band. The analysis of propagation mode shows that the power cable wiring installation can be use to inject and extract the PLC signal in two ways, DM and CM mode, using different ways such as phase, neutral and ground conductors and number of connections of these wires can be used to provide more than one path for data communication. These fundamental concepts are provided to suffice basic understanding about some relevant issues related to the design of PLC coupling circuits.

Chapter 4 has introduced a design and characterization of a capacitive, SISO and LV non-adaptive PLC coupling circuit designed for narrowband and broadband frequency bands. The design of appropriate PLC coupling circuits is detailed showing the electric protection devices used on primary stage based on MOV and GDT, and on secondary stage, near to PLC transceivers, based on Zener diodes. The combination of high-pass and low-pass analog filter to design a band-pass filter which eliminates the high power mains signal and high-frequency signal is discussed and used to limit the frequency band in narrowband and broadband PLC coupling circuit. Each component of the PLC coupling circuit prototype such as connectors, capacitors, inductors and RF transformer was chosen to work in the desired frequency band and avoid distortion in the magnitude frequency response. Moreover, the PCB was designed following the microstrip technique to well-define impedance of 50 Ω. The narrowband and broadband prototypes design was analyzed showing the schematic circuits, PCB, the values of components for each PLC coupling circuit and finally the performance of the developed PLC coupling circuits was shown measuring their scattering parameters. The measuring scattering parameters show that the PLC coupling circuit added with de microstrip technique offers satisfactory results.

In Chapter 3 has presented a measurement campaign carried out on in-home and LV electric power grid. In this regard, the Chapter 3 focuses on measurement, characterization, statistical analysis and the procedure to model the access impedance of in-home at Brazilian LV electric power grid. Based on a large set of access impedance measures covering the frequency band between 2 and 500 MHz, we have obtained a statistical model for both resistance and reactance components of the access impedance. This model assumes that the access impedance is a random process in the frequency

domain and is capable of generating samples functions of such access impedance. The model is proposed following six steps whose information will be very important to know the value of the resistance and reactance of the electric power grid impedance and thus design PLC coupling circuits with the previous knowledge of the values that the electric power grid impedance can most likely assume. This measurement campaign has provided relevant information about the access impedances in typical Brazilian residences and facilities and it shows that electric power grid access impedance is mostly inductive and the resistive component varies between 25 and 100 Ω in 90 % analyzing the CDF curve. In order to select the best distribution model, a statistical analysis of the data set of measured access impedance was shown based on Lognormal, Exponential, Gamma, Inverse Gaussian, Logistic, Log-logistic, Nakagami, Normal, Weibull and t-location scale distributions. The results show that the resistance is best modeled by the Log-logistic distribution and the reactance is best modeled by the t-location scale distribution.

Finally, Chapter 5 has discussed the prototype of an adaptive PLC coupling circuit showing its effectiveness matching the impedance and providing maximum power transfer to the electric power grid. The necessity to investigate an adaptive PLC coupling circuit arises due to the time-varying nature of residential loads. In this fickle environment, a non-adaptive PLC coupling circuit 50 Ω fails to achieve its purpose. In this concern, in order to enhance the impedance matching, a discuss about an adaptive PLC coupling circuit which automatically matches to the varying impedance, providing better perceptive of PLC in real applications is presented. Since the complete matching with the time-varying impedance of the PLC transmission media is very difficult, only the resistance of electric power grid impedance is proposed to be match. The reactance component is absorbed by the input reactance of the analog low-pass filter of the adaptive PLC coupling circuit. In order to verify the performance of the implemented couplers we compare the system composed of a non-adaptive PLC coupling circuit 50 Ω together with an adaptive PLC coupling circuit and another system composed of two adaptive PLC coupling circuits. Based on the analyzed results, the best impedance matching is achieved for the PLC coupling circuits with input impedances of 50 Ω and 100 Ω and the PLC coupling circuits with input impedance of 25 Ω showed the worst results for the S_{11} and S_{12} scattering parameters. Considering the results we can conclude that an adaptive PLC coupling circuit proved its effectiveness in performing the impedance matching compared with the non-adaptive PLC coupling circuit.

6.1 FUTURE WORKS

Future research efforts that can be carried out are as follows:

- To develop other methods to measure the access impedance and compare with the results of the measurement campaign obtained in Chapter 3 using the same access impedance model, which constitutes an important tool to be used for design non-adaptive and adaptive PLC coupling circuits.
- To propose other types of adaptive PLC coupling circuits that can offer impedance matching for the reactance and resistance of electric power grid simultaneously by improving better insertion loss and return loss.
- To promote another impedance measurement campaign to characterize electric power grid impedance in the SIMO, MISO and MIMO configurations outdoor and in-vehicle electric power grid and design improved versions of adaptive coupling circuits based on measurements.

REFERENCES

[1] C. Ke, Q. Chenxi, Z. Tingtao, and H. Xiaoguang, "Research of automatic meter reading system based on broadband carrier in the power line," in *Proc. Industrial Electronics and Applications (ICIEA)*, June 2011, pp. 2763–2767.

[2] J. Nguimbis, S. Cheng, Y. Zhang, and L. Xiong, "Coupling unit topology for optimal signaling through the low-voltage powerline communication network," *IEEE Transactions on Power Delivery*, vol. 19, no. 3, pp. 1065–1071, Jul. 2004.

[3] M. V. Ribeiro, "*Técnicas de processamento de sinais aplicadas a transmissão de dados via rede elétrica e ao monitoramento da qualidade de energia*," Ph.D. dissertation, Universidade de Campinas UNICAMP, Apr 2005.

[4] P. Van Rensburg and H. Ferreira, "Dual coupler for dedicated switching with loads," in *Proc. International Symposium on Power Line Communications and Its Applications*, Mar. 2007, pp. 53–58.

[5] M. Seijo, G. López, J. Matanza, and J. I. Moreno, "Planning and performance challenges in power line communications networks for smart grids," *International Journal of Distributed Sensor Networks*, vol. 12, no. 3, pp. 892– 981, Jan. 2016.

[6] H. Gassara, M. Bali, F. Duval, F. Rouissi, and A. Ghazel, "Coupling interface circuit design for experimental characterization of the narrowband power line communication channel," in *Proc. IEEE International Symposium on Electromagnetic Compatibility*, Aug. 2012, pp. 1–6.

[7] L. G. da Silva Costa, "Circuitos de acoplamento para transceptores PLC," Dissertação de Mestrado, Universidade Federal de Juiz de Fora - UFJF, Feb 2012.

[8] Y. Xiaoxian, Z. Tao, Z. BaoHui, Y. Fengchun, D. Jiandong, and S. Minghui, "Research of impedance characteristics for medium-voltage power networks," *IEEE Trans. on Power Delivery*, vol. 22, no. 2, pp. 870–878, Apr. 2007.

[9] P. Van Rensburg and H. Ferreira, "Coupler winding ratio selection for effective narrowband power-line communications," *IEEE Trans. on Power Delivery*, vol. 23, no. 1, pp. 140–149, Jan. 2008.

[10] M. Sibanda, P. Van Rensburg, and H. Ferreira, "Impedance matching with low-cost, passive components for narrowband PLC," in *Proc. IEEE International Symposium on Power Line Communications and Its Applications*, Apr. 2011, pp. 335–340.

[11] "Keysight technologies." http://www.keysight.com/en/pc-1297113, Jun 2016.

[12] M. Schwartz, "Carrier-wave telephony over power lines: Early history [history of communications]," *Trans. on Communications Magazine*, vol. 47, no. 1, pp. 14–18, Jan. 2009.

[13] O. G. Hooijen, "A channel model for the low-voltage power-line channel; measurement and simulation results," in *Proc. Internatonal Symposium on Power line Communications and its Applications*, Apr. 1997, pp. 51–56.

[14] H. Meng, S. Chen, Y. Guan, C. Law, P. So, E. Gunawan, and T. Lie, "Modeling of transfer characteristics for the broadband power line communication channel," *IEEE Trans. on Power Delivery.*, vol. 19, no. 3, pp. 1057–1064, Jul. 2004,.

[15] A. Pinomaa, J. Ahola, A. Kosonen, and P. Nuutinen, "Power line communication network for a customer-end AC grid in an LVDC distribution system," in *Proc. IEEE International Conference on Smart Grid Communications*, Nov. 2014, pp. 224–229.

[16] S. Chen, M. Setta, X. Chen, and C. G. Parini, "Ultra wideband powerline communication (PLC) above 30 MHz," *Institution of Engineering and Technology Communications*, vol. 3, no. 10, pp. 1587–1596, Oct. 2009.

[17] E. A. Teixeira, E. L. Rege, F. S. Marques, E. M. de Souza, T. M. Johnson, and M. V. Ribeiro, "Regulation issues relating to broadband PLC: A Brazilian experience and perspective," in *Proc. IEEE International Symposium on Power Line Communications and Its Applications*, Mar. 2007, pp. 523–527.

[18] K. Dostert, *Powerline Communications*. Prentice Hall, 2001.

[19] J. Granado, A. Torralba, and J. Chavez, "Using broadband power line communications in non-conventional applications," *IEEE Trans. on Consumer Electronics*, vol. 57, no. 3, pp. 1092–1098, Aug. 2011.

[20] H. Ferreira, H. Grove, O. Hooijen, and A. J. Han Vinck, "Power line communications: an overview," in *Proc. IEEE African Electrical Technology Conference*, vol. 2, Sep. 1996, pp. 558–563.

[21] X. Carcelle, *Power Line Communications in Practice*. New York: Artech House, 2006.

[22] T. R. Oliveira, W. A. Finamore, and M. V. Ribeiro, "A sounding method based on OFDM modulation for PLC channel measurement," in *Proc. IEEE International Symposium on Power Line Communications and Its Applications*, Mar. 2013, pp. 185–190.

[23] A. A. M. Picorone, T. R. Oliveira, and M. V. Ribeiro, "PLC channel estimation based on pilots signal for OFDM modulation: A review," *IEEE Latin America Transactions*, vol. 12, no. 4, pp. 580–589, Jun. 2014.

[24] J. Dias, F. P. V. de Campos, M. L. R. de Campos, E. L. Pinto, and M. V. Ribeiro, "Time-varying channel characterization based on SVM under the impulsive noise presence," in *Proc. IEEE International Symposium on Power Line Communications and Its Applications*, Mar. 2010, pp. 261–266.

[25] G. R. Colen, H. Schettino, D. Fernandes, L. M. Sirimarco, F. P. Campos, W. A. Finamore, H. A. Latchman, and M. V. Ribeiro, "A temporal compressive resource allocation technique for complexity reduction in plc transceivers," *Trans. on Emerging Telecommunications Technologies*, vol. 1, no. 1, pp. 1–12, May 2015.

[26] M. V. Ribeiro, G. R. Colen, Z. Quan, H. V. Poor *et al.*, "Clustered-orthogonal frequency division multiplexing for power line communication: when is it beneficial?" *IET Communications*, vol. 8, no. 13, pp. 2336–2347, Apr. 2014.

[27] M. V. Ribeiro, R. R. Lopes, J. M. T. Romano, and C. A. Duque, "Impulse noise mitigation based on computational intelligence for improved bit rate in PLC-DMT," *IEEE Trans. on Power Delivery*, vol. 21, no. 1, pp. 94–101, Jan. 2006.

[28] R. M. Oliveira, M. S. Facina, M. V. Ribeiro, and A. B. Vieira, "Performance evaluation of in-home broadband plc systems using a cooperative MAC protocol," *Computer Networks*, vol. 95, pp. 62–76, Dec. 2016.

[29] C. Boddie, "Telephone communication over power lines by high frequency currents," *in Proc. of the Institute of Radio Engineers*, vol. 15, no. 7, pp. 559–640, July 1927.

[30] T. R. Oliveira, C. A. G. Marques, M. S. Pereira, S. L. Netto, and M. V. Ribeiro, "The characterization of hybrid PLC-wireless channels: A preliminary analysis," in *Proc. IEEE International Symposium on Power Line Communications and Its Applications*, Mar. 2013, pp. 98–102.

[31] T. R. Oliveira, F. J. A. Andrade, A. A. M. Picorone, H. A. Latchman, S. L. Netto, and M. V. Ribeiro, "Characterization of hybrid communication channel in indoor scenario," *Journal of Communication and Information System.*, vol. 31, no. 1, pp. 224 – 235, Nov. 2016.

[32] Z. W. Swana, P. A. J. van Rensburg, and H. C. Ferreira, "Is resistive coupling feasible for the reception of power-line communications data?" in *Proc. International Symposium on Power Line Communications and Its Application*, May 2015, pp. 47–52.

[33] J. Anatory and T. N., *Broadband Power-line Communication Systems Theory and Applications*. Boston: Wit Press, 2010.

[34] L. Simonovich, "Relative permittivity variation surrounding PCB via hole structures," in *Proc. IEEE Workshop on Signal Propagation on Interconnects*, May 2008, pp. 1–4.

[35] D. Moongilan, "Minimizing radiated emissions from PCBs using grid-like ground plane impedance matching techniques," in *Proc. International Symposium on Electromagnetic Compatibility*, vol. 3, Aug. 2005, pp. 971–976.

[36] G. Smithson, "Practical RF printed circuit board design," in *How to Design RF Circuits, IEE Training Course*, Jul. 2000, pp. 11/1–11/6.

[37] T. T. Yan and M. Z. M. Jenu, "Capacitive and inductive couplings of PCB traces," in *Proc. Telecommunication systems Congresses*, vol. 1, Sep. 2000, pp. 186–191.

[38] M. Rajesh, P. Bhartia, and I. J. Bahl, *RF and Microwave Coupled Line Circuits*, 2nd, Ed. Boston: Artech House, 2007.

[39] R. Mongia, I. Bahl, and P. Jit Bharitia, *RF and Microwave Coupled-line Circuits*. Norwood: Artech House, 1999.

[40] S. C. Thierauf, *High-Speed Circuit Board Signal Integrity*. New York: Artech House, 2004.

[41] G. Gonzalez, R. Linares Y.M., J. De La Rosa, and W. Fonseca, "Ground plane impedance analysis of printed circuit board," in *Proc. IEEE International Symposium on Electromagnetic Compatibility*, vol. 2, Aug. 1999, pp. 712–715.

[42] D. Brooks, *Signal Integrity Issues and Printed Circuit Board Design*. Boston: Prentice Hall, 2003.

[43] R. Ludwig and G. Bogdanov, *RF Circuit Design, Theory and Applications*. New Delhi, India: Prentice Hall, 2009.

[44] K. Fezzani, C. Rebai, and A. Ghazel, "Analysis and optimization of power line coupling circuit for CENELEC-PLC modem," in *Proc. IEEE International Conference on Electronics, Circuits and Systems*, Dec. 2006, pp. 676–679.

[45] Z. Tao, Y. Xiaoxian, and Z. BaoHui, "Influence and modification of coupling device on low voltage power network channel characterization measurement," in *Proc. IEEE Power and Energy Society Transmission and Distribution Conference and Exhibition: Asia and Pacific*, Apr. 2005, pp. 1–5.

[46] W. A. Davis and K. Agarwal, *Radio Frequency Circuit Design*, K. Chang, Ed. New York: John Wiley and Sons, 2001.

[47] J. Biernacki and D. Czarkowski, "High frequency transformer modeling," in *Proc. IEEE International Symposium on Circuits and Systems*, vol. 2, May 2001, pp. 676–679.

[48] P. J. Van Rensburg and H. C. Ferreira, "Coupling circuitry: understanding the functions of different components," in *Proc. International Symposium in Power Line Communications and Its Applications*, vol. 1, Mar. 2003, pp. 204–209.

[49] M. K. Kazimierczuk, *Radio Frequency Circuit Designg*. New York: John Wiley and Sons, 2009.

[50] V. Dumbrava and L. Svilainis, "RF transformer model parameters measurement," in *Proc. Design and Diagnostics of Electronic Circuits and Systems*, Apr. 2007, pp. 1–5.

[51] M. S. Damnjanovic, L. D. Zivanov, S. M. Djuric, A. M. Maric, A. B. Menicanin, G. J. Radosavljevic, and N. V. Blaz, "Characterization and modelling of miniature ferrite transformer for high frequency applications," *Microelectronics International Magazine*, vol. 29, no. 2, pp. 83–89, Jan. 2012.

[52] Y. Sun and G. Amaratunga, "High-current adaptive impedance matching in narrowband power-line communication systems," in *Proc. IEEE International Symposium on Power Line Communications and Its Applications*, Apr. 2011, pp. 329–334.

[53] F. Corripio, J. Arrabal, L. del Rio, and J. Munoz, "Analysis of the cyclic short-term variation of indoor power line channels," *IEEE Journal on Selected Areas in Communications*, vol. 24, no. 7, pp. 1327–1338, Jul. 2006.

[54] A. Tonello, F. Versolatto, and A. Pittolo, "In-home power line communication channel: statistical characterization," *IEEE Trans. on Communications*, vol. 62, no. 6, pp. 2096–2106, Jun. 2014.

[55] L. G. S. Costa, A. A. M. Picorone, A. C. M. de Queiroz, V. L. R. Costa, and M. V. Ribeiro, "Caracterização da impedância de acesso à rede de energia elétrica residencial para uso em sistemas PLC," *XXXIII Simpósio Brasileiro de Telecomunicações*, pp. 1–5, Sep. 2015.

[56] G. R. Colen, C. A. G. Marques, T. R. Oliveira, F. P. V. de Campos, and M. V. Ribeiro, "Measurement setup for characterizing low-voltage and outdoor electric distribution grids for PLC systems," in *Proc. Conference On Innovative Smart Grid Technologies Latin America*, Apr. 2013, pp. 1–5.

[57] R. Vines, H. Trussell, K. Shuey, and J. O'Neal, J.B., "Impedance of the residential power-distribution circuit," *IEEE Trans. on Electromagnetic Compatibility*, vol. EMC-27, no. 1, pp. 6–12, Feb. 1985.

[58] E. Karadeniz and I. Cavdar, "Measurements of impedance and attenuation at CENELEC bands for power line communications systems," *Sensors*, pp. 8027–8036, Dec. 2008.

[59] J. Malack and J. Engstrom, "RF impedance of United States and European power lines," *IEEE Trans. on Electromagnetic Compatibility*, vol. EMC-18, no. 1, pp. 36–38, Feb. 1976.

[60] J. R. Nicholson and J. Malack, "RF impedance of power lines and line impedance stabilization networks in conducted interference measurements," *IEEE Trans. on Electromagnetic Compatibility*, vol. EMC-15, no. 2, pp. 84–86, May 1973.

[61] H. Tian, R. Yuan, F. Li, Z. Huang, S. Wang, S. Li, and K. Zhong, "Measurement on narrow band power line communication channel impedance of distribution network," in *Proc. International Conference on Consumer Electronics, Communications and Networks*, Apr. 2011, pp. 454–457.

[62] R. Araneo, S. Celozzi, and G. Lovat, "Design of impedance matching couplers for Power Line Communications," in *Proc. IEEE International Symposium in Electromagnetic Compatibility*, Aug. 2009, pp. 64–69.

[63] L. Qi, S. Jingzhao, and F. Zhenghe, "Adaptive impedance matching in power line communication," in *Proc. International Conference in Microwave and Millimeter Wave Technology*, Aug. 2004, pp. 887–890.

[64] S. Despande, I. Prasanna, and S. Panda, "An adaptive impedance matching technique for narrowband power line communication in residential smart grids," *International Journal of Engineering Research and Technology*, vol. 2, p. 9, Sep. 2013.

[65] A. A. Atayero, A. A. Alatishe, and Y. A. Ivanov, "Power line communication technologies: Modeling and simulation of PRIME physical layer," in *Proc. World Congress on Engineering and Computer Science*, vol. 2, Oct. 2012, pp. 24–26.

[66] C. P. Rui, N. N. Barsoum, A. W. K. Ming, and W. K. Ing, "Adaptive impedance matching network with digital capacitor in narrowband power line communication," in *Proc. IEEE International Symposium on Industrial Electronics*, May 2013, pp. 1–5.

[67] C.-Y. Park, K.-H. Jung, and W.-H. Choi, "Coupling circuitary for impedance adaptation in power line communications using VCGIC," *in Proc. IEEE International Symposium on Power Line Communications and Its Applications*, pp. 293–298, Apr. 2008.

[68] W.-H. Choi and C. Y. Park, "A simple line coupler with adaptive impedance matching for power line communication," in *Proc. IEEE International Symposium on Power Line Communications and Its Applications*, Mar. 2007, pp. 187–191.

[69] M. Sibanda, P. van Rensburg, and H. Ferreira, "A compact economical plc bandpass coupler with impedance matching," in *Proc. IEEE International Symposium on Power Line Communications and Its Applications*, Mar. 2013, pp. 339–344.

[70] S. Yang, H. Li, M. Goldberg, X. Carcelle, F. Onado, and S. Rowland, "Broadband impedance matching circuit design using numerical optimisation techniques and field measurements," in *Proc. IEEE International Symposium on Power Line Communications and Its Applications*, Mar. 2007, pp. 425–430.

[71] R. Araneo, S. Celozzi, G. Lovat, and F. Maradei, "Multi-port impedance matching technique for power line communications," in *Proc. IEEE International Symposium on Power Line Communications and Its Applications*, Apr. 2011, pp. 96–101.

[72] J. Kennedy and R. Eberhart, "Particle swarm optimization," in *Proc. Conference on Neural Networks*, vol. 4, Nov. 1995, pp. 1942–1948.

[73] S. Wei, W. Gao, L. Zhang, and Z. Cao, "High frequency and broadband coupling characteristics of filter circuit based on low voltage power lines," *in Proc. Advanced in Control Engineering and Information Science*, vol. 15, pp. 1978–1982, Aug. 2011.

[74] H. Ueda and T. Tsuboi, "A sampling theorem for periodic functions with no minus frequency component and its application," in *Proc. Asia-Pacific Conference on Communications*, Aug 2013, pp. 225–230.

[75] C. Bowick, *RF Circuit Design*, 2nd, Ed. Burlington: Howard W. Sams and Cos, 2008.

[76] J. Zdunek, "Generation of filter functions from a given model," *Institute of Electrical Engineers*, vol. 110, no. 2, pp. 282–294, Feb. 1963.

[77] C. P. Serra, *Teoria e Projeto de Filtros*. Campinas, Brazil: Cartigraf, 1983.

[78] A. C. M. de Queiroz and L. P. Caloba, "Passive symmetrical RLC filters suitable for active simulation," in *Proc. IEEE International Symposium in Circuits and Systems*, vol. 3, Jun. 1988, pp. 2411–2414.

[79] B. Zarikoff and D. Malone, "Experiments with radiated interference from in-home power line communication networks," in *Proc. IEEE International Conference on Communications*, Jun. 2012, pp. 3414–3418.

[80] E. A. Teixeira, F. S. Marques, S. G. de Araujo, E. M. de Souza, T. M. Johnson, and M. V. Ribeiro, "Modeling and performance analysis of PLC channels with external interference in outdoor and indoor environments," in *Proc. IEEE International Symposium on Power Line Communications and Its Applications*, Apr. 2008, pp. 222–227.

[81] F. Leccese, "Study and characterization of a new protection system against surges and over voltages for domestic telecommunication networks," in *Proc. International Telecommunications Energy Conference*, Sep. 2007, pp. 363–368.

[82] V. Kamat, "Protection mechanism for modern telecommunications," in *Proc. International Conference in Electromagnetic Interference and Compatibility*, Dec. 1997, pp. 45–50.

[83] T. Imamura and A. Ametani, "Investigation of transient induced voltage to a communication line from an overhead power transmission line," *Generation, Transmission and Distribution*, vol. 137, no. 2, pp. 129–138, Mar. 1990.

[84] A. Gayen, A. Dhar, B. Das, and D. Poddar, "Study of the induced voltage on an overhead line due to lightning discharge," in *Proc. International Conference in Electromagnetic Interference and Compatibility*, Feb. 2006, pp. 353–357.

[85] W. Vijayananda and S. Alahakoon, "Surge arrester with improved reliability and protection level for low bandwidth data communication in high voltage installations," in *Proc. Australasian Universities Power Engineering Conference*, Dec. 2010, pp. 1–6.

[86] H. Iwao, H. Kijima, and K. Takato, "An influence on transmission characteristics of power line communication when using surge protective devices," in *Proc. IEEE International Symposium in Power Line Communications and Its Applications*, Apr. 2008, pp. 218–221.

[87] H. C. Ferreira, L. Lampe, J. Newbury, and T. G. Swart, *Power Line Communications Theory and Applications for Narrowband and Broadband Communications over Power Lines*. New York: John Wiley and Sons, 2010.

[88] M. Hove, T. O. Sanya, A. J. Snyders, I. R. Jandrell, and H. C. Ferreira, "The effect of type of transient voltage suppressor on the signal response of a coupling circuit for power line communications," in *Proc. IEEE African Electrical Technology Conference*, Sep. 2011, pp. 1–6.

[89] M. Drabkin, "Surge protection of low-voltage AC power by MOV-based SPDs," in *Proc. 10th International Conference in Harmonics and Quality of Power*, vol. 1, Oct. 2002, pp. 13–16.

[90] J. Wei and D. Gerling, "Simulation and modelling of power passive components for EMI prediction," in *Proc. IET International Conference on Power Electronics, Machines and Drives*, Mar. 2012, pp. 1–6.

[91] S. Chickamenahalli, H. Braunisch, S. Srinivasan, J. He, U. Shrivastava, and B. Sankman, "RF packaging and passives: design, fabrication, measurement, and validation of package embedded inductors," *IEEE Trans. on Advanced Packaging*, vol. 28, no. 4, pp. 665–673, Nov. 2005.

[92] M. Bartoli, A. Reatti, and M. Kazimierczuk, "High-frequency models of ferrite core inductors," in *Proc. International Conference on Industrial Electronics, Control and Instrumentation*, vol. 3, Sep. 1994, pp. 1670–1675.

[93] R. Lafferty, "Measuring the self-resonant frequency of capacitors," *IEEE Trans. on Components, Hybrids, and Manufacturing Technology*, vol. 5, no. 4, pp. 528–530, Dec. 1982.

[94] H. Hrasnica, A. Haidine, and R. Lehnert, *Broadband Powerline Communications: Network Design*. Chinchester, England: John Wiley and Sons, 2004.

[95] I. Whyte, "Distribution network powerline carrier communication system," U.S. Patent 3 942 170, Mar. 2, 1976. [Online]. Available: https://www.google.tl/patents/US3942170

[96] L. G. S. Costa, A. A. M. Picorone, A. C. M. de Queiroz, V. L. R. Costa, and M. V. Ribeiro, "Projeto e caracterização de acopladores para power line communications," in *Proc. XXXIII Simpósio Brasileiro de Telecomunicações*, Sep. 2015, pp. 1–5.

[97] E. Wade and H. Asada, "Design of a broadcasting modem for a DC PLC scheme," *IEEE/ASME Trans. on Mechatronics*, vol. 11, no. 5, pp. 533–540, Oct. 2006.

[98] F. Grassi and S. Pignari, "Coupling/decoupling circuits for powerline communications in differential DC power buses," in *Proc. IEEE International Symposium on Power Line Communications and Its Applications*, Mar. 2012, pp. 392–397.

[99] H.-K. Podszeck, *Carrier Communication over Power Lines*. New York: Springer, 1972.

[100] A. Pinomaa, J. Ahola, A. Kosonen, and P. Nuutinen, "Homeplug green PHY for the LVDC PLC concept: Applicability study," in *Proc. IEEE International Symposium on Power Line Communications and its Applications*, Mar. 2015, pp. 205–210.

[101] J.-J. Lee, D.-S. In, H.-M. Oh, S. Shon, and D.-H. Nam, "Neutral inductive coupling for improved underground medium voltage BPLC," in *Proc. IEEE International Symposium on Power Line Communications and Its Applications*, Mar. 2010, pp. 67–71.

[102] J. Binkofski, "Influence of the properties of magnetic materials," in *Proc. IEEE International Symposium on Power Line Communications and Its Applications*, Apr. 2005, pp. 281–284.

[103] C. Kikkert, "Power transformer modelling and MV PLC coupling networks," in *Proc. IEEE Power and Energy Society Innovative Smart Grid Technologies Asia*, Nov. 2011, pp. 1–6.

[104] D.-S. In, S. Shon, and J. J. Lee, "A study on the implementation of inductive coupler with Rogowski coil for BPLC," in *Proc. International Conference on Advanced Technologies for Communications*, Oct. 2008, pp. 327–330.

[105] Q. Yu, T. Holmes, and K. Naishadham, "RF equivalent circuit modeling of ferrite-core inductors and characterization of core materials," *IEEE Trans. on Electromagnetic Compatibility*, vol. 44, no. 1, pp. 258–262, Feb. 2002.

[106] O. Bilal, E. Liu, Y. Gao, and T. O. Korhonen, "Design of bidirectional coupling circuit for broadband power-line communications," *Journal of Electromagnetic Analysis and Applications*, vol. 4, no. 4, pp. 162–166, Apr. 2012.

[107] T. R. Oliveira, C. A. G. Marques, M. S. Pereira, S. L. Netto, and M. V. Ribeiro, "The characterization of hybrid PLC-wireless channels: A preliminary analysis," in *Proc. IEEE International Symposium on Power Line Communications and Its Applications*, Mar. 2013, pp. 98–102.

[108] T. R. Oliveira, "*The characterization of hybrid PLC-wireless and PLC channels in the frequency band between 1.7 and 100 MHz for data communication*," Ph.D. dissertation, Federal University of Juiz de Fora, 2015.

[109] S. Jordaan, P. A. Janse van Rensburg, A. S. De Beer, and H. C. Ferreira, "Long-wire half wave dipole antenna integrated into power cabling," Australian Patent 2 013 101 645, 2 17, 2013.

[110] A. Emleh, A. de Beer, H. Ferreira, and A. J. Han Vinck, "Interference detection on powerline communications channel when in-building wiring system acts as an antenna," in *Proc. International Symposium Electronic in Marine*, Sep. 2013, pp. 141–144.

[111] T. R. Oliveira, F. J. Andrade, L. G. S. Costa, M. S. Pereira, and M. V. Ribeiro, "Measurement of hybrid PLC-wireless channels for indoor and broadband data communication," in *Proc. XXXI Simpósio Brasileiro de Telecomunicações*, vol. 1, no. 1, Sep. 2013, pp. 1–5.

[112] S. Jordaan, P. Janse van Rensburg, A. de Beer, H. Ferreira, and A. J. Han Vinck, "A preliminary investigation of the UHF properties of LV cable for WiFi over power line communications," in *Proc. IEEE International Symposium on Power Line Communications and its Applications*, Mar. 2015, pp. 35–40.

[113] L. Lampe, T. A. M., and T. G. Swart, *Power Line Communications: Principles, Standards and Applications from Multimedia to Smart Grid*. New Deli: John Wiley & Sons, 2016.

[114] "IEEE guide for power-line carrier applications," *IEEE Std 643-2004, Revision of IEEE Std 643-1980*, pp. 1–134, Aug. 2005.

[115] "American national standard requirements for power-line carrier coupling capacitors and coupling capacitor voltage transformers," *ANSI C93.1-1999*, pp. 41–42, May 1999.

[116] G. Franklin, "A practical guide to harmonic frequency interference affecting high-voltage power-line carrier coupling systems," *IEEE Trans. on Power Delivery*, vol. 24, no. 2, pp. 630–641, Apr. 2009.

[117] B. A. Mork, D. Ishchenko, X. Wang, A. Yerrabelli, R. Quest, and C. Kinne, "Power line carrier communications system modeling," in *Proc. International Conference on Power Systems Transients*, Jun. 2005, pp. 1–6.

[118] P. Wouters and P. van der Wielen, "Effect of cable load impedance on coupling schemes for MV power line communication," in *Proc. IEEE Bologna Power Technology Conference*, vol. 2, Jun. 2003, p. 7.

[119] F. Campagna, M. Quarantelli, and R. Pighi, "High-frequency characterization of a medium voltage PLC transmission system," in *Proc. Third Workshop on Power Line Communications*, Oct. 2009, pp. 1–4.

[120] F. Issa, O. Devaux, E. Marthe, and F. Rachidi, "Influence of power switching on power line communications in medium voltage networks," in *Proc. IEEE International Conference on Communications*, vol. 1, Jun. 2004, pp. 114–117.

[121] S. S. Ali, A. Bhattacharya, and D. R. Poddar, "Design of bidirectional coupling circuit for broadband power-line communications," *Journal of Electromagnetic Analysis and Applications*, vol. 4, pp. 162–166, Apr. 2012.

[122] M. Rastogi, D. K. Mitra, and A. Bhattacharya, "A novel implementation of bidirectional coupling circuit for broadband, high-voltage, power-line communications," in *Proc. Asia-Pacific Conference on Communications*, Oct. 2005, pp. 38–42.

[123] J.-J. Lee, D.-S. In, H.-M. Oh, S. Shon, and D.-H. Nam, "Neutral inductive coupling for improved underground medium voltage BPLC," in *Proc. IEEE International Symposium on Power Line Communications and Its Applications*, Mar. 2010, pp. 67–71.

[124] X. Y. Wang and X. Gao, "The typical designs of PLC network in MV distribution network," in *Proc. IEEE International Symposium on Power Line Communications and Its Applications*, Mar. 2012, pp. 19–23.

[125] T. T. Ku, C. S. Chen, C. H. Lin, M. S. Kang, and H. J. Chuang, "Identification of customers served by distribution transformer using power line carrier technology," in *Proc. IEEE Conference on Industrial Electronics and Applications*, May 2009, pp. 3476–3481.

[126] J. Anatory, N. Theethayi, M. Kissaka, N. Mvungi, and R. Thottappillil, "The effects of load impedance, line length, and branches in the BPLC: Transmission-lines analysis for medium-voltage channel," *IEEE Trans. on Power Delivery*, vol. 22, no. 4, pp. 2156–2162, Oct. 2007.

[127] F. J. A. Andrade, C. A. G. Marques, T. R. Oliveira, F. P. V. Campos, E. J. de Oliveira, and M. V. Ribeiro, "Preliminary analysis of additive noise on outdoor and low voltage electric power grid in Brazil," in *Proc. IEEE International Symposium on Power Line Communications and Its Applications*, Mar. 2013, pp. 109–113.

[128] A. Kosonen and J. Ahola, "Comparison of signal coupling methods for power line communication between a motor and an inverter," in *Proc. Lappeenranta University of Technology*, Aug. 2010, pp. 431–440.

[129] A. Pinomaa, J. Ahola, and A. Kosonen, "Power-line communication-based network architecture for LVDC distribution system," in *Proc. IEEE International Symposium on Power Line Communications and Its Applications*, Apr. 2011, pp. 358–363.

[130] F. Grassi, S. A. Pignari, and J. Wolf, "Channel characterization and emc assessment of a plc system for spacecraft dc differential power buses," *IEEE Trans. on Electromagnetic Compatibility*, vol. 53, no. 3, pp. 664–675, Aug. 2011.

[131] A. Pinomaa, J. Ahola, A. Kosonen, and P. Nuutinen, "Applicability of narrow-band power line communication in an LVDC distribution network," in *Proc. IEEE International Symposium on Power Line Communications and its Applications*, Mar. 2014, pp. 232–237.

[132] A. Kosonen, A. Pinomaa, J. Ahola, and P. Nuutinen, "Noise analysis of a power-line communication channel in an LVDC smart grid concept," in *Proc. IEEE International Symposium on Power Line Communications and Its Applications*, Mar. 2013, pp. 41–46.

[133] F. Versolatto and A. Tonello, "An MTL theory approach for the simulation of MIMO power-line communication channels," *IEEE Trans. on Power Delivery*, vol. 26, no. 3, pp. 1710–1717, Jul. 2011.

[134] A. Perez, A. M. Sanchez, J. R. Regue, M. Ribo, R. Aquilue, P. Rodriguez-Cepeda, and F. J. Pajares, "Circuital and modal characterization of the power-line network in the PLC band," *IEEE Trans. on Power Delivery*, vol. 24, no. 3, pp. 1182–1189, Jul. 2009.

[135] T. Pang, P. So, K. See, and A. Kamarul, "Modeling and analysis of common-mode current propagation in broadband power-line communication networks," *IEEE Trans. on Power Delivery*, vol. 23, no. 1, pp. 171–179, Jan. 2008.

[136] L. Berger, A. Schwager, P. Pagani, and P. D. Schneider, *MIMO Power Line Communications: Narrow and Broadband Standards, Eletromagnetic Compatibility and Advanced Processing.* Boca Raton: CRC Press, 2014.

[137] M. S. P. Facina, H. A. Latchman, H. V. Poor, and M. V. Ribeiro, "Cooperative in-home power line communication: Analyses based on a measurement campaign," *IEEE Trans. on Communications*, vol. 64, no. 2, pp. 778–789, Feb. 2016.

[138] A. Schwager, D. Schneider, W. Baschlin, A. Dilly, and J. Speidel, "MIMO PLC: Theory, measurements and system setup," in *Proc. IEEE International Symposium on Power Line Communications and Its Applications*, Apr. 2011, pp. 48–53.

[139] S. Chen, M. Setta, X. Chen, and C. G. Parini, "Ultra wideband powerline communication (PLC) above 30 MHz," *Institution of Engineering and Technology Communications*, vol. 3, no. 10, pp. 1587–1596, Oct. 2009.

[140] F. J. Canete, J. A. Cortes, L. Diez, and J. T. Entrambasaguas, "A channel model proposal for indoor power line communications," *IEEE Communications Magazine*, vol. 49, no. 12, pp. 166–174, 2011.

[141] H. Ferreira and P. Van Rensburg, "Coupling circuitry: Understanding the functions of different components," *7th International Symposium on Power Line Communications and Its Applications*, vol. 1, pp. 204–206, Mar. 2003.

[142] R. N. Gore, E. A. Andarawis, and D. M. Davenport, "Design methodology for powerline coupling circuit: a system-level and monte carlo simulation based approach," in *Proc. International Symposium on Power Line Communications and Its Applications*. IEEE, Apr. 2005, pp. 270–274.

[143] P. A. J. Van Rensburg and H. C. Ferreira, "Step-by-step design of a coupling circuit with bi-directional transmission capabilities," in *Proc. International Symposium on Power Line Communications and Its Applications*, Apr. 2004.

[144] P. Van Rensburg and H. Ferreira, "Classifying typical residential rooms for narrow-band impedance adaptation," in *Proc. IEEE International Symposium on Power Line Communications and Its Applications*, Mar. 2007, pp. 47–52.

[145] IEEE, "1901.2-2013 - IEEE Standard for Low-Frequency (less than 500 kHz) Narrowband Power Line Communications for Smart Grid Applications," https://standards.ieee.org/findstds/standard/1901.2-2013.html, Feb. 2015.

[146] "Anatel," http://www.anatel.gov.br/legislacao/resolucoes/2009/101-resolucao-527, 2016.

[147] "Dv Tecnologia," http://www.dvtecnologia.com.br/, 2015.

[148] H. C. Ferreira, L. Lampe, J. Newbury, and T. G. Swart, *Power Line Communications: Theory and Applications for Narrowband and Broadband Communications of Power Lines*. Boca Raton: John Wiley and Sons Lt, 2010.

[149] S. S. Ali, A. Bhattacharya, and D. R. Poddar, "Design of bidirectional coupling circuit for broadband power-line communications," *Journal of Electromagnetic Analysis and Applications*, vol. 4, no. 4, pp. 162–166, Apr. 2012.

[150] "Coilcraft," http://www.coilcraft.com/, 2015.

[151] Minicircuits, "Mini Circuits - Global Leader of RF and Microwave Components," http://www.minicircuits.com/homepage/homepage.html, Feb. 2017.

[152] B. S. Yarman, *Design of Ultra Wideband Antenna Matching Networks*, 1st ed. Stambul, TK: Springer, 2008.

[153] A. T. Ceramics, "American Technical Ceramics Corporation," http://www.atceramics.com/, Feb. 2017.

[154] M. I. Montrose, *EMC and the Printed Circuit Board*, 1st ed. New York, USA: IEEE Press Series on Electronics Technology and Wiley Interscience, 1999.

[155] "Altium designer," http://www.altium.com/altium-designer/overview, 2015.

[156] K. Technologies, "Keysight Technologies," http://www.keysight.com/, Jun. 2017.

[157] L. G. S. Costa, A. C. M. Queiroz, B. Adebisi, V. L. R. Costa, and M. V. Ribeiro, "Coupling for power line communications: A survey," *Journal of Communication and Information Systems*, vol. 32, no. 1, pp. 8–22, Feb. 2017.

[158] G. R. Colen, L. G. Oliveira, A. J. Han Vinck, and M. V. Ribeiro, "Statistical analysis and modeling of a new parameter for resource allocation in multicarrier PLC systems," *Trans. on Emerging Telecommuniations Technologies*, vol. 1, pp. 1–11, Feb. 2016.

[159] L. G. de Oliveira, G. R. Colen, M. V. Ribeiro, and A. H. Vinck, "Narrowband interference error correction in coded OFDM-based PLC systems," in *Proc. International Symposium on Power Line Communications and its Applications*, Mar. 2016, pp. 13–18.

[160] M. V. Ribeiro, G. R. Colen, F. V. De Campos, Z. Quan, and H. V. Poor, "Clustered-orthogonal frequency division multiplexing for power line communication: when is it beneficial?" *IET Communications*, vol. 8, no. 13, pp. 2336–2347, Sep. 2014.

[161] M. V. Ribeiro, F. P. Campos, G. R. Colen, H. V. Schettino, D. Fernandes, L. M. Sirimarco, V. Fernandes, and A. A. Picorone, "A novel power line communication system for outdoor electric power grids," in *Proc. International Symposium on Power Line Communications and its Applications*, Mar. 2015, pp. 228–233.

[162] S. D. A. Sanabria, V. R. P. Bonilla, and J. M. D. B. Tobar, "Test methodology for impedance characterization of a low voltage power line channel for broadband communication applications," in *Proc. IEEE Colombian Conference on Communications and Computing*, Jun. 2014, pp. 1–6.

[163] T. R. Oliveira, C. A. Marques, W. A. Finamore, S. L. Netto, and M. V. Ribeiro, "A methodology for estimating frequency responses of electric power grids," *Journal of Control, Automation and Electrical Systems*, vol. 25, no. 6, pp. 720–731, Sep. 2014.

[164] R. M. Vines, H. J. Trussell, K. C. Shuey, and J. B. O'Neal, "Impedance of the residential power-distribution circuit," *IEEE Trans. on Electromagnetic Compatibility*, vol. 27, no. 1, pp. 6–12, Feb. 1985.

[165] P. S. Henry, "Interference characteristics of broadband power line communication systems using aerial medium voltage wires," *IEEE Communications Magazine*, vol. 43, no. 4, pp. 92–98, Apr. 2005.

[166] M. A. O. Kharraz, C. Lavenu, P. Jensen, D. Picard, and M. Serhir, "Characterization of the input impedance of household appliances in the FCC frequency band," in *Proc. IEEE International Symposium on Power Line Communications and its Applications*, Apr. 2017, pp. 1–6.

[167] M. Karduri, M. D. Cox, and N. J. Champagne, "Near-field coupling between broadband over power line (BPL) and high-frequency communication systems," *IEEE Trans. on Power Delivery*, vol. 21, no. 4, pp. 1885–1891, Oct. 2006.

[168] M. Thompson and J. K. Fidler, "Determination of the impedance matching domain of impedance matching networks," *IEEE Trans. on Circuits and Systems I: Regular Papers*, vol. 51, no. 10, pp. 2098–2106, Oct. 2004.

[169] P. R. Chin, A. K. M. Wong, K. I. Wong, and N. Barsoum, "Modelling of LCRC adaptive impedance matching circuit in narrowband Power Line Communication," in *Proc. 11th International Conference on Power Electronics and Drive Systems*, Jun. 2015, pp. 132–135.

[170] J. A. Cortés, A. Sanz, P. Estopiñán, and J. I. García, "Analysis of narrowband power line communication channels for advanced metering infrastructure," *EURASIP Journal on Advances in Signal Processing*, vol. 1, no. 1, p. 27, Mar. 2015.

[171] B. Rasool, A. Rasool, and I. Khan, "Impedance characterization of power line communication networks," *Arabian Journal for Science and Engineering*, vol. 39, no. 8, pp. 6255–6267, Jun. 2014.

[172] S. S. Dash and A. V. Panda, "Interpretation of different channel configurations and modulation techniques over power line communication," in *Proc. International Conference on Communication and Signal Processing*, Apr. 2016, pp. 420–425.

[173] E. Takmaz, "Impedance, attenuation and noise measurements for power line communication," in *Proc. 4th International Istanbul Smart Grid Congress and Fair*, May 2016, pp. 1–4.

[174] L. T. Tang, P. L. So, E. Gunawan, Y. L. Guan, S. Chen, and T. T. Lie, "Characterization and modeling of in building power lines for high-speed data transmission," *IEEE Power Engineering Review*, vol. 22, no. 9, pp. 58–58, Sep. 2002.

[175] Y.-J. Park and K.-H. Kim, "Investigation and measurement of indoor low-voltage powerline impedance for high data rate powerline communications," *Korea Electrotechnology Research Institute*, vol. 41, no. 8, pp. 93–98, Aug. 2004.

[176] Y.-S. Kim and J.-C. Kim, "Characteristic impedances in low-voltage distribution systems for power line communication," *Journal of Electrical Engineering and Technology*, vol. 2, no. 1, pp. 29–34, Mar. 2007.

[177] Y. Zhou, M. Zhai, and G. Xing, "Measurement methods of low voltage power-line communication channel impedances," in *Proc. International Conference on Advanced Computational Intelligence*, Oct. 2012, pp. 1004–1008.

[178] Z. Tao, Z. Baohui, and Y. Xiaoxian, "Study of 1MHz to 30 MHz impedance characterization in the low voltage networks," in *Proc. 18th International Conference and Exhibition on Electricity Distribution*, Jun. 2005, pp. 1–5.

[179] T. R. Oliveira, A. A. Picorone, S. L. Netto, and M. V. Ribeiro, "Characterization of Brazilian in-home power line channels for data communication," *Electric Power Systems Research*, vol. 150, pp. 188–197, Sep. 2017.

[180] C. R. B. Cabral, V. H. Lachos, and C. B. Zeller, "Multivariate measurement error models using finite mixtures of skew-student t distributions," *Journal of Multivariate Analysis*, vol. 124, no. 1, pp. 179–198, Feb. 2014.

[181] C. C. Dorea, C. R. Goncalves, and P. A. Resende, "Simulation results for Markov model seletion: AIC, BIC and EDC," in *Proc. World Congress on Engineering and Computer Science*, vol. 2, Oct. 2014, pp. 899–901.

[182] L. Tang, P. So, E. Gunawan, Y. Guan, S. Chen, and T. Lie, "Characterization and modeling of in-building power lines for high-speed data transmission," *IEEE Transactions on Power Delivery*, vol. 18, no. 1, pp. 69–77, Jan 2003.

[183] P. So and Y. Ma, "Development of a test bed for power line communications," *IEEE Transactions on Consumer Electronics*, vol. 50, no. 4, pp. 1174–1182, Nov 2004.

[184] M. De Piante and A. M. Tonello, "On impedance matching in a power-line-communication system," *IEEE Transactions on Circuits and Systems II: Express Briefs*, vol. 63, no. 7, pp. 653–657, Jan. 2016.

[185] M. Sigle, W. Liu, and K. Dostert, "On the impedance of the low-voltage distribution grid at frequencies up to 500 khz," in *Proc. International Symposium on Power Line Communications*, Mar. 2012, pp. 30–34.

[186] P. Van Rensburg and H. Ferreira, "Design of a bidirectional impedance-adapting transformer coupling circuit for low-voltage Power-line Communications," *IEEE Transactions on Power Delivery*, vol. 20, no. 1, pp. 64–70, Jan. 2005.

[187] P. Van Rensburg and H. Ferreira, "Design and evaluation of a dual impedance-adapting power-line communications coupler," *IEEE Transactions on Power Delivery*, vol. 25, no. 2, pp. 667–673, April 2010.

[188] W.-H. Choi and C. yeon Park, "A simple line coupler with adaptive impedance matching for power line communication," in *Proc. International Symposium on Power Line Communications and Its Applications*, Mar. 2007, pp. 187–191.

[189] F. Munoz, R. Carvajal, A. Torralba, L. Franquelo, E. ZRamos, and J. Pinilla, "Adapt: mixed-signal ASIC for impedance adaptation in power line communications using fuzzy logic," in *Proc. The 25th Annual Conference of the IEEE Industrial Electronics Society*, vol. 2. IEEE, Nov. 1999, pp. 509–513.

[190] D. Brown, W. Engeler, J. Tiemann, N. Lavoo, R. Carlson, and R. Connery, "High-frequency mos digital capacitor," *IEEE Transactions on Electron Devices*, vol. 22, no. 10, pp. 938–944, 1975.

[191] P. Nisbet, M. He, and L. Zhao, "Transformerless impedance matching networks for automotive power line communication," *Journal of Electrical and Electronics Engineering Research*, vol. 6, no. 2, pp. 13–20, 2014.

[192] R. M. Fano, "Theoretical limitations on the broadband matching of arbitrary impedances," *Journal of the Franklin Institute*, vol. 249, no. 1, pp. 57–83, Jan. 1950.

[193] P. Mlynek, J. Misurec, M. Koutny, and P. Silhavy, "Two-port network transfer function for power line topology modeling." *Radioengineering*, vol. 21, no. 1, pp. 356–363, Apr. 2012.

[194] E. Kelechi and M. G. Chinedum, "ABCD Parameter model for Two-port Networks," *International Journal of Advanced Engineering Research and Technology*, vol. 3, no. 10, pp. 334–339, Oct. 2015.

[195] D. M. Pozar, *Microwave Engineering*, 4th ed. New York, USA: John Wiley & Sons, 2011.

[196] A. C. M. de Queiroz, "Wideband asymmetrical bandpass LC-ladder matching networks for low-noise amplifiers," in *Proc. International Conference on Electronics, Circuits and Systems*. IEEE, Sep. 2008, pp. 974–977.

[197] "Nodemcu." https://nodemcu.readthedocs.io/en/master/, Jul 2017.

[198] "Analog devices," http://www.analog.com/media/en/technical-documentation, Jul 2017.

[199] "Peregrine semiconductor," http://http://www.psemi.com/, Jul 2017.

[200] "Keysight technoligies," http://www.keysight.com/en/pdx-x201745-pn-N9912A, Jul 2017.

[201] A. C. De Queiroz and L. P. Calôba, "Optimal filter overdesign," in *Proc. 36th Midwest Symposium on Circuits and Systems*. IEEE, Aug. 1993, pp. 1388–1391.

[202] R. Schaumann, M. S. Ghausi, and K. R. Laker, *Design of Analog Filters*, 1st ed. New Jersey, USA: Prentice Hall, 1981.

[203] P. A. C. M. de Queiroz, "Home page of dr. antônio carlos moreirão de queiroz," http://www.coe.ufrj.br/~acmq/programs/, Jun. 2017.

[204] A. S. Sedra and P. O. Brackett, *Filter Theory and Design*, 1st ed. New York, USA: Pitman Publishing, 1978.

APPENDIX A – DESIGN OF 4^{th} ORDER IRREGULAR ANALOG LOW-PASS FILTER

This appendix describes the design of the broadband and analog low-pass irregular filter [201], which will be used in the impedance matching circuit of the bank of impedance matching circuits, showed in Fig. 50. The use of these analog filters is due to its simpler structure for broadband impedance matching of unequal resistances termination at the input and output ports [196]. We assume that the broadband and analog low-pass irregular filter is doubly matched, in other words, its input and output port are matched.

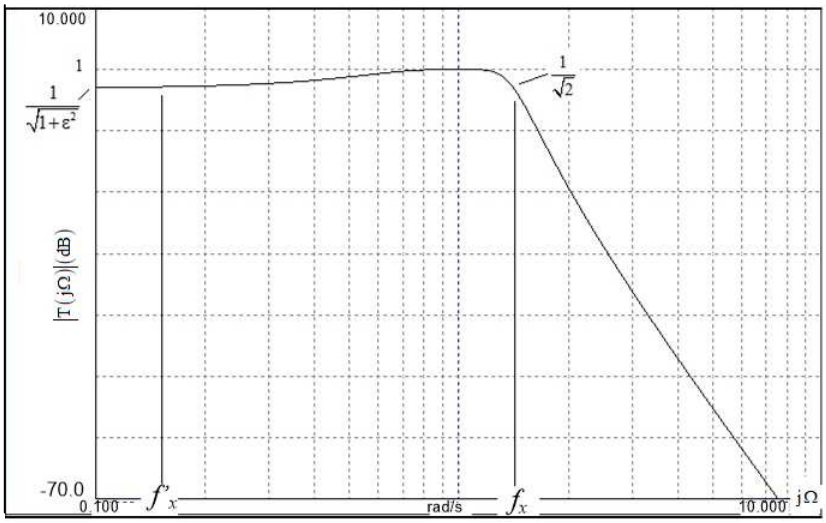

Figure 75: Frequency response magnitude analog and low-pass irregular filter.

Fig. 75 shows the frequency response magnitude of an broadband and analog low-pass irregular filter. Note that $\frac{1}{\sqrt{2}}$ is the cut-off frequency, $\frac{1}{\sqrt{1+\varepsilon^2}}$ is the ripple of magnitude response and f_x and f'_x are the band-pass limits. The first task is design this filter to obtain a realizable $T(j\Omega)$ which satisfies the target specifications. The magnitude of the frequency response of this filter is given by

$$|T\left(j\Omega\right)| = \frac{1}{\sqrt{1+\varepsilon^2 K(j\Omega)^2}}, \tag{A.1}$$

where $\varepsilon \in \mathbb{R}$ is a constant which is calculated in function of input R_S and output R_L resistance terminations. $K(j\Omega)$ is obtained from the *Feldtkeller's* equation [202], such that

$$|K(j\Omega)|^2 = \frac{1}{|T(j\Omega)|^2} - 1, \tag{A.2}$$

in which is $K(j\Omega) = F(j\Omega)/P(j\Omega)$ the even rational polynomial function ratio, $F(j\Omega)$ is the reflection zero polynomial, $P(j\Omega)$ are the transmission zero polynomial [203].

Considering a 4^{th} order analog low-pass irregular filter that has the structure showed in Fig. 76, R_S and R_L are the resistance termination of the filter and the inductors L_1 to L_4 and the capacitors C_1 to C_4 constitute the broadband and analog low-pass irregular filter. P_{in} is the power delivered by the input port of the broadband and analog low-pass irregular filter and P_{out} is the power delivered to the R_L. The desired band-pass insertion loss is shown in Fig. 75 around the normalized frequency response of 1 rad/s, between f'_x and f_x, which is designed from the characteristic function

$$K(j\Omega) = \varepsilon\left(j\Omega^2 + 1\right)^2 = \frac{F(j\Omega)}{P(j\Omega)}. \tag{A.3}$$

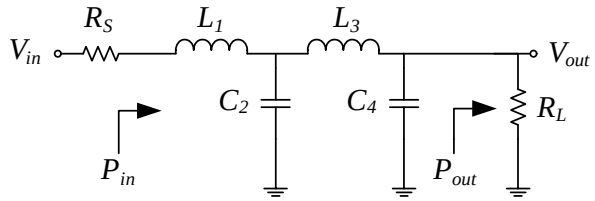

(a) $R_L > R_S$

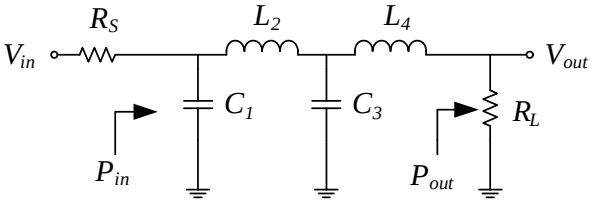

(b) $R_S > R_L$

Figure 76: 4^{th} order broadband and analog low-pass irregular filter for impedance matching.

The frequency response $H(j\Omega) = E(j\Omega)/P(j\Omega)$ corresponding to this characteristic function is obtained by solving the *Feldtkeller's* equation, which is given by

$$E(j\Omega)E(-j\Omega) = P(j\Omega)P(-j\Omega) + F(j\Omega)F(-sj\Omega). \tag{A.4}$$

In this way, the ratio between $K(j\Omega)$ and the so-called transduction function $H(j\Omega)$ is expressed as

$$\frac{K\left(j\Omega\right)}{H\left(j\Omega\right)} = \frac{R_S - Z_I}{R_S + Z_I} = \rho_1\left(j\Omega\right) \tag{A.5}$$

where $Z_I \in \mathbb{R}$ is the input impedance of the broadband and analog low-pass irregular filter in Fig. 76 and $\rho_1(s)$ is the reflection function [204]. Based on (A.5), $H(j\Omega) = E(j\Omega)/P(sj\Omega)$ and $K(j\Omega) = F(j\Omega)/P(j\Omega)$, we have $\rho_1(j\Omega) = F(j\Omega)/E(j\Omega)$. From $F(j\Omega)$ and $E(j\Omega)$, the input impedances or admittances of the broadband and analog low-pass irregular filter between the terminations can be found, and the structure, shown in Fig. 76 can be obtained. For the broadband and analog low-pass irregular filter, the impedance termination seen by the input termination R_S, is expressed by [202]

$$Z_I\left(0\right) = R_S\frac{H(0) + K(0)}{H(0) - K(0)} = \frac{\sqrt{1+\varepsilon^2} + \varepsilon}{\sqrt{1+\varepsilon^2} - \varepsilon} = R_L, \tag{A.6}$$

where $H(0)$ and $K(0)$ denote the value of which the magnitude function is assumed for $\rho_1(s) = 0$ that is the maximum power transfer. This implies that the input impedance Z_I must be real and have the same value of the resistance of the source. For functions with zeros of reflection at $j\Omega = 0$ this condition is easy to be fulfilled, because for $j\Omega = 0$ the input impedance of an analog low-pass filter of a ladder network R_S is equal to R_L [202].

$$\frac{1}{\varepsilon} = \sqrt{\left(\frac{R_L + R_S}{R_L - R_S}\right)^2 - 1}. \tag{A.7}$$

A key limitation of this design is the relation between R_L and R_S. Based on (A.7) it is straightforward to write

$$\left(\frac{R_L + R_S}{R_L - R_S}\right)^2 - 1 = \left(j\Omega^2 - 1\right)^4 \tag{A.8}$$

or

$$\frac{R_L + R_S}{R_L - R_S} = \sqrt{\left(j\Omega^2 - 1\right)^4 + 1}. \tag{A.9}$$

For the sake of simplicity, we can adopt that

$$\gamma = \sqrt{\left(j\Omega^2 - 1\right)^4 + 1}, \tag{A.10}$$

$$R_L + R_S = \gamma\left(R_L - R_S\right) \tag{A.11}$$

and

$$R_L = R_S \frac{\gamma + 1}{\gamma - 1}. \tag{A.12}$$

For the cut-off frequency of the broadband and analog low-pass irregular filter designed for -3 dB, the constant γ is equal to $\gamma = \sqrt{2}$ and the relation between R_L and R_S is 5.828. However, this relation is not adequate, because for a relation 1:5.828, $R_L = 50\ \Omega$ and $R_S = 8.579\ \Omega$ and for the relation 5.828:1, $R_S = 291.4\ \Omega$ and $R_L = 50\ \Omega$, which is not a useful result because of the range of access impedance value. In Chapter 3, the statistical analysis of resistance component probabilities showed that 90% of the values of resistance components are below 127 Ω and above 11.64 Ω.

In order to overcome this problem, we redesign the filter to obtain a relation between R_L and R_S equal to for 1:2 or 2:1 and, as a consequence, to keep the input impedance of irregular filter between 25 Ω and 100 Ω. The values of R_S equal to 25 Ω and 100 Ω are used because based on Chapter 3. Following (A.7), a new value of $\varepsilon = 0.353553390593$ is obtained and the cut-off point of the broadband and analog low-pass irregular filter is expanded to $j\Omega = 1.6376$ rad/s.

To illustrate the design of such broadband and analog low-pass irregular filter, a simulation was performed using the HK Software considering the broadband and analog low-pass irregular filter matching with $R_S = 2\ \Omega$ and $R_L = 1\ \Omega$. In this case, $F(j\Omega) = \varepsilon(j\Omega^2 + 1)^2 = \varepsilon(j\Omega^4 + 2j\Omega + 1)$, $P(j\Omega) = 1$, $\varepsilon = 0.353553390593$, and $E(j\Omega) = \varepsilon(j\Omega^4 + 2.4467j\Omega^3 + 4.9932j\Omega^2 + 5.0950j\Omega + 3)$. In this way, using the Ladder program [203], we obtain the normalized values of the LC broadband and analog low-pass irregular filter in Fig. 76(b), for $R_S > R_L$, expanding the LC ladder from the impedance seen by the R_L impedance termination. The values of each component are $R_L = 1\ \Omega$, $R_S = 2\ \Omega$, $C_1 = 0.408710973035821$ F, $L_2 = 1.730090033879250$ H, $C_3 = 0.865045016940072$ F, $L_4 = 0.817421946071220$ H. A similar approach is used when $R_S < R_L$ and the normalized values of L and C components is the same, but the broadband and analog low-pass irregular filter is mirrored as can be seen in Fig. 76(a).

To visualize the result of this design, a circuit simulation was performed and the insertion loss obtained is shown in Fig. 77. Note that the cut-off frequency is 1.6376 rad/s and the maximum transfer power is located at 1 rad/s, where the gain is maximally flat. The attenuation in the band-pass of the filter is 3 dB ($10\log_{10}(1/2)$), because of the impedance terminations of the broadband and analog low-pass irregular filter $R_L = 1\ \Omega$ and $R_S = 2\ \Omega$. Based on the attained results, it can be concluded that the constant value of ε, which is calculated by the ratio between the terminations,

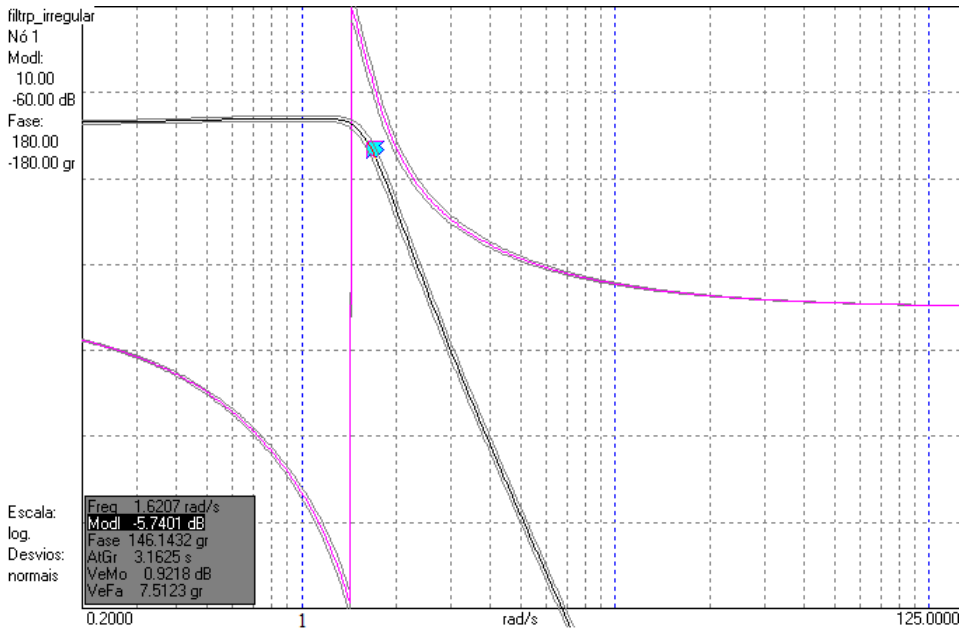

Figure 77: Frequency response magnitude of broadband and analog low-pass irregular filter for s =1.6376 rad/s.

controls the bandwidth of the broadband and analog low-pass irregular filter.

According to the design procedure [196], the values of components are normalized ones. To obtain the correct values for the capacitor and inductor, the following equations apply:

$$L_n^x = 1.6376\frac{Z_I L_n}{2\pi f_c} \tag{A.13}$$

and

$$C_n^x = 1.6376\frac{C_n}{Z_I 2\pi f_c} \tag{A.14}$$

where L_n and C_n is the normalized value of the inductor and capacitor, respectively, calculated by the HK and Ladder software and f_c is the cut-off frequency. The index n denotes the n^{th} inductor and capacitor of the low-pass irregular filter.

The impedance matching performance attained by the broadband and analog low-pass irregular filter can be measured by the amount of power delivered to the load compared with the maximum power deliverable by the source. It is well known that maximum power is delivered to the load when the load impedance and the source impedance are conjugate of each other. When these impedances are represented by resistances, the maximum power is delivered when the two resistances are equal.

From now on, we assume that the broadband and analog low-pass irregular filter in Fig. 76(a) and (b) are lossless and calculate the power delivered by the source P_{in}

and the power delivered to the load P_{out}. They are, respectively,

$$P_{in} = \left(\frac{V_{in}}{2}\right)^2 \frac{1}{2R_S} \tag{A.15}$$

and

$$P_{out} = \frac{{V_{out}}^2}{R_L}. \tag{A.16}$$

Note that if the broadband and analog low-pass irregular filter, designed to provide impedance matching, is lossless, the maximum power available occurs if P_{in}=P_{out}. In other words,

$$\frac{{V_{in}}^2}{4R_S} = \frac{{V_{out}}^2}{R_L} \quad \equiv \quad \frac{V_{out}}{V_{in}} = \frac{1}{2}\sqrt{\frac{R_L}{R_S}}. \tag{A.17}$$

where $\equiv$ denotes equivalence.

Similarly, we can calculate the DC gain of the filter, when the voltage $V_{out} = V_{in}/2$ and the impedance matching occurs if $R_S = R_L$, by writing

$$DC_{gain} = \frac{R_L}{R_S + R_L} = \frac{V_{out}}{V_{in}}. \tag{A.18}$$

By defining the ratio V_{out}/V_{in} with (A.17) and (A.18) a comparison between ratios with and without impedance matching can be accomplished.

Several tests were performed to analyze (A.18), in which the normalized impedance R_S is equal to 1 Ω and R_L is equal to 2 Ω ($R_S < R_L$). Similarly, the relation R_L is equal to 1 Ω and R_S is equal to 2 Ω ($R_S > R_L$) can be assumed and both cases are depicted in the Figs 76(a) and (b). Based on (A.18), Tab. 18 summarizes both ratios V_{out}/V_{in} obtained with and without impedance matching. To obtain these results, Tab. 18 shows that the gain obtained is 6% with the ratio of 1:2 and 2:1 between R_S and R_L.

Table 18: V_{out}/V_{in} with and without impedance matching.

R_S/R_L	Type	V_{out}/V_{in}	Total ratio
1:2	without impedance matching	$\frac{2}{3}$	$\frac{\frac{\sqrt{2}}{2}}{\frac{2}{3}} = \frac{\frac{1}{2\sqrt{2}}}{\frac{1}{3}} = 1.06066$
	with impedance matching	$\frac{\sqrt{2}}{2}$	
2:1	without impedance matching	$\frac{1}{3}$	
	with impedance matching	$\frac{1}{2\sqrt{2}}$	

The designs of this broadband and analog low-pass irregular filter aforementioned match the impedance of the resistive component between the PLC coupling circuit and the electric power grid. However, to match the impedance of reactive component between the electric power grid and the PLC coupling circuits an attractive way is to incorporate the reactive component as part of the matching network (in our case the electric power grid) or, equivalently, absorbing them into the electric power grid. To provide impedance matching with the access impedance of the reactive component of the electric power grid with the PLC coupling circuit, the L_1 inductor component, see Fig. 76(a), is chosen to absorb part of the reactance of the electric power grid. However, according to the measurements of the access impedance of the electric power grid, discussed in Chapter 3, the average value of the inductance, obtained in the measurement campaign, is bigger than the value of the L_1 inductor designed in the broadband and analog low-pass irregular filter. Thus, the impedance matching between the inductor L_1 of the PLC coupling circuit with the inductive component of the electric power grid depends on the value of the inductive component of the electric power grid. If the inductive reactance of the electric power grid and the L_1 inductor of the broadband and analog low-pass irregular filter are equal, the impedance matching occurs. On the other hand, if the reactive component of the electric power grid has a different value of the inductor L_1, the bandwidth of the broadband and analog low-pass irregular filter may increase or decrease. The same analysis can be applied to the capacitive component C_1, when the analog low-pass irregular filter is matching the impedance with a capacitive component of the electric power grid as showed in Fig. 76(b).

APPENDIX B – PUBLICATIONS

Journal:

- Costa, Luís Guilherme; Queiroz, Antônio Carlos Moreirão de; Adebisi, Bamidele; Costa, Vinícius Lagrota Rodrigues da; Ribeiro, Moisés Vidal. Coupling for Power Line Communications: A Survey. Journal of Communication and Information Systems, v. 32, p. 8-22, 2017.

Conference:

- Oliveira, Thiago Rodrigues; Andrade, Fernando José de Almeida ; Costa, Luís Guilherme; Pereira, Michelle Soares; Ribeiro, Moisés Vidal. Measurement of Hybrid PLC Wireless Channels for Indoor and Broadband Data Communication. Proc. XXXI Simpósio Brasileiro de Telecomunicações, 2013, Fortaleza.
- Costa, Luís Guilherme; Picorone, Antônio Ângelo Massiagia; Queiroz, Antônio Carlos Moreirão de; Costa, Vinícius Lagrota Rodrigues da; Ribeiro, Moisés Vidal. Projeto e Caracterização de Acopladores para Power Line Communications. Proc. XXXIII Simpósio Brasileiro de Telecomunicações, 2015, Juiz de Fora.
- Costa, Luís Guilherme; Picorone, Antônio Ângelo Massiagia; Queiroz, Antônio Carlos Moreirão de; Costa, Vinícius Lagrota Rodrigues da; Ribeiro, Moisés Vidal. Caracterização da Impedância de Acesso à Rede de Energia Elétrica Residencial para Uso em Sistemas Power Line Communications. Proc. XXXIII Simpósio Brasileiro de Telecomunicações, 2015, Juiz de Fora.